Abstract

Title of Dissertation: EXPERIMENTAL STUDIES OF THE PRODUCTION OF NITROGEN OXIDES BY SIMULATED LIGHTNING SPARKS

Yujin Wang

Doctor of Philosophy, 1998

Dissertation directed by: Alan DeSilva

Professor

Institute for Physical Science and Technology

Department of Physics

Lightning flashes have been simulated with arcs at ambient conditions. Each simulated flash consisted of a weakly ionized leader channel initialized by a 250 kV pulse about one half microsecond long from a Marx generator followed by a high current stroke from the discharge of a 1035 μF main capacitor bank through the pre-ionized leader channel. The leader channel was initialized up to 20 cm under

atmospheric pressure. The arcs were successfully created up to 4 cm under atmospheric pressure and longer sparks were available under lower pressure.

The experimental arcs matched the cloud-ground (CG) strokes in current waveform, current amplitude and energy dissipation. The current waveform of arcs, primarily determined by an external resistor, agreed well with the overall of CG strokes on the global average. Arc current arrived at its peak from zero in about 30 μs and decayed thereafter with a RC decay time constant of about 350 μs. The current amplitude of the simulated lightning depended on the charge voltage on the main capacitor bank. The peak current increased from 5.0 kA to 30 kA as the main capacitor was charged from 3.0 kV to 10.0 kV, which covers about 50% of the global CG stroke in peak current. Experimental measurements have shown that the energy dissipation of the simulated lightning fell in the range of a typical CG lightning stroke. The energy deposited per unit length of spark increased from 3 to 8×10^3 J/m as the spark peak current changed from 3.0 kA to 10.0 kA discharging at atmospheric pressure.

NO_x production by the simulated lightning has been measured with chemiluminescent techniques. The results showed that the NO_x yield of a lightning flash not only depends on its energy deposition but also strongly depends on the dynamic discharge process. The NO production rate per unit of energy increased with the energy dissipated, rather than remaining constant as previously assumed in most estimates of the global NO_x production by lightning. The NO production per unit length of the simulated lightning strongly depended on the spark peak current, and it was proportional to the density of the initial air in the range that corresponds

to the atmospheric density from the ground to a cloud. About 11% of the NO produced by a spark was oxidized into NO_2 after a discharge by the atmospheric O_3 and the O_3 produced during the discharge.

The global NO_x production by lightning was estimated with the Flash-Extrapolation-Approach (FEA) from our observation of the NO production by the simulated lightning in combination with the lighting frequency data observed in the United States. The NO_x yield by a global "average" CG flash was estimated as 1.51×10^{26} NO_x molecules, in which the multiplicity of strokes in a flash and the tortuosity of a flash channel were included. We calculated that the global NO_x production by lightning as 2.84 to 11.4 TgN/year by taking the global lightning frequency as 30 to 100 flashes/second respectively. This result shows that the lightning may have been overestimated as a source of the global NO_x emission into the atmosphere.

EXPERIMENTAL STUDIES OF THE PRODUCTION OF NITROGEN OXIDES BY SIMULATED LIGHTNING SPARKS

By

Yujin Wang

Dissertation submitted to the Faculty of the Graduate School of the
University of Maryland at College Park in partial fulfillment
of the requirements for the degree of
Doctor of Philosophy
1998

Advisory Committee:

Professor Alan DeSilva, Chairman /Advisor
Professor Russell Dickerson
Professor George Goldenbaum
Doctor Parvez Guzdar
Doctor Kenneth Pickering

Dedication

To
my wife, Yinghua
and
our beloved daughter, Cherrie

Acknowledgments

I wish to express my deepest gratitude to my graduate advisor, Professor Alan DeSilva, for his guidance and support throughout the course of this work, and for carefully reading many iterations of this thesis. Without his ceaseless encouragement and help, this work would not have been completed.

I would like to thank Professors George Goldenbaum and Russell Dickerson for their interest and valuable advice, their patience in reading the initial version and their suggestions which make the thesis more presentable. At each step of our experiments, Dr. Goldenbaum had worked with me carefully and provided all the critical simulation and models in data analysis. From Dr. Dickerson I began to learn the complexities of the world of the atmospheric chemistry. The close working relationship we developed during the past years showed me the rewards of interdisciplinary study. I would like to give my special gratitude to Drs. Parvez Guzdar and Kenneth Pickering for serving on my Ph.D. committee, and in reading and modifying the final version of this thesis.

I thank Mr. Ken Diller for his encouragement and creative support, which solved many technical problems with minimum resources. I would like to thank Dr. Hezhong Guo, Dr. Raymond Elton, Dr. Enrique Iglesias, Dr. Julius Goldhar, Dr. Ellen Williams, Dr. Michael Coplan, Dr. Xiaoqing Xu, Dr. Xiao Yuan, Mr. Victor Yun, Dr. John Rodgers, Mr. Jay Pyle, Mr. Doug Cohen, Mr. Nolan Ballew, Mr. Paul Chin, and Mr. Ed Condon for their technical support and personal help.

I thank Dr. Jeffrey Stehr, Ms. Kristen Hallock, Dr. Bruce Doddridge, Dr. Kevin Rhoads, and other members of the Atmospheric Chemistry group for their help in building the gas phase titration system, and for numerous discussions in calibration of the chemiluminescent NO_x analyzer and in measurement of NO_x in our experiments. I also thank my friends and fellow graduate students Dr. Shiawei Chen, Dr. Jack Cheng, Dr. John Curry, Mr. David Gershon, Mr. Joseph Katsourus, Dr. Yongzhang Leng, Dr. Chunbo Liu, Dr. Weizhong Wang, Mr. Weijun Chen, Mr. Yun Zhou, Ms. Yun Li, and Mr. James Weaver for their wonderful support and friendship.

I thank Ms. Margaret Hess, Ms. Marilyn Spelling, Ms. Diane Mancuso and other members at the Institute for Plasma Research, and the Institute for Physical Science and Technology at University of Maryland for providing me the necessary support during my graduate study.

I thank Mrs. DeSilva for her caring and love to my family and me.

Finally, I thank my wife, Yinghua, who has had to bear all of the necessary sacrifices and uncertainties, and my family for their love, encouragement and support throughout my graduate study.

Table of Contents

Lists of Tables

Lists of Figures

Chapter I. Introduction

The sum of NO and NO_2 are always designated here as NO_x. They are two important compounds of the reactive nitrogen trace species (NO, N_2O_5, NO_2, NO_3, HNO_2, HNO_3, etc.) in the Earth's atmospheric-biospheric system. In the atmosphere, NO_2 absorbs over the entire visible and UV of the solar radiation. When it absorbs a UV photon in wavelength less than 420 nm, it photolyzes as

$$NO_2 + h\nu \rightarrow NO + O \qquad (1.1)$$

Because O_3 absorbs the solar radiation in wavelengths less than 330 nm in the outer atmosphere, most of the UV solar radiation in the troposphere is in wavelengths longer than 290 nm--the long wavelength limit of O_2 absorption. Therefore, NO_2 is the most important source of the atomic oxygen in the troposphere (Seinfeld and Pandis, 1998). The atomic oxygen is responsible for the production of O_3.

NO_x is the key catalyst in O_3 formation in the troposphere and thus plays a major role in the formation of other tropospheric oxidants such as OH, HO_2 and RO_2 (R refers to an alkyl radical), when CO, non-methane hydrocarbons and water are present (Hagen-Smith, 1958; Fehsenfeld et al., 1988). Locally high levels of O_3 have been observed in urban or continental areas with high levels of NO_x that are primarily emitted by anthropogenic sources (Levy, 1971; Crutzen 1979; Logan et al., 1981; Liu et al., 1983).

The tropospheric NO_x after conversion to nitrates can be deposited in the ground by dry deposition or precipitation. These deposited nitrates are an important source of the fixed nitrogen to be absorbed and utilized by plants in biosynthesis. Nitrate particles from the NO_x also result in visibility impairment, human health and

material damage (Haggen-Smith, 1958;Brimblecombe, 1986). A comprehensive understanding of the sources of the atmospheric NO_x is essential to study atmospheric chemistry and global climate changes.

Table 1.1 lists the anthropogenic and natural sources of atmospheric NO_x. The primary sources of anthropogenic emissions are burning of fossil fuel and industrial production of fertilizers. The natural sources include biomass burning (Dhar and Ram, 1993), oxidation of N_2 in the hot gas mixture of lightning sparks (von Leibig, 1857), or other minor sources (Brimblecombe, 1986). As shown in Table 1.1 and Table 1.2, lightning has the largest uncertainty in all these sources of the atmospheric NO_x emissions. The global annual NO_x production by lightning was reported (Table 1.2) from as little as 1 TgN/year (1 Tg = 10^{12} g) to more than 200 TgN/year (Lawrence et al., 1995).

The objectives of this research are to simulate natural lightning with an arc in atmosphere, and study the production of NO_x by the simulated lightning. Global NO_x production by lightning is estimated from our experimental observations and reported data of global lightning. Therefore, a more constrained estimate of global NO_x production by lightning is available to accurately assess the role of each source in the budget of the atmospheric NO_x.

1.1 Previous Studies of Lightning NO_x Production

Global NO_x production by lightning has been estimated based on theoretical calculation, studies of laboratory discharge, and field measurements of NO and NO_2

Table 1.1 Global Sources of NO_x

Source	Investigators	Magnitude(TgN/year)
Fossil fuel	Hameed and Dignon [1988]	22
	Levy and Moxim [1989]	21.2
	Benkovitz et al. [1996]	22.2
	Levy et al. [1996]	21.4
Subsonic aircraft	Beck et al. [1992]	1
	Wuebbles et al. [1993]	0.45
Stratosphere	Kasibhatla et al.[1991]	0.64
Biomass burning	Hao et al. [1989]	~6
	Levy et al. [1991]	8.5
	Penner et al. [1991]	5.8
	Dignon et al. [1992]	~5
Soil biogenic	Müller [1992]	4.7
emissions	Yienger and Levy [1995]	5.5
Lightning	see Table 1.2 & 1.3	1~220

Table 1.2 Estimates of the Amount of Nitrogen Fixed by Lightning

Investigators	Nitrogen per Year (TgN/year)
Tuck [1976]	4.2
Chameides et al. [1977]	30 ~ 40
Chameides [1979]	4.2 - 90
Dawson [1980]	3
Hill et al. [1980]	4.4
Hameed et al. [1981]	2.1
Levine et al. [1981]	1.8
Kowalczyck [1982]	5.7
Ehhalt and Drummond [1982]	5
Peyrous and Lapeyee [1982]	9
Logan [1983]	8
Drapcho et al. [1983]	30
Borucki and Chameides [1984]	2.6
Franzblau and Popp [1989]	220
Liaw et al. [1990]	9.1-152
Penner et al. [1991]	3-10
Lawrence et al. [1995]	1-8
Kumar [1995]	2
Levy et al. [1996]	2-6
Price et al. [1997]	12.5±2.2

associated with thunderstorms. There exist large uncertainties on both the mechanism of NO_x production by lightning and the lightning parameters, such as the channel length, the lightning frequency, and the total energy dissipation by each lightning flash. The NO_x production per unit energy has been given by different mechanisms from $1.6x10^{16}$ to 17×10^{16} molecules/Joule (Table 1.3). Widespread values of the lightning parameters have been adopted, for instance, the channel length between 2 km and 10 km, the global lightning frequency from 100 to 1600 flashes/second, and the energy dissipation from 10^8 to 10^{10} J/flash.

In 1857, von Leibig proposed lightning as a global source of the atmospheric NO_x which is removed into the biosphere as NO_3^- in rainwater. Thereafter, some early studies were undertaken to investigate the correlation between the lightning intensity and the contents of NO_3^- in rainwater. They estimated the contribution of lightning to the atmospheric NO_x and nitrogen fixation for the biosphere (Hutchinson, 1954; Viemeister, 1960; Visser, 1961). However, these early studies found that lightning was not a major source of the atmospheric NO_x; for example, Hutchinson (1954) calculated that less than 20% of the NO_3^- in rainwater is related to the NO_x produced in lightning.

These studies underestimated the production of NO_x by lightning when they only accounted for the content of NO_3^- in rainwater. The rainwater acquires most of its NO_3^- by dissolving HNO_3 (Chameides, 1975) that is converted from the NO_x produced by lightning discharge. NO_x reacts with the OH radicals via the chain process

$$NO + O_3 \rightarrow NO_2 + O_2 \qquad (1.2)$$

Table 1.3 Estimates of NO Production Rate in Lightning

Methods	Investigators	P (10^{16} NO/J)
Theoretical	Truck [1976]	3
Calculation	Chameides et al. [1977]	3-7.5
	Griffing [1977]	5±1
	Hill et al.[1980]	16
	Borucki and Chameides [1984]	9±2
	Goldenbaum and Dickerson [1993]	15
Laboratory	Chameides [1979]	8-17
spark	Chameides et al. [1977]	6 ±1
	Levine et al. [1981]	5 ±2
	Peyrous and Lapeye [1982]	2 ±0.5
	Borucki and Chameides [1984]	9±2
	Stark et al.[1996]	3-12
Atmospheric	Noxon [1976]	20-30
Measurement	Drapcho et al. [1983].	25-2500
Review	Liaw et al. [1990]	2.46-41.1
	Lawrence et al. [1995]	7.2

$$NO_2 + OH + M \rightarrow HNO_3 + M \quad (1.3)$$

where M is a molecule to remove the excess energy. The lifetime of the chain conversion process is 12-20 hours from NO and NO_2 to HNO_3 (Chameides, 1977). It is much longer than the typical thunderstorm lifetime of one hour. Only a portion of the NO_x produced by lightning can be converted into HNO_3 during thunderstorms.

Some other field observations also directly measured the NO_x production related to thunderstorms. Using an absorption spectrometer to measure the overburden of NO_2 via the scattered sunlight during thunderstorms, Noxon (1976) found a higher content of NO_2 below a thunderstorm than in the surrounding air. He obtained the NO_x production as 1×10^{26} to 4×10^{26} NO_2/flash (Noxon, 1976, 1978), and estimated the global annual NO_x production of 2 to 30 TgN/year if the entire NO produced by lightning was converted to NO_2.

Although field measurements of NO_x avoid many uncertainties associated with lightning parameters and correlation functions that result from scaling up a laboratory spark to natural lightning flashes, there exist many uncertainties in estimating the NO_x amount because of the atmospheric complexity. In addition, NO_x production by a lightning stroke depends on the properties of the discharging channel such as temperature, density, conductivity, current, and spark radius. These parameters vary from one lightning flash to another one even may vary along a lightning channel. Thus, it is impossible to extrapolate the global NO_x accurately with a limited number of field measurements.

The better approach to estimate the global NO_x production by lightning lies on the studies of NO_x production by laboratory sparks. Since the 1970's, many experiments have been undertaken to measure the NO_x production by laboratory sparks which imitated lightning (Chameides et al., 1977; Levine et al, 1981; Peyrous and Lapeyre, 1982; Borucki et al., 1984; Lawrence et al., 1995; Stark et al., 1996). These experiments have investigated the simulated lightning sparks with a very broad range of energy and spark length. The discharge energy has varied from 3.6 x 10^{-2} (Chameides et al., 1977) to 12 x 10^{3} joules (Stark et al., 1996), and the spark length has changed from less than one centimeter to over one meter. These studies reported the NO production rate, the number of NO molecules per unit of discharge energy, as 2 to 17 x 10^{16} NO/J (Table 1.2). They estimated the global NO production as 1.8 to 47 TgN N/year based on a channel length of 5-10 km and energy inputs from 10^{4} to 10^{5} J/m (Liaw et al., 1990).

On the basis of simulated sparks, these approaches have estimated the NO production by lightning using two major assumptions. First, laboratory discharges and natural lightning were assumed to have the same characteristics such as the mechanism of energy transport, dynamics of the spark expansion, and the thermal proprieties of discharging electrodes (which are clouds and ground for lightning discharges). Secondly, NO production by sparks was assumed to increase linearly with discharge energy, and the global NO production was estimated by multiplying the NO production per unit of energy with the estimated global flash energy.

1.2. The Shock-Wave and Hot-Channel Mechanisms

Two mechanisms have been developed in modeling the dynamic expansion of the lightning spark channel: the shock-wave model and the hot-channel model based on ohmic heating. The shock-wave mechanism assumes that the release of energy in a line (spark plasma) creates a pressure discontinuity that drives a shock. As the shock propagates outward, the shock front compresses and heats air in the region just behind the shock front (Lin, 1954). The hot-channel mechanism considers the spark energy dissipation by ohmic heating of the ionized air in the conductive hot channel. The hot channel expands slowly and mixes with surrounding cold air during discharge. Both of the models result in the heating of air and NO formation in the hot gas mixture via the Zel'dovich mechanism (Zel'dovich and Raizer, 1966).

The formed NO is "frozen" out as the hot gas mixture cools to

$$\tau_{equil} = \tau_{cooling} \qquad (1.4)$$

where τ_{equil} is the relaxation time constant to thermochemical equilibrium of NO formation and dissociation, τ_{equil} is the cooling time constant of the hot column. The NO "freezing" mixing ratio strongly depends on the "freezing" temperature. It could vary from 0.8 to 1.6% as the "freezing" temperature decreases from 2300 K to 2000 K.

Chameides et al. (1976) estimated the upper limit and the lower limit of the NO production by lightning with the shock wave model. They assumed that the lightning stroke releases its energy instantaneously along an ideal plasma line, then

the gas mixture expands and cools as a strong shock wave. The energy to heat the surrounding air equals the energy lost in the shock, which is (Lin, 1954)

$$\frac{E^{'}}{E_0} = \frac{169.8}{T}[0.02\,\mathrm{T}^{1/\gamma} - 0.5] \qquad (1.5)$$

where E_0 is the initial energy released into the shock, E' is the energy to heat surrounding air, T is the shock front temperature and γ is the ratio of specific heats. The amount of NO produced is determined by the NO "freezing" mixing ratio and the volume of gas involved in the NO production. The upper limit is given as 7.4×10^{16} NO/J assuming that the hot gas mixture cools quickly and all air heated above 2300 K are involved in NO production. The lower limit is given as 2.9×10^{16} NO/J if only those molecules within the shock wave front are heated sufficiently to produce NO, and the hot gas mixture cools slowly.

The shock-wave model greatly simplifies the energy dissipation process in lightning because the lightning energy is released in a relatively long duration (10-100μS). Based on numerical simulation of lightning, Hill et al. (1979; 1980) pointed out that the shock-wave model is not energetic enough to fix nitrogen by the amount observed in laboratory sparks or field measurements. Furthermore, Stark et al. (1996) found that the temperature immediately behind the shock front can reach a maximum of 2480 K, but the temperature is not maintained long enough for significant NO production.

Goldenbaum and Dickerson (1993) calculated the NO production as a function of energy using a two step model. The first step modeled the expansion of gases by one-dimensional fluid dynamics with the mass density of atmosphere, considering the discharge as axially symmetric and uniform along the discharge

axis. The discharge channel is heated instantaneously forming a finite radius plasma core. The second step calculated the chemical reaction rates and concentrations of all species during expansion of the discharge channel at each time step. The NO mixing ratio in this hot region reaches its maximum in ~1 μs and then drops slowly. As the channel expands, a shock wave moves away from the high pressure core. Core expansion causes a slow reduction in temperature and a rapid drop in gas density, which increases the lifetime of NO. Therefore, the NO formed is "frozen out" at a high concentration before appreciable expansion has taken place. The calculation showed that the NO production depends non-linearly on the energy density in the initial column. At ambient pressure, the NO production per unit of the initial energy reaches the maximum of 2.6×10^{17} NO/J for a channel with initial energy density of about 3.5 MJ/m^3.

The hot channel model predicts the NO amount to be an order of magnitude higher than the shock-wave model does. It attributes the "freezing" of NO formed to either the drop of temperature or the drop of pressure in the discharge channel. However, Stark et al. (1996) maintained that NO_x is “frozen out” due to the reduction in temperature in the core region. In their experiment, they measured the NO "freezing" mixing ratio by adding varying concentrations of NO to an N_2:O_2 mixture and monitoring the NO production after discharges under a pressure of 27 mbar. The results indicated that the rapid drop in gas density in a lightning discharge core is accompanied by much higher temperature (over 20,000 ^oK) (Plooster, 1971) than the temperature calculated by Goldenbaum and Dickerson.

The NO lifetime should be decreasing as the density drops due to the rise of temperature, precluding any "freezing" of NO at stage of the discharge process.

1.3. Objectives

The potential problem of extrapolating NO_x production from a laboratory spark to a natural lightning stroke is the scale difference between a natural lightning stroke and a laboratory spark. The laboratory electrical discharges are shorter than natural lightning discharges, so one must compare the parameters per unit length. A natural lightning spark is ~10^4 meter long and it deposits energy of 10^4-10^5 J/m (Dawson, 1980). The laboratory sparks have only been to one meter long depositing energy of 10^1 to 10^5 J/m (Chameides et al. 1977; Levine, 1981; Peyrous and Lapeyre, 1982; Stark et al., 1996). The objectives of this dissertation are to create laboratory sparks simulating natural lightning strokes, to study the NO production by the simulated lightning spark, and to scale the global NO_x production by lightning from laboratory sparks. It includes the following topics:

1. Simulate lightning flashes with induced arcs under ambient pressure. These arcs match natural lightning in several aspects, not only the electric field strength but also the energy density, and current waveform and magnitude.

2. Diagnose the simulated lightning sparks. These diagnostics include the expansion of the discharging channel and the process of energy dissipation. In previously reported experiments, researchers always related the NO production with the stored energy, neglecting the effects of discharge current profile. In this work, the current profile and the voltage across the spark are directly measured. The

energy dissipated by a spark, rather than the energy stored in the capacitor, is accounted to evaluate the correlation between the NO production and its energy dissipation.

3. Measure the NO_x production with the chemiluminescent technique. Previously, it has always been assumed that the NO production by a lightning spark linearly increases with its energy dissipation ignoring the dynamic difference between sparks on their energy transport processes and spark expansion. In this work, we study the dependence of NO_x production on lightning parameters, which include spark peak current, energy density, air density along a spark channel and the presence of water.

4. Estimate the global NO_x production by lightning. The Flash-Extrapolation Approach (FEA) has always calculated g(NO), the NO_x yield by a global average lightning flash, from the amount of lightning energy and a parameter p(NO) that refers to the NO production per unit of energy. Because energy is not a primary lightning parameter and p(NO) strongly depends on the dynamic process of discharging, there is very large uncertainty in estimates of g(NO). In this work, g(NO) is extrapolated on the basis of spark peak current, considering the dependence of NO production on air density and the effect of water. The estimates of g(NO) and G(NO), the global NO_x production are therefore greatly improved.

Chapter II Characteristics of Lightning

Lightning occurs when a sufficiently large electric charge is accumulated in some region of the atmosphere that the electric fields associated with the charge cause electrical breakdown of the air. Most lightning occurs in thunderclouds, but they also occur in snowstorms, sandstorms, clouds over erupting volcanoes and even the clear air (Gifford, 1950; Baskin, 1952). In thunderclouds, lightning can take place between a cloud and the earth (cloud-ground discharges), entirely within a cloud (intra-cloud discharges), between two clouds (cloud-cloud discharge), or occasionally between a cloud and the surrounding air (cloud-air discharges). The cloud-ground discharges (CG) occur in the region where the air pressure is much higher than the regions in which the intra-cloud discharges (IC) or the cloud-cloud-discharges (CC) occur. The CG discharges are always more energetic than the intra-cloud discharges (IC) or the cloud-cloud-discharges (CC) (Krehbiel, 1986; Lawrence et al., 1995; Price et al., 1997). The NO_x production by a lightning strongly depends on the amount of energy dissipated and the air pressure (Goldenbaum and Dickerson, 1993) where the lightning occurs. Therefore, although IC and CC occur most frequently, we only focus our discussion on the CG discharges because they may be more efficient in producing NO_x and their energetics and frequency are better understood.

2.1. Lightning Discharge Mechanism

A CG discharge, termed a flash, may be composed of several component discharges or return strokes that are usually separated by about 40 milliseconds

(Berger and Vogelsanger, 1966; Williams and Brook, 1963). Each return stroke has a luminous phase lasting some tenths of a millisecond. It is initialized by a weakly luminous discharge leader that propagates from a cloud to ground. A return stroke travels from ground to cloud immediately after its leader reaches ground, following the channel ionized by its leader (Figure 2.1).

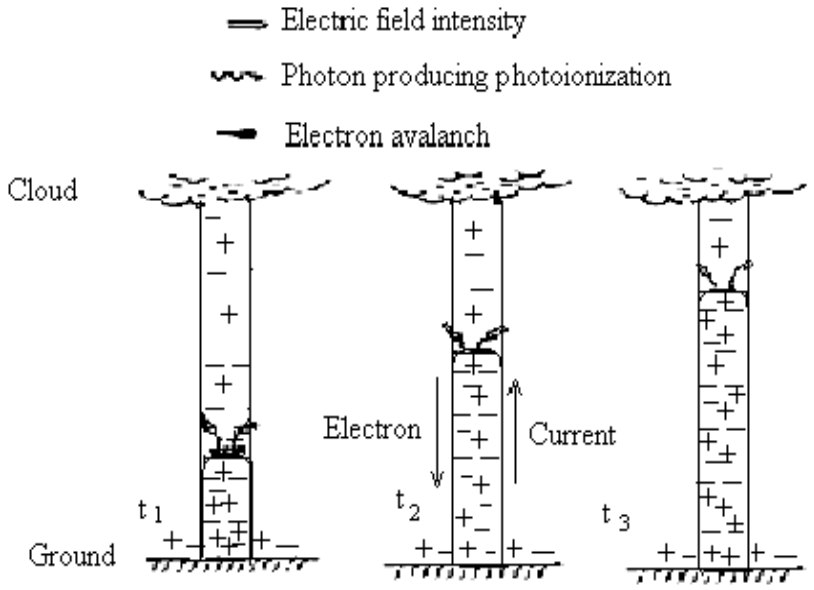

Figure 2.1 General features of the return stroke of a negative cloud ground flash. $t_1<t_2<t_3$.

There are two different kinds of return stroke leaders: the stepped leader preceding the first return stroke in a flash, and the dart leader preceding the second or any subsequent return stroke. A stepped leader (Figure 2.2.a) begins with a local breakdown between the positive and negative region in a thundercloud. This breakdown makes mobile the electric charges which were previously attached to ice and water particles and results in a strong concentration of negative charge within the cloud. These strongly concentrated negative charges produce a local strong

electric field which causes a negatively charged column to propagate toward the earth. The column is called a stepped leader because it moves downward in steps of typically 50 meters length and a pause time of about 50 μs between steps. A dart leader (Figure 2.2.b) traverses the pre-ionized channel surviving from the previous return stroke while electric charges are moving from more distant cloud regions to the spark channel. The dart leader is a luminous column about 50 meter long but it travels continuously to earth. A dart leader increases the degree of spark channel ionization and deposits charges along the channel. A stepped leader travels at a typical velocity about 1.5×10^5 m/s, while a dart leader travels at a typical velocity about 2.5×10^6m/s.

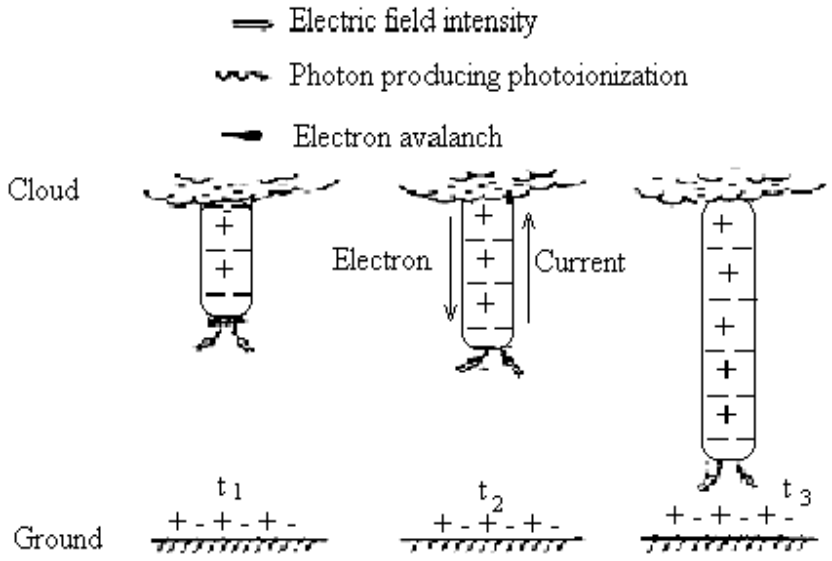

Figure 2.2.a. General features of a stepped leader in virgin air. $t_1<t_2<t_3$

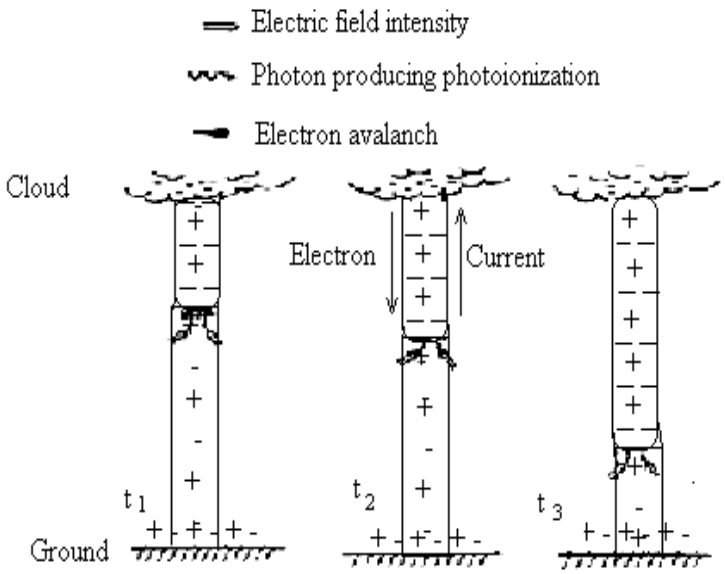

Figure 2.2.b. General Features of a Dart Leader. $t_1<t_2<t_3$.

When a downward leader from a cloud is close to the ground, it is met by a very fast upward moving connection leader. A return stroke (Figure 2.1) begins when the downward leader comes into contact with the upward connecting leader. The return stroke discharges the charges accumulated in the leader and part of the cloud charges to earth. After one return stroke has stopped, the flash may be ended or followed by a dart leader which grows up in the previous return stroke discharge channel. The dart leader will initiate a subsequent return stroke if the cloud can accumulate enough charges in about 40 milliseconds after the previous return stroke. Each succeeding return stroke always drains charge from more distant regions of the cloud if additional charges are available. The return strokes started with different leaders could have great different characteristics such as the velocity of spark propagation, current rise time and the amount of transferred charge. For example, the first return stroke is always branched, but no branch has been observed

for a subsequent return stroke because the dart leader finds a hot channel reaching all the way to earth.

2.2 Electromagnetic Field of Lightning

Over the region associated with a lightning discharge, the electric field distribution is determined by the charges, and the magnetic field distribution is associated with the current, which is constituted by the moving of charges within a cloud or between a cloud and ground. The electric and magnetic fields associated with lightning are the primary parameters in lightning study because the are easily measured in field observation. They are useful to investigate the distribution and transportation of cloud charge, and to estimate the magnitude of stroke current. Recently, the electric field signature has been used to study the characteristics of different return strokes (Rakov and Uman, 1994) in the same flash.

When a lightning stroke changes the charge and current distribution in a relatively short time interval, it radiates electromagnetic waves in a wide frequency range. The radio frequency observation could be used to locate the origin and the process of development of the lightning, and to estimate the propagating speeds horizontally and vertically (Rhodes et al. 1994).

A. Electric charges of lightning

On the basis of many observations, including aircraft measurements over thunderstorms, some important qualifications have been derived for the distributions

of lightning electric charge (Brook and Ogawa, 1977; Krehbiel et al, 1979; Price et al., 1997a; Rhouma and Auriol, 1997):

(a). Most of CG flashes occur between negative cloud charges and earth. The magnitude of charge released by a discrete return stroke ranges from 20 C to 1 C or less. In the same flash, the first return stroke always transfers more charge than the subsequent ones.

(b). Sources of charges for successive return strokes of one flash develop over a large horizontal distance (up to 8 km).

(c). Most thunderclouds appear to have positive charge in their upper region and a somewhat larger quantity of negative charge lower in the cloud. Both the positive and negative charge centers are located 5 to 12 km above ground.

(d). The net field change due to individual strokes corresponds well to the removal of a small spherical symmetric region of charges from the cloud.

B. Stroke potential

A stroke potential is the potential between cloud and ground to lead a CG discharge or the potential between the positive charge center and negative charge center to lead a CC discharge or an IC discharge. It could be estimated from the electric field distribution

$$V=\int E \, dl \qquad (2.1)$$

where V is the stroke potential, E is electric field, the integration goes over the path of a lightning. The stroke potential of a CG discharge is the cloud potential. Because a lightning flash can only move a small portion of the electric charges stored in the

cloud to ground, the cloud potential does not vary significantly over the lifetime of a single lightning flash. From storm to storm, the cloud potential may vary but it is fairly constant during a particular storm. As clouds become increasingly electrified during a storm's development, breakdown simply occurs more often, resulting in greater lightning frequency but not the cloud potential.

The breakdown electric field is 3×10^6 V/m under ground air pressure, but the electric field to cause a lightning flash could be much lower. A lightning flash is initialized by a stepped leader which begins with a local high electric field in a thundercloud. A stepped leader only needs a local electric field that is much lower than 3×10^6 V/m because the air pressure is much lower than the ground air pressure at its beginning height. When a stepped leader travels toward ground, it moves electric charge from the cloud to the leader head and enhances the local electric field. Field observations found that the maximum electric fields in thunderstorms could be as high as 4.5×10^5 V/m (Winn et al., 1974). In general, the electric breakdown field could be taken as approximately 5×10^5 V/m for its mean value. The negative charge center is located in the cloud between 5 and 7 km above the ground (Krehiel, 1986). Therefore, the cloud potential could be $2.5\text{-}3.5 \times 10^8$ V, and $0.5\text{-}3 \times 10^8$ V is expected for IC and CC discharges since the length of an IC or CC discharge is between 1 and 6 km (Ogawa and Brook, 1964; Krehiel, 1986).

2.3. Stroke Currents

The lightning current consists of the displacement current and the conductive current. The displacement current flows into the earth as a lightning

Table 2.1 Lightning Parameters--Downward Flashes (Berger et al., 1975)

	Parameter		Percentage exceeding tabulated value		
Number	Peak current exceeding 2 kA	Unit	95%	50%	5%
101	Negative 1st return strokes	kA	14	30	80
135	Negative subsequent strokes	kA	4.6	12	30
25	Positive flashes	kA	4.6	35	250
	Charges				
93	Negative first return strokes	C	1.1	5.2	24
122	Negative subsequent stokes	C	0.2	1.4	11
94	Negative flashes	C	1.3	1.4	40
26	Positive flashes	C	20	80	350
	Time to peak current				
89	Negative first return strokes	μs	1.8	5.5	18
118	Negative subsequent stokes	μs	0.22	0.95	4.5
19	Positive flashes	μs	3.5	22	200
	Decay time to half-value				
90	Negative first return strokes	μs	30	75	200
122	Negative subsequent stokes	μs	6.5	32	120
21	Positive flashes	μs	25	230	2,000

leader moves toward the earth. The conductive current is designated as the return stroke current. It begins when a return streamer from ground touches the corona sheath preceding and surrounding the leader channel. The return stroke current increases very rapidly and continues to flow until the local cloud charges have been neutralized or to be followed by a subsequent return stroke. In this section, we only discuss the return stroke currents because they dominate the charge neutralization and energy dissipation of lightning flashes.

A. Statistics of stroke current peak

The amplitude of a return stroke is affected by the nature of its initiating leader and by the polarity of the flash (Garbagnati et al., 1973; Berge et al., 1975; Krehbiel et al., 1979; Price et al. 1997a). A stepped leader initializes the first return stroke of a multi-stroke flash in which the first return stroke usually discharges with the highest current. A positive cloud charge may lead to a positive flash to earth. The positive flashes occur much less frequently than the negative flashes from negative clouds to earth, but they are much more intense than negative flashes.

Table 2.1 lists the data obtained from 101 negative flashes and 26 positive flashes from Mount San Salvatore (Berge et al., 1975). The median of peak current is 30 kA for the first negative return strokes, but it is 12 kA the subsequent strokes. All the positive flashes have only one return stroke and the median of peak current is 35 kA for the less frequent flashes. Only 5% of all negative first return strokes have peak current over 80 kA, while 5% of the positive return strokes have peak current over 250 kA.

Figure 2.3 shows the frequency distributions of the peak currents in the 930,323 cloud-ground flashes obtained by the U.S. National Lightning Detection Network (Price, 1997) for the period June-August 1988. Only the first return strokes were recorded for either the negative or the positive flashes. About 98.7% (918, 579) of these flashes are negative. The negative flashes have a mean peak current of 35.7 kA and a median value of 30.3 kA. The positive flashes have a mean peak current of 61.4 kA and a median value of 55.4 kA.

B. Analytical expression of stroke current

A typical return current can be simply expressed as a double exponential of the form (Stekolnikov, 1941; Bruce and Golde, 1941)

$$I = I_0[e^{-\alpha t} - e^{-\beta t}] \qquad (2.2)$$

The values of I_0, α and β determine the peak current, the decay and rise time from and to the peak. I_0 is primarily determined by the amount of charges neutralized by the stroke, while the values of α and β depends on the properties of the spark channel such as the charge density along the leader channel, the velocity of the return stroke and the rate of recombination of the charges on the leader during the return stroke process. There are notable differences in the values of I_0, α and β between negative and positive flashes, or between the first and the subsequent return strokes in a multi-stroke flash (Table 2.1). The first negative return strokes may be modeled by taking I_0 = 35.7 kA, $\alpha = 1.3 \times 10^4$ s^{-1}, and $\beta = 1.8 \times 10^5$ s^{-1}. The subsequent strokes may be modeled by taking I_0 = 15.4 kA, $\alpha = 3.1 \times 10^4$ s^{-1}, and $\beta = 1.1 \times 10^6$ s^{-1} (Pierce, 1977; Uman, 1987; Price et al., 1997).

The above stroke current expression (Eq. 2.2) was derived with the assumption that the current amplitude is constant at any instant along the return stroke channel. The assumption is wrong in a real lightning spark, at least during the early phase of a return stroke. A better expression was developed regarding the spark channel as a quasi-transmission line charged by the leader and then discharged by the ascending return stroke (Dennis and Pierce, 1964; Barlow et al, 1954; Little, 1978).

$$I = I_0[e^{-\alpha t} - e^{-\beta t}] + I_1[e^{-\delta t} - e^{-\varepsilon t}] \qquad (2.3)$$

where I_0 represents the current discharging cloud charges, and I_1 represents the low current discharging the electric charges along the spark channel deposited by the leader. The low current discharge could be modeled by taking $\delta = 1 \times 10^3\ s^{-1}$, $\varepsilon = 1 \times 10^4\ s^{-1}$, and $I_1 = 2$ kA to model the low current discharge.

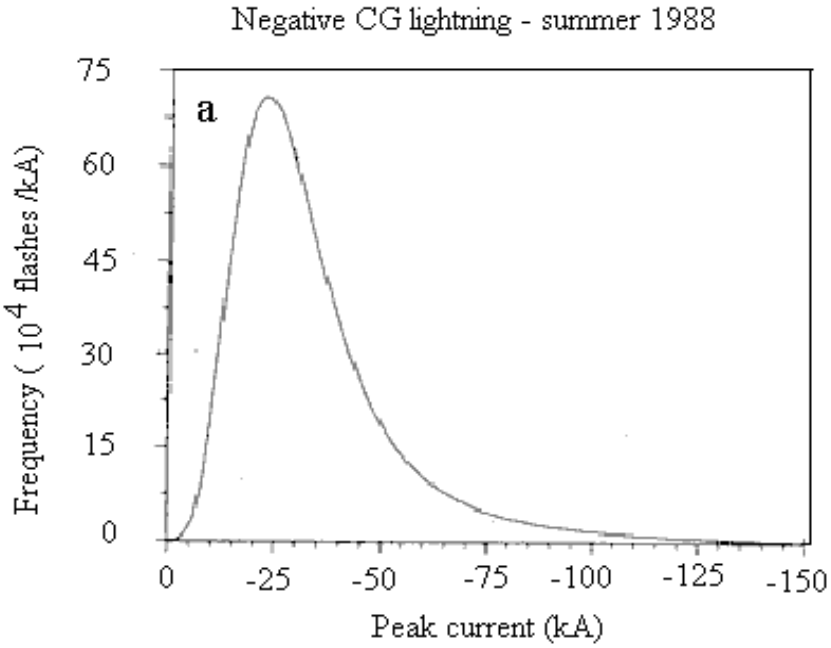

Figure 2.3.a Frequency distribution of negative cloud-ground lightning flashes observed by the U.S. National Lightning Detection Network in the United States during the summer 1988. (Price et al., 1997)

Total negative flashes = 918,579

Mean peak current = 35.7 kA

Median peak current = 30.3 kA

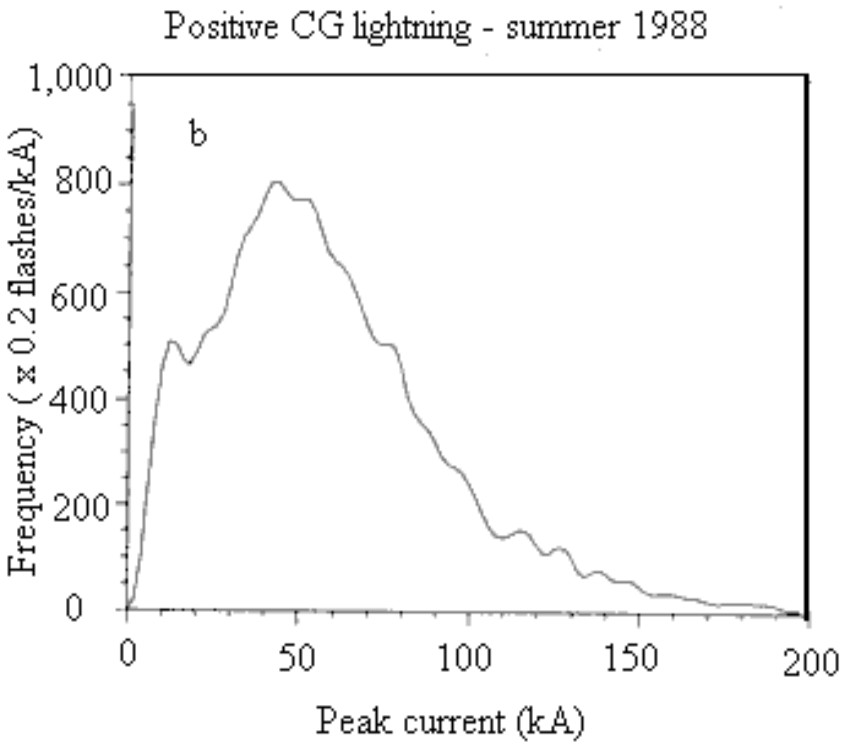

Figure 2.3.b. Frequency distribution of positive cloud-ground lightning flashes observed by the U.S. National Lightning Detection Network in the United States during the summer 1988. (Price et al., 1997)

Total positive flashes = 11,744

Mean peak current = 61.4 kA

Median peak current = 55.4 kA

2.4. Energy Dissipation of Lightning

The amount of energy dissipated by a lightning flash or return stroke cannot be directly measured like other primary parameters. It can only be indirectly estimated from field observations of the primary parameters on the basis of theoretical models of the cloud charge distribution and the return stroke evolution (Cooray, 1997). These primary parameters could be the electric field, the magnetic field, the electromagnetic radiation or the return stroke current. Table 2.2 lists the results of the electrostatic and optical radiant estimates.

A. Electrostatic estimates

The electrostatic method calculates the energy dissipated by a stroke assuming the thunderstorm is like a capacitor, as

$$E = \frac{1}{2} QV^2 \qquad (2.4)$$

where V is the cloud potential and Q is the electric charge removed by a flash from cloud to ground. The cloud potential V has been estimated early in Section 2.2.A that is about 3.0 x 10^8 V for a cloud of 6.0 km high. The electric charge Q can be calculated with the observed electric field distribution or the return stroke current, as

$$Q=\int I(t)\, dt \qquad (2.5)$$

here I(t) is the measured current of a flash, the integration is over the time interval of a flash (return stroke). The typical value of Q is 10 C for the first return stroke and 5 C for subsequent strokes (Price, 1997). Thus, the energy dissipated is 1.5 GJ (10^9J) and 0.75 GJ for the first return strokes and subsequent strokes respectively.

Table 2.2 Estimates of Energy Dissipated by Lightning Flashes

	Investigators	Flash Energy (10^8 J/flash)
Optical	Connor [1967]	2.8
	Krider et al. [1968]	5.2
	Barasch [1970]	3.0
	Mackerras [1973]	5.2
	Turman [1978]	4.9 (IC discharges)
		7.5 (CG discharges)
	Guo and Krider [1982]	1.2
	Average (±s.d)	4±2
Electrical	Wilson [1920]	1
	Malan [1963]	6
	Connor [1967]	2.5
	Uman [1969]	10
	Mackerras [1973]	3.7
	Berger [1977]	2
	Hill [1979]	0.5
	Average (± 1 s.d)	4±3

B. Optical radiant estimates

This method determines the energy dissipated by a stroke from the optical radiant energy measured in a spectral region. The electric energy is related with the optical radiant energy assuming that the lightning strokes have the same radiant efficiency as the long laboratory sparks. The optical radiant efficiency could be estimated from the observed radiation of a long laboratory spark whose electric power was known accurately (Guo and Krider, 1982).

If the lightning spark is approximated by a point source, the total optical power $P_{optical}$ is

$$P_{optical} = 4\pi R^2 L_{rad} \qquad (2.6)$$

where L_{rad} is the measured optical radiation power at a distance R from the spark. The total optical radiation energy produced by a return stroke is

$$E_{optical} = \int P_{optical}\, dt \qquad (2.7)$$

where the integration goes over time interval of that stroke. Usually the total energy is estimated using just the peak of $P_{optical}$ (Guo and Krider, 1982) and the "Characteristic width" of the optical radiation from a return stroke. The total optical energy is

$$E_{optical} = P_{optical}(peak) * t_c \qquad (2.8)$$

where the $P_{optical}(peak)$ is the peak value of the obtained radiant signal for a return stroke and t_c is the “Characteristic width” of the return. The popularly used radiation efficiency is 0.8% which was based on laboratory studies of a 4 m spark in air using the Lite-Mite sensor (Krider et al., 1968).

The electrical energy of a return stroke is

$$E = \frac{E_{optical}}{\eta_{rad}} \tag{2.9}$$

here η_{rad} is the optical radiant efficiency for lightning sparks and long laboratory sparks. As shown in Table 2.2, the results agree with that from electrostatic estimates very well that a CG flash dissipates about 4 GJ energy on average.

These optical estimates of the energy dissipated by a return stroke neglect any atmospheric extinction from lightning sources to detectors, any multiple scattering or absorption by cloud drops and any reflection from other clouds or ground. They always underestimated the flash energy because of their neglect of such effects for lightning radiation. For instance, it was reported that the mean peak of optical radiant power of all strokes was 1.3×10^9 W (Guo and Krider, 1982) for the lightning in Florida, but that for the lightning in Arizona was 5.7×10^9 W (Krider et al., 1966). Since similar techniques were used in both the observations, one reason for the larger signal difference may have been due to generally greater visibility under thunderstorm conditions in Arizona.

2.5 Summary

A CG flash may occur between ground and a positive cloud or a negative cloud. The positive flashes always have only one stroke, and they occur much less frequent than the negative flashes. A negative flash may be composed of many strokes which include the first stroke initialized by a stepped leader in virgin air and several subsequent strokes. A subsequent stroke is preceded by a dart leader

following through the path of its previous discharge channel. Usually, a succeeding stroke drains charge from more distant region of the cloud.

The magnitude of stroke current and the amount of charge neutralized by a discrete stroke vary widely. The positive strokes are always more intense than the negative ones and the first strokes are always more intense than the subsequent strokes. Based on field observations and theoretical simulations, the parameters of CG negative flashes are summarized as following:

Average height of cloud center = 6 km

Breakdown electric field = 5×10^5 V/m

Average cloud potential of negative flashes = 3×10^6 kV

Charge released = 10 C for the first return stroke

= 5 C for a subsequent stroke

Energy dissipation = 1.5 GJ for the first return stroke

= 0.75 GJ for a subsequent stroke

Peak current = 30.5 kA for the first return stroke

= 13.2 kA for a subsequent stroke

Current rise time = 5 μs for the first return stroke

= 1 μs for a subsequent stroke

Current decay time = 75 μs for the first return stroke

= 30 μs for a subsequent stroke

Chapter III. Mechanism of NO_x Production by Lightning

When a return stroke goes up, it transports the energy stored in a cloud into the spark column by ohmic heating as the dissociation, ionization, excitation, and kinetic motion of the channel particles. The dissociation of N_2 and O_2, the primary components of atmospheric air, increases with the temperature. The free N and O drive the formation of NO and NO_2 as the gas mixture establishes its thermal chemical equilibrium at high temperature. The concentrations of NO and NO_2 in this hot gas mixture are extremely temperature dependent because of the high activation in dissociating O_2 and N_2. During the lightning discharge, the hot gas mixture also loses its energy by radiation, expansion of the column and turbulent mixing with surrounding cold air. As the hot column expands, both the column temperature and the pressure in the spark core drop rapidly. The formed NO_x can be "frozen" by a rapid drop of either temperature or pressure. After a lightning flash, net NO_x is "frozen" into the surrounding air.

3.1. Hydrodynamic Expansion of Spark Channel

If lightning discharges along an axially symmetric and uniform channel, the lightning column can be described with only one geometric variable, r, the cylindrical coordinate of a system with the origin at its center. The radial velocity of the only geometric variable will represent the dynamic expansion of the lightning column. The radial velocity is defined as

$$u = \partial r / \partial t \qquad (3.1)$$

The dynamic expansion of the spark channel is determined by the conservation of mass, momentum, and energy. The mass conservation equation is

$$\left(\frac{\partial}{\partial t}+u\frac{\partial}{\partial r}\right)\rho=-\rho\left(\frac{1}{r}\right)\frac{\partial(\mathrm{ur})}{\partial t} \tag{3.2}$$

The momentum conservation equation is

$$\rho\left(\frac{\partial}{\partial t}+\mathrm{u}\frac{\partial}{\partial r}\right)\mathrm{u}=-\frac{\partial(\mathrm{P}+\Pi)}{\partial t} \tag{3.3}$$

And the energy conservation equation is

$$\rho\left(\frac{\partial}{\partial \mathrm{t}}+\mathrm{u}\frac{\partial}{\partial \mathrm{r}}\right)\varepsilon=-(\mathrm{P}+\Pi)\frac{1}{\mathrm{r}}\frac{\partial(\mathrm{ru})}{\partial \mathrm{r}}+\sigma\mathrm{E}^{2}-\mathrm{P}_{\mathrm{rad}} \tag{3.4}$$

In these equations, ρ is the mass density, ε is the specific energy, σ is the conductivity, Π is the stress tensor, P is pressure, E is the electric field and P_{rad} is the power of radiation loss from the discharge channel.

A. Solution of the fluid dynamic equations

To solve the hydrodynamic equations (3.1 -3.4), we need information about the atmospheric composition and the properties of each species. Goldenbaum and Dickerson (1993) took account of the atmospheric gases with a mixture of 79% nitrogen and 21% oxygen and introduced an additional variable T, the temperature, and two additional state equations to describe the thermodynamics of the gas mixture. The state equations are the “thermal” equation

$$P = P(\rho, T) \tag{3.5}$$

and the “caloric” equation

$$\varepsilon = \varepsilon(\rho, T) \tag{3.6}$$

If the radiation loss was ignored, the specific energy and pressure of each species can be determined by Saha equations assuming the dissociation equilibrium occurs first, and then first and second ionization occur during the expanding of the hot channel. Transforming the differential equations into difference forms with grid of spark radius and temperature steps, the temperature and pressure could be calculated with Eq. 3.1-3.6 at each time step with given initial conditions.

Assuming lightning arc releases the cloud energy instantaneously into an initial spark core with finite radius, the behavior of the spark channel could be simulated with a starting core and internal energy density. For example, a typical lightning flash can drive the core temperature to a maximum of 5300 K. It was calculated that the column pressure falls to about 1/5 of ambient pressure within about 16 μs before dramatically expanding. As it expands outward, the spark column temperature drops off to about 3000 K in about 70 μs.

B. Ohmic heating of spark channel

In high-density plasma like a lightning discharge column, electron-electron and ion-ion collisions establish a local equilibrium within each component. The electric conductivity (σ) which is a collective parameter of a plasma, is primarily determined by the combination of elastic electron-ion collisions, elastic and ionizing electron-neutral collision, and collective electron-ion collisions (Braginskii, 1965).

The calculated electrical conductivity has been collected by Borovsky (Borovsky, 1995) as an approximate fitting function of the air temperature.

$$\sigma = 1.03 \times 10^{-54} T^{14.25} \ \Omega^{-1} \text{cm}^{-1}; \qquad 2{,}500 \text{ K} \leq T \leq 5{,}000 \text{ K} \qquad (3.7)$$

$$\sigma = 9.0 \times 10^{-37} T^{9.4} \ \Omega^{-1}cm^{-1} \ ; \quad 5{,}000 \text{ K} \le T \le 9{,}350 \text{ K} \qquad (3.8)$$

$$\sigma = 3.67 \times 10^{-12} T^{3.2} \ \Omega^{-1}cm^{-1}; \quad 9{,}350 \text{ K} \le T \le 15{,}000 \text{ K} \qquad (3.9)$$

$$\sigma = 8.44 \times 10^{-4} T^{1.2} \ \Omega^{-1}cm^{-1}; \quad T \ge 15{,}000 \text{ K} \qquad (3.10)$$

This is a continuous function of T. Above 10,000 K, the electrical conductivity is nearly independent of the air density and of the free-electron density (Alfven and Falthammar, 1963). In the temperature range 10,000 K - 20,000 K, it is in the range of 22 - 110 Ω^{-1} cm^{-1}, which can be compared with the conductivity of common metals, 5.6×10^3 - 5.6×10^6 Ω^{-1} cm^{-1}. If a lightning channel expands axially and local thermal equilibrium is always established, then the spark channel can be divided into cylindrical annuli with the conductivity in each annulus determined by the local temperature and density. The ohmic heating (σE^2) of a lightning discharge can be given by the electric conductivity and electric field distribution in a discharge column.

The formulae in Eq. 3.7-10 only work for relatively high temperature ($T \ge$ 2,500 K). They can not be used to calculate the conductivity of a lightning leader because a leader has a very low temperature (1,500 K) and degree of ionization. A lighting leader only dissipates a small portion of the flash energy. The NO yield is not too sensitive to the leader energy. Therefore, the ohmic heating of the lightning leader has never been included in the simulation of NO production by a lightning discharge. If it is of interest, the average conductivity of leader can be estimated with known parameters of lightning leaders, such as current, dimension, distribution of charges and the electric fields. For instance, the electric field of a leader channel can be taken as 2.5 kV/cm and the leader current is in the range of 0.5-5 A (Ortega

et al., 1991). Supposing that the lightning leader is a uniform cylindrical channel with a constant radius of 1.5 mm, the average conductivity was estimated (Fofana and Be'roual, 1994) as $0.003\ \Omega^{-1}cm^{-1} \le \sigma \le 0.03\ \Omega^{-1}\ cm^{-1}$.

C. Radiation loss of spark channel

The radiation and absorption of hot air involve almost all electronic transition mechanisms, including the bound-bound transitions, bound-free transitions and free-free transitions. The bound-bound transitions correspond to electronic transitions in atoms, molecules, and ions from one discrete level to another. These transitions result in the radiation and absorption of line spectra of atoms or band spectra of molecules, in which the electronic transitions are accompanied by changes in vibrational and rotational modes. The bound-free transition involves a bound state of particle and a free electron with arbitrary kinetic energy. The free electron can assume any positive energy, so the bound-free transitions have continuous radiation and absorption spectra. The free-free transitions also lead to continuous radiation and absorption spectra that are usually called bremsstrahlung radiation. These transitions occur when a free electron travels through the electric field of an ion or even passes close a neutral atom. The free electron can emit a photon without losing all its kinetic energy and remains free, or absorbs a photon and acquires additional kinetic energy.

Air is transparent to visible light at temperature below 2,000 K. It only emits infrared radiation attributed to the Schumann-Runge bands of oxygen molecules. At moderate temperatures of the order 2,000 ~ 4000 K, its radiation is mainly attributed

to the presence of small amounts of nitrogen dioxide (NO_2). NO_2 molecules radiate and absorb strongly in both visible and ultraviolet regions. In the range of 15,000 ~ 20,000 K, all molecules are almost completely dissociated into atoms. These atoms are in turn ionized appreciably, so the radiation is composed of the continuous spectrum caused by the photoelectric capture of electrons by ions and the bremsstrahlung radiation of electrons in the field of the ions.

In the spark channel of lightning, both the air temperature and density vary widely. The air temperature may go up to 30,000 K in the discharge core. Air density ranges from ~$4\rho_0$ (behind the shock wave propagating in air at standard temperature and density $\rho_0 = 2.67 \times 10^{19}\ cm^{-3}$) to very low densities ~10^{-3}-10^{-4} ρ_0 in the central region of lightning at high altitudes. The most interesting temperature range is below ~15,000 K for the study of NO production by a lightning. It is a range in which all of the above mechanisms participate in the radiation. The relative roles of each mechanism strongly depend on the temperature and density, or even on the light frequency. The radiation losses, P_{rad} in Eq. 3.4, are associated with the following continuous and quasi-continuous radiation: <a> The molecular radiation of N_2, O_2, N_2^+ (ion), NO, NO_2. <b> The photoelectric captures by species of O_2, N_2, NO, O, N, and O^-. <c> The free-free transitions in the fields of O^+, N^+, NO^+, O_2^+, and N_2^+ ions, and also, possible, in the fields of neutral atoms and molecules. Actual calculations of the radiation loss require knowledge of the concentrations of free electrons and all the above components (Zel'dovich and Raizer, 1966).

3.2 Production of NO in Lightning Spark Channel

The mechanism of nitrogen oxidation at high temperature has been studied extensively (Zel'dovich, Sadovnikov and Frank-Kamenetskii, 1947; Raizer, 1959; Hill, 1979; Seinfeld, 1986). Theoretical studies have simulated NO_x formation in various hot air mixtures based on the Zel'dovich mechanism (Zel'dovich and Raizer, 1966). Experimental observations have studied the NO_x during the combustion processes in a wide temperature range. The NO_x formation rate is strongly temperature dependent because the thermal NO_x forming reactions involve the dissociation of the stable O_2 and N_2 molecules. The NO_x formation favors to high temperature and high O_2 concentration. NO is formed from N_2 and O_2 molecules in the hot air mixture in the heating phase and it "freezes" into the surrounding cold air as the hot channel expands outward. The final NO yield by a lightning flash is determined by the cooling rate, the air density behind the shock front, the radius of the discharge channel and the ambient pressure air (Hill, 1979; Goldenbaum and Dickerson, 1993).

A. Chain mechanism of nitrogen oxidation in hot air

In a hot air mixture, nitrogen is oxidized into NO by oxygen via the chain reactions.

$$O + N_2 \xleftrightarrow{k_1,k_2} NO + N - 75.5\,\text{kcal/mole} \qquad (3.11)$$

$$N + O_2 \xleftrightarrow{k_3,k_4} NO + O + 32.5\,\text{kcal/mole} \qquad (3.12)$$

Where $k_1 = 1.16 \times 10^{-10}\, e^{-75{,}500/RT}$ cm^3 $molecule^{-1}s^{-1}$ and $k_3 = 2.21 \times 10^{-14} T e^{-7{,}080/RT}$ cm^3 $molecule^{-1}s^{-1}$ are forward reaction rate constants, $k_2 = 2.57 \times 10^{-11}$ cm^3

molecule^{-1} sec^{-1} and $k_4 = 5.3 \times 10^{-15}\, Te^{-39,100/RT}$ cm^3 molecule^{-1} s^{-1} are backward reaction rate constants (Ammann and Timmins, 1966; Eremin, 1981), R=2 cal/mole•deg is the gas constant. The endothermic reaction 3.11 requires high activation energy not less than 75.5 kcal/mole, but the exothermic reaction 3.12 has low activation energy of 7.08 kcal /mole. Therefore, the reaction 3.12 proceeds very rapidly in the forward reaction and the overall rate of the chain reactions are controlled by reaction 3.11.

Free O atoms play an active role in the chain reactions (Gaydon and Hurle, 1963). Since the reaction 3.11 controls the overall chain reaction, the free N atoms liberated in reaction 3.11 will immediately react with the molecular oxygen restoring free O atoms. The equilibrium concentration of free O remains constant during the chain reactions so that it does not affect the chain reactions of nitrogen oxidation. It is only determined by the O_2 concentration and temperature because of the high O_2 concentration, corresponding to the dissociation of O_2

$$O_2 + M \xleftrightarrow{k_5, k_6} 2O + M \qquad (3.13)$$

where M denotes a third body, O_2 or N_2. $k_5 = 1.876 \times 10^{-6}\, T^{-1/2}\, e^{-118,000/RT}$ cm^3 molecule^{-1} s^{-1}, $k_6 = 2.6 \times 10^{-33}$ cm^6 molecule^{-2} s^{-1} denote the forward and backward reaction constants. The reaction 3.13 has high activation energy of 118 kcal, so the reaction strongly depends on temperature and it will not become important until a high temperature is reached. At high temperature, the high concentration of O_2 establishes its equilibrium faster than the nitrogen oxidation (Zel'dovich, Sadovnikov and Frank-Kamenetskii, 1947).

B. Kinetics of NO formation

From the kinetics of the process, rates of change of NO, N and O concentration can be expressed as

$$\frac{d[NO]}{dt} = k_1[O][N_2] + k_3[N][O_2] - k_2[NO][N] - k_4[NO][O] \tag{3.14}$$

$$\frac{d[O]}{dt} = -\frac{d[N]}{dt} = -k_1[O][N_2] + k_3[N][O_2] + k_2[NO][N] - k_4[NO][O] \tag{3.15}$$

where the concentrations are expressed in molecules/cm^3. Since [O] is constant during the chain reactions, the right side of Eq. 3.15 equals to zero. Thus, [N] can be expressed in term of [O], [O_2], [N_2] and [NO]. It yields

$$\frac{d[NO]}{dt} = k_f[N_2][O_2] - k_b[NO]^2 \tag{3.16}$$

where k_f and k_b are the overall rate constants for the forward and backward reactions, which are

$$k_f = \frac{2k_1k_3[O]}{k_3[O_2] + k_2[NO]} \tag{3.17}$$

$$k_b = \frac{2k_2k_4[O]}{k_3[O_2] + k_2[NO]} \tag{3.18}$$

These expressions are valid below 4500K because dissociation of N_2 into N becomes important above 4500K that the variation of [N] can not be expressed with Eq. 3.15.

The reaction 3.13 determines [O] from [O_2] as

$$[O] = \left(\frac{k_5}{k_6}[O_2]\right)^{1/2} = 2.686\times10^{13}\,T^{-1/4}e^{-59{,}000/RT}[O_2]^{1/2} \tag{3.19}$$

Using the fact that [NO] is much less than [O_2] and Eq. 3.14, yields

$$k_f = \frac{2k_1[O]}{[O_2]} = \frac{6.23\times10^4 T^{-1/4} e^{-134{,}500/RT}}{[O_2]^{1/2}} \quad \text{cm}^{3/2}\,\text{molecules}^{-1/2}\,\text{s}^{-1} \qquad (3.20)$$

$$k_b = \frac{2k_2k_4[O]}{k_3[O_2]} = \frac{331T^{-1/4} e^{-91{,}020/RT}}{[O_2]^{1/2}} \quad \text{cm}^{3/2}\,\text{molecules}^{-1/2}\,\text{s}^{-1} \qquad (3.21)$$

The term $k_f[N_2][O_2]$ of Eq. 3.16 represents the rate of NO formation in the hot air mixture. It becomes $2k_1[N_2][O]$ when the expression for k_f (Eq. 3.20) is substituted. Since $k_1[N_2][O]$ is the rate the first oxidation reaction (3.11), two NO molecules are formed by each of the first event because the second oxidation reaction (3.12) follows the first one "instantaneously".

When the thermal chemical equilibrium is established in a hot air mixture, the rate equation of NO becomes

$$k_f[N_2]_0[O_2]_0 - k_b[NO]_0^2 = 0 \qquad (3.22a)$$

or

$$[NO]_0^2 = \frac{k_f}{k_b}[N_2]_0[O_2]_0 \qquad (3.22b)$$

where the subscript "0" denotes the equilibrium state of a species. The equilibrium NO concentration can be calculated using $[O_2]$ and temperature. Table 3.1 lists the calculated results of dissociated and even slightly ionized air mixture in standard density for several temperatures.

C. NO "Freezing"

As the thermal chemical reactions approach equilibrium, we have $[NO] \approx [NO]_0$. The rate equation of NO, Eq. 3.16, can be expressed as

$$\frac{d[NO]}{dt} = k_b([NO]_0^2 - [NO]^2) \approx 2k_b[NO]_0([NO]_0 - [NO]) \tag{3.23}$$

This is a relaxation process with [NO] varying as

$$[NO] = [NO]_0 e^{-t/\tau} \tag{3.24}$$

Where τ is the relaxation time characterizing the rate of approach to equilibrium, which is

$$\tau = \frac{1}{2k_b[NO]_0} \tag{3.25}$$

The relaxation time decreases rapidly with temperature or reduction of density. For example, at one atmospheric pressure, the relaxation is over 1,000 years at 1000 K but it is less than 1 μs at 4,000 K (Table 3.2). If the density drops to one tenth of the ambient at around 4,000 K, the relaxation time increases to more than 50 μs (Goldenbaum and Dickerson, 1993).

A return stroke heats the air in the lightning column to a temperature over 4,000K. At this temperature, the gas mixture establishes its thermal chemical equilibrium in less than one μs with very high content of NO (Table 3.1, 8.4% at 4, 000 K). As the spark column expands outward, it cools due to the radiation energy loss, conversion of energy into the kinetic energy of shock wave and the turbulent mixing with the surrounding cold air. The equilibrium NO content in the mixture decreases with its temperature. If the lightning column were to cool sufficiently slowly that

Table 3.1 Equilibrium Composition of Dissociated and Slightly Ionized Air.

$\rho=\rho_0=1.29\times10^{-3}$ g/cm^{-3} (Standard density) (Zel'dovich and Raizer)

T, ^oK	N_2	N	O_2	O	NO	N^+	O^+	NO^+
2000	0.788	-----	0.205	-----	0.007	-----	-----	-----
4000	0.749	0.0004	0.100	0.134	0.084	-----	-----	-----
6000	0.744	0.044	0.006	0.356	0.050	-----	-----	-----
8000	0.571	0.416	0.007	0.393	0.024	-----	-----	-----
10,000	0.222	1.124	-----	0.407	0.009	0.0034	-----	0.0015
12,000	0.050	1.458	-----	0.411	0.003	0.020	0.0034	0.001
15,000	0.006	-----	-----	-----	-----	0.096	0.015	-----

Table 3.2 Relaxation Time for the Equilibrium of Nitrogen

Oxidation $N_2 + O_2 \leftrightarrow 2$ NO, $\rho=\rho_0=1.29\times10^{-3}$ g/cm^{-3} (Zel'dovich and Raizer)

T, ^oK	1000	1700	2000	2300	2600	3000	4000
τ,sec	2.2×10^{12}	140	1	5.3×10^{-3}	1.4×10^{-3}	7.8×10^{-5}	7.2×10^{-7}

$\tau_{cooling} > \tau$, then the gas mixture would reach its thermal-chemical equilibrium at every step and all formed NO would be dissociated when the spark column cools to ambient temperature.

Actually, both the temperature and the density in the lightning column drops very quickly and the gas mixture does not remain in equilibrium in the whole cooling process. At some temperature, about 2500 K (Goldenbaum and Dickerson, 1993) ~ 2660 K (Borucki and Chameides, 1984), there exists $\tau_{cooling}(T) \cong \tau(T)$. Further cooling of the gas mixture results in the rate of approach to thermal-chemical equilibrium being much slower than the rate of cooling of the air, and the NO concentration no longer follows its equilibrium concentration below this temperature. Net NO is "frozen out" at this temperature. The amount of NO produced by a lightning discharge is determined by the amount of air which reaches the "freezing" temperature and the "freezing" concentration of NO in the gas mixture at this temperature.

3.3 Conversion of NO to NO_2

A. NO oxidation in hot spark channel

Before and after the "freezing" of NO in a lightning column, the concentration of NO is very high in this column. For instance, at 2,660K, the equilibrium NO concentration is about 2.7% for the air with standard density ρ_0=1.29 g/cm^{-3} (Borucki and Chameides, 1984). The high content of NO can be oxidized into NO_2 by the abundance of O_2 in the hot gas mixture via the following reactions (Zel'dovich and Raizer, 1966).

$$2NO + O_2 \xleftrightarrow{k_1', k_2'} 2NO_2 + 25.6\text{kcal/mole} \tag{3.26}$$

$$NO + O_2 \xleftrightarrow{K_3', K_4'} NO_2 + O - 45\text{kcal/mole} \tag{3.27}$$

The reaction 3.26 is exothermic, its forward reaction rate constant is $k_1' = 2.94\times10^{-34} T^{-2} e^{530/RT}$. The equilibrium shifts in the direction of NO oxidation with decrease in temperature because of the negative activation energy. This reaction has wide industrial application and has been well studied experimentally at temperature below 1,000K. In the temperature range from 353 to 845K, the calculated reaction rate constants were in good agreement with experimental observations (Ramstetter, 1922; Goody, 1995).

At low temperature, the NO_2 oxidation is dominated by reaction 3.26. The $[NO_2]$ rate equation can be written as

$$\begin{aligned}\frac{d[NO_2]}{dt} &= 2\{k_1'[NO]^2[O_2] - k_2'[NO_2]^2\} \\ &= 2k_2'([NO_2]_0^2 - [NO_2]^2)\end{aligned} \tag{3.28}$$

Where $[NO_2]_0$ is the equilibrium concentration of NO_2. Similar to the Eq. 3.23, the relaxation time to thermal-chemical equilibrium is

$$\tau' = \frac{1}{4k_2'[NO_2]_0} \tag{3.29}$$

Where $[NO_2]_0$ is the equilibrium NO_2 concentration in the air mixture which depends on the temperature and the true amount of the O_2. Table 3.3 shows the relaxation time constants calculated at high temperatures with a statistical method (Glasstone et al., 1941), which have not been investigated experimentally.

Table 3.3 Relaxation Time for the Equilibrium of NO_2 in Hot Air. τ' denotes termolecular reaction (3.23) and τ'' denotes bimolecular reaction (3.24). $\rho=\rho_0=1.29\times10^{-3}$ g/cm^{-3} (Zel'dovich and Raizer)

T, ^oK	1600	1800	2000	2300	2600	3000	4000
τ', sec	0.09	0.04	2.2×10^{-2}	4.5×10^{-3}	1.5×10^{-3}	5.5×10^{-4}	1.1×10^{-6}
τ'', sec	0.69	0.09	0.1×10^{-1}	0.9×10^{-3}	1.4×10^{-4}	2.1×10^{-5}	1.0×10^{-6}

At high temperature, and especially at low densities, the reaction 3.27 competes with the reaction 3.26. Despite the fact that this reaction requires high activation energy, it has advantage over the reaction 3.26 because it occurs by binary, rather than the three-body molecular collisions. It varies the NO_2 concentration with the rate equation

$$\frac{d[NO_2]}{dt} = k_3'[NO][O_2] - k_4'[NO_2][O] = k_4'[O]_0([NO_2]_0 - [NO_2]) \tag{3.30}$$

and the relaxation time constant

$$\tau'' = \frac{1}{k_2''[O]} \tag{3.31}$$

The calculated relaxation time constants for the thermal chemical equilibrium of reaction 3.27 are also shown in Table 3.3. It indicates that the reaction 3.27 proceeds more rapidly in the temperature of ~2,000 to ~3,000K. When air density is low, it approaches thermal chemical equilibrium more quickly than the reaction (3.26).

The qualitative feature of NO oxidation in the hot air mixture can be elucidated by considering the overall reaction

$$NO + \frac{1}{2}O_2 \xleftrightarrow{K'} NO_2 \qquad (3.32)$$

with the equilibrium constant (Seinfeld, 1986)

$$K' = \frac{[NO_2]}{[NO][O_2]^{1/2}} = 1.016\times10^{-23} e^{13,720/RT} \quad \text{molecules}^{-1/2}\text{cm}^{3/2} \qquad (3.33)$$

Supposing that the formed NO is "frozen" to surrounding air at 2660 K (Borucki and Chameides, 1984) with ratio of 2.7%, the equilibrium ratio of NO_2/NO is 0.15 % estimated with Eq. 3.33. (Similar to the NO "freezing", the NO_2 oxidation reaction no longer remains in thermal-chemical equilibrium as cooling of the gas mixture proceeds.) The ratio of NO_2/NO will be "frozen" at a value corresponding to the equilibrium ratio at a temperature.

Because the reaction 3.26 shifts to the forward direction at low temperature, it establishes thermal chemical equilibrium more rapidly than all other involved reactions. As shown in Table 3.2, reaction 3.26 arrives at its thermal chemical equilibrium with the time constant of 0.09 seconds at 1600 K, the lifetime of a typical lightning. The "freezing" temperature of NO_2/NO should be lower than that of NO. Let us consider the extreme case that all the NO "frozen" stays in a limited region as the lightning column is expanding. The mixing ratio of NO is 2.7% when the lightning column cools below 2660 K. If the equilibrium NO_2/NO ratio is "frozen" at 1600 K, its value is 0.81%. Therefore, we conclude that most of the NO_x formed in a hot air mixture of lightning will exist as NO.

B. NO oxidation by atmospheric O_2

After a lightning discharge, the NO formed in the hot column may be further oxidized by O_2 as it entrains the surrounding cooler air. At low temperature, the reaction 3.26 has advantage over the reaction 3.27

$$2NO + O_2 \xleftrightarrow{k_1', k_2'} 2NO_2 + 25.6\text{kcal/mole} \quad (3.26)$$

$$NO + O_2 \xleftrightarrow{K_3', K_4'} NO_2 + O - 45\text{kcal/mole} \quad (3.27)$$

At ambient temperature, k_3' is much less than k_1' for the exothermic reaction. For example, at 298 K, $k_1' = 1.93 \times 10^{-38}$ $cm^6 molecules^{-2} s^{-1}$ and $k_3' = 1.38 \times 10^{-55}$ $cm^3 molecules^{-2} s^{-1}$ (Hill et al., 1980). Thus, NO oxidation is dominated by reaction 3.26 in the atmosphere, and the NO concentration varies as

$$\frac{d[NO]}{dt} = -2k_1'[O_2][NO]^2 \quad (3.34)$$

The amount of oxygen is excess for reaction 3.26 in the atmosphere, the third order reaction will reduce to a pseudo second order reaction. The NO concentration decreases with a coefficient of $2k_1'[O_2]$. The concentration of atmospheric oxygen is about 5.17×10^{18} cm^{-3} at 298K, so $2k_1'[O_2] = 1.96 \times 10^{-19}$ cm^3 $molecules^{-1} s^{-1}$. The half-life time NO is related with its reaction constant by

$$t_{1/2} = \frac{1}{2k_1'[O_2][NO]_i} \quad (3.35)$$

where $[NO]_i$ is the initial NO concentration.

We can estimate the half-life time of NO formed by a lightning after completely mixing with surrounding air. Assuming the initial NO concentration as $[NO]_i$ = 1 ppm = 2.46×10^{13} molecules cm^{-3}, the half-life time of NO is 2.07×10^5

seconds or about two days. Actually, the typical lifetime of thunderstorm is about one hour. Integrating Eq. 3.34, it shows that about 1.8% of the 1 ppm NO could be oxidized into NO_2 in one hour. The atmospheric background NO concentration is much lower than 1 ppm, so the actual lifetime of NO formed by a lightning may be longer than that given by Eq. 3.35. Therefore, if the formed NO is only oxidized by the atmospheric O_2, its life time is very long so that most NO_x formed will exist as NO before it is oxidized by O_3 or other atmospheric oxidants.

C. NO oxidation by O_3

The NO formed by lightning can be oxidized by ozone O_3, including the atmospheric O_3 and the O_3 produced in lightning discharge.

$$NO + O_3 \xleftrightarrow{k_f', k_b'} NO_2 + O_2 \qquad (3.36)$$

where $k_f' = 1.8 \times 10^{-14}$ $cm^3\ s^{-1}$ and $k_b' = 7.4 \times 10^{-56}$ $cm^3\ s^{-1}$ are the forward and backward reaction rate constants at 300 K respectively. This oxidation is more significant than that driven by O_2 because of the high activity of O_3. This reaction may last for a long time if there exist enough O_3 (Hill et al., 1980). The NO concentration varies as

$$\frac{d[NO]}{dt} = -k_f'[O_3][NO] \qquad (3.37).$$

When NO concentration is very low or a local high NO content mixes with the surrounding atmosphere very quickly, the atmospheric O_3 remains constant such that the reaction 3.36 reduces to a first order reaction. NO concentration will decrease with the rate determined by the reaction rate constants of the original

second order and the atmospheric ozone concentration. In middle altitude, the atmospheric ozone concentration is nearly constants about 15 ppb or 3.7×10^{11} molecules/cm^3. Thus, $k_f^{'}[O_3] = 6.7 \times 10^{-3}\ s^{-1}$, the half-life time of the pseudo first order reaction is

$$t_{1/2} = \frac{0.693}{k_f^{'}[O_3]} \tag{3.38}$$

The half-life time of NO is about 100 seconds for an atmospheric ozone concentration of 15 ppb. It means that the local high NO content could be oxidized by atmospheric O_3 in a short time if there are enough O_3 molecules.

In a thunderstorm region, NO concentration could be very high. We have used 1 ppm in last the section. If only the atmospheric O_3 exists as 15 ppb, O_3 will deplete more quickly than the NO formed by lightning. The local atmospheric O_3 can only oxidize ~1% of the formed NO. The average dimension of a thunderstorm is about 10 km in radius, so the horizontal motion can not mix atmosphere completely in so large range during the lifetime of a thunderstorm. Therefore, most of the NO_x formed by lightning will remain as NO after the thunderstorm if the atmospheric O_2 is the only resource for reaction 3.36. However, a lightning discharge also produces O_3 (Orville, 1967; Donohoe et al, 1977; Hill, 1979; Stark et al, 1996). The UV radiation of lightning discharge photolyzes oxygen molecules and produce a large amount of O_3 in the corona discharge sheath of the spark channel. It is estimated as much as ~1% of oxygen molecules could be photolyzed into O_3. Thus, the O_3 formed during lightning is more significant source in reaction 3.36 to oxidize lightning NO. In a high ozone region after lightning stokes, the NO lifetime is dominated by lightning O_3 yield.

3.4 Summary

The thermal formation of NO from atmospheric O_2 and N_2 involves the dissociation of stable molecules (O_2, N_2) and the thermal chemical reactions of free atoms with molecules ($N+O_2$, $O+N_2$). All these reactions have high activation energy, so that tempearture primarily determines both the equilibrium NO concentration and the relaxation time approaching thermal chemical equilibrium in hot air. At high temperature, both the NO formation and dissociation process vary rapidly. The thermal equilibrium NO mixing ratio reaches a maximum of about 8.4 % at 4000 K in the hot air with density of $\rho_0 = 1.29 \times 10^{-3}$ g/cm^3.

A lightning flash can heat air in a discharge column by ohmic heating, which depends on the distribution of electric field and the electric conductivity of the discharge column. In addition to conversion of its internal energy into the expansion of shock wave, the hot discharge column also losses its energy by radiation. In the temperature range of interest in NO formation, the electric conductivity of hot air can be uniquely calculated from air temperature, and the radiation loss, from the temperature and concentration of each components in the gas mixture and that of free electrons. Knowing the ohmic heating and the radiation loss of hot air, temperature, density, internal energy of each species in the lightning discharge channel could be numerically calculated at every time step using hydrodynamic equations.

At each time step, the NO mixing ratio in a lightning discharge column can be computed from the results of hydrodynamic equations and dynamics of the

reactions related to thermal NO formation. A lightning flash can heat the air in its discharge column up to 30,000 K. At this temperature, both the NO formation and NO dissociation reaction proceed quickly such that an equilibrium amount of NO is formed and rapidly quenched. As the hot column cools from its maximum temperature, the gas mixture establishes thermal chemical equilibrium locally at high temperature, so the equilibrium NO concentration first increases then decreases. When the cooling rate equals the rate to estiblish thermal chemical equilibrium, the hot air column reaches the "freezing" temperature. Below this temperature, the hot air column does not remain its thermal chemical equilibrium and the net NO is "frozen" into atmosphere with Zel'dovich mechanism. For a hot air mixture with density $\rho = 1.29 \times 10^{-3}$ g/cm^3 (the standard air density at standard temperature), the "freezing" temperature is 2660 K and the NO "freezing" ratio is 2.7% by volume.

Almost all of the NO_x formed by a lightning will exist as NO after the lightning discharge. The oxidation of NO into NO_2 by O_2 is negligible during the lightning discharge. In a thunderstorm region, the NO oxidation is dominated by the O_3 produced by lightning. In the NO_x redistribution process by convective updrafts and downdrafts, NO could be oxidized by atmospheric O_3.

Chapter IV Laboratory Simulation of Lightning Discharges

A natural lightning flash may have more than one return strokes, which are high current pulses flowing through the ionized channels initialized by low current leaders (stepped leader or dart leader). Each return stroke discharges the electric charge contained both in a cloud and in the leader channel in which charge was deposited as the leader traveled from its origin in the cloud to ground. In our studies, lightning flashes were simulated with the arcs in ambient air (composition, temperature, and pressure). A laboratory spark simulated a lightning flash with a single stroke discharging a simple series LRC system. The LRC system discharged a 1035 μF main capacitor bank through a pre-ionized leader channel to form a return stroke. A short high voltage pulse that provided by a 10-stage compact Marx generator initialized the pre-ionized leader.

The LCR system simulated the return stroke of natural lightning flash in both amplitude and waveform. The peak currents of experimental sparks were changed from 2.0 kA up to 35 kA, covering over 50 % of global lightning flashes in amplitude. The current waveform of experimental sparks matched the global average waveform of natural return strokes. Unlike a natural return stroke, whose current waveform depends on the parameter of the leader discharge, the current waveform of the experimental spark was primarily determined by the main capacitor and the resistance and inductance of the discharging loop. It was almost independent of the leader discharge because the capacitance of Marx generator was much less than that of the main capacitor bank.

The experimental sparks were diagnosed with electrical and photographic

techniques, including simultaneous measurement of current profile and voltage across the spark and photographic recording of spark expansion. After each discharge, the energy dissipation was directly measured from the observed current and voltage. This reduces the great uncertainty caused from energy estimation in studying the correlation between NO production and energy dissipation. Photographic observation revealed dynamic expansion of the arc that is the critical parameter in simulating the behavior of lightning discharge channel and its NO production.

4.1 Experimental Set-up

A schematic of the lightning simulation system is shown in Figure 2.1. It consisted of a stainless steel vessel to allow quantitative study of the gas phase reaction stimulated by an arc, and the electrical components to create a simulating spark. Different power supply systems were adopted in charging the Marx generator for the leader discharge, the plasma gun for closing the separation switch gap and the main capacitor bank. The Marx generator and trigger capacitor of the plasma gun were charged with low current (5 mA), high voltage (30 kV) DC power supplies. The main capacitor bank was charged with high current (1 A), high voltage (20 kV) power supply. The remote controlling system and the data acquisition systems are not shown in Figure 2.1. They were separated from the high voltage system and some of them were shielded in screen rooms.

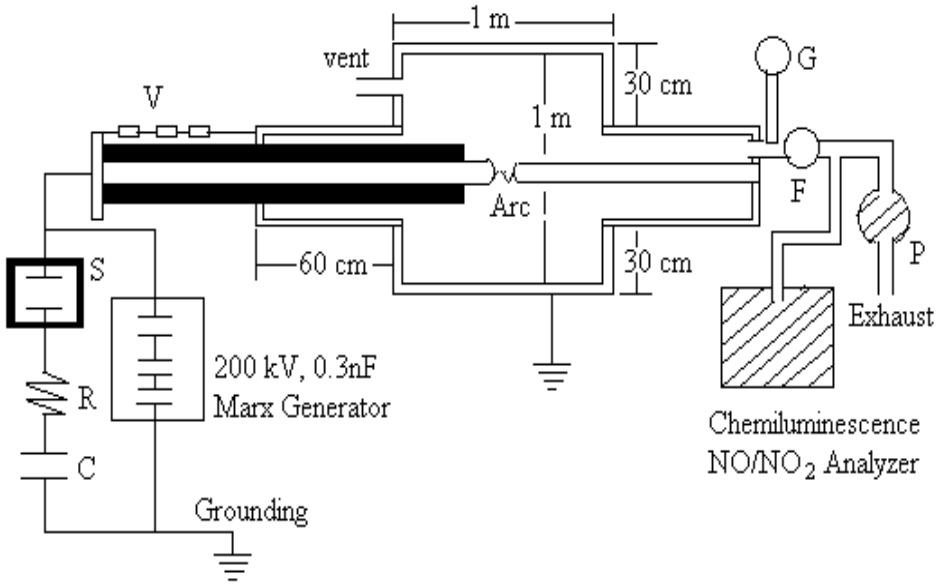

Figure 4.1 Schematics of apparatus

S --- SF_6 switch gap, pressurized up to 2 ATM. V --- Spark voltage measuring resistors, 820Ω. R --- Steel resistor, 0.23Ω. C --- Main capacitor bank, 1035 μF. G --- Pressure gauge. F --- MKS mass flow meter, 200 L/min. P --- Exhausting pump.

A. Reaction vessel, electrodes, and capacitor bank

Experimental sparks were made between two electrodes mounted in the steel vessel, which has a diameter and length of one meter. The vessel is grounded and has cylindrical extensions of 40 cm long and 60 cm in diameter at each end. A digital temperature-humidity gauge was installed to monitor the relative humidity and temperature in the vessel.

Two brass electrodes of 2" diameter, one grounded and another one at high voltage, project coaxially from each end into the reaction vessel. The electrodes have hemispherical tips of Elkonite, a tungsten-copper mixture that is commonly used in switches to minimize erosion due to sputtering. The grounded electrode is connected with the vessel, while the high voltage electrode is isolated from the vessel with PVC pipes. The position of the grounded electrode is adjustable to set the length of spark gap.

The main capacitor bank of 1035 μF simulates the lightning cloud in storing a large amount of electric charge to discharge through a return stroke channel. For each shot, the main capacitor bank was charged to the desired operating voltage as the first step. Then it discharged following a leader channel to form the main return stroke current. The capacitor bank consists of sixteen 11 kV capacitors in parallel. Each capacitor has inductance less than 50 nH, so the inductance of main capacitor should be less than 3 nH.

B. Isolation switch

The Marx generator outputs a 250 kV high voltage pulse that lasts about

one-half microsecond. To form a leader channel under ambient pressure, the Marx pulse has to be isolated from the main capacitor bank. If the main capacitor bank were connected with the Marx generator directly, it would present low impedance to the Marx pulse and effectively short-circuit it to ground. This isolation was accomplished by a SF_6 spark gap (Figure 4.1). The spark gap (2 cm wide) was pressurized to about 2.5 ATM (absolute) that was sufficient to hold off a 250 kV Marx pulse long enough to establish a leader channel between two electrodes.

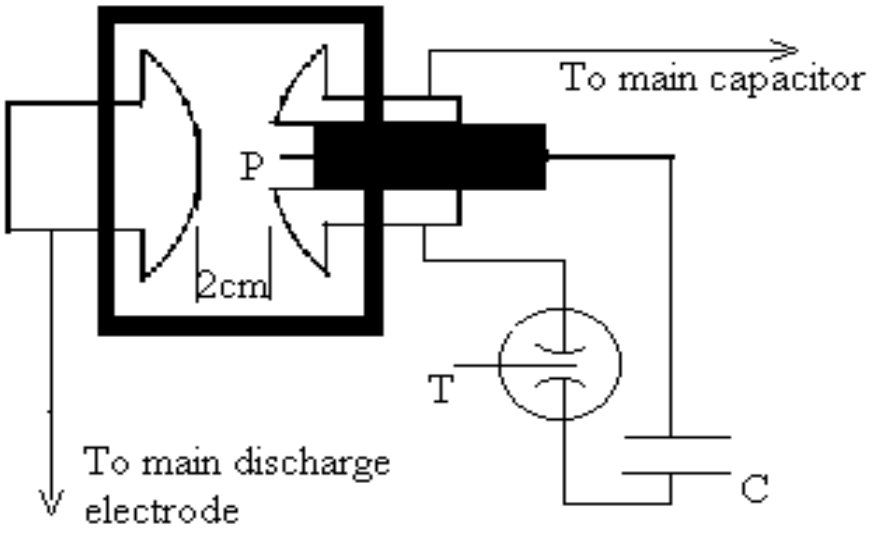

Figure 4.2. Cross section of the SF_6 switch

P--- Tungsten trigger pin of the plasma gun. T--- Thyratron trigger pin, 30 kV. C--- Trigger capacitor of the plasma gun, 4 μF.

The SF_6 switch has to be closed immediately after discharge of the Marx generator. Otherwise, the surrounding air would quench the ionized leader very quickly. We operated the switch using a miniature plasma gun (Figure 4.2) installed in one of the gap electrodes. The plasma gun injected a plasma jet across the switch gap driven by discharging a 4μF capacitor. The triggering capacitor was charged to 20--25 kV and fired through a trigatron spark gap switch that was in turn trigged by a Thyratron.

This SF_6 switch gap has to be closed on command sometime after the discharge of the Marx generator. If the switch were closed early, the main capacitor would be connected with the high voltage electrode before any conductive channel existed between electrodes. Then the main capacitor bank would not only short circuit the Marx pulse but also discharge through the voltage measuring circuit and burn the voltage measuring resistors (Figure 4.1). We closed the SF_6 switch gap with a signal coupled from the current of the leader channel.

The length of the main arc depends on the charge voltage of the main capacitor bank and the degree of ionization between the main electrodes when the SF_6 switch is closed. The Marx generator outputs a 250 kV Marx pulse which can initialize a leader channel up to 20 cm long at ambient pressure. The main capacitor bank was charged up to 10 kV, which was much lower than the Marx voltage. Since the SF_6 switch closure took 80 μs, most ions in the leader channel had been quenched by the surrounding air by the time the switch is closed. Therefore, when the main capacitor bank was charged to 10 kV, it could only successfully discharge with a gap ≤ 4 cm at one atmosphere pressure or ≤ 8 cm at one-half atmosphere

pressure.

C. Inductance and resistance

The total system inductance consisted of the inductance of the main capacitor bank and that of the discharge loop. It was hard to know the inductance of each component in this system, but the total inductance could be estimated from the ringing period of the discharge current. When the two main electrodes were replaced by a 2" diameter copper pipe, the system reduces to a simple LRC discharge loop. Connecting the electrode to main capacitor bank with a solid dielectric switch, the LRC discharge current rang with a period

$$T = 2\pi/\omega = 2\pi(LC)^{1/2} \qquad (4.1)$$

Figure 4.3 shows the measured current profile, where the ringing period is 330 μs. Thus, the total inductance of the system is about 2.66 μH.

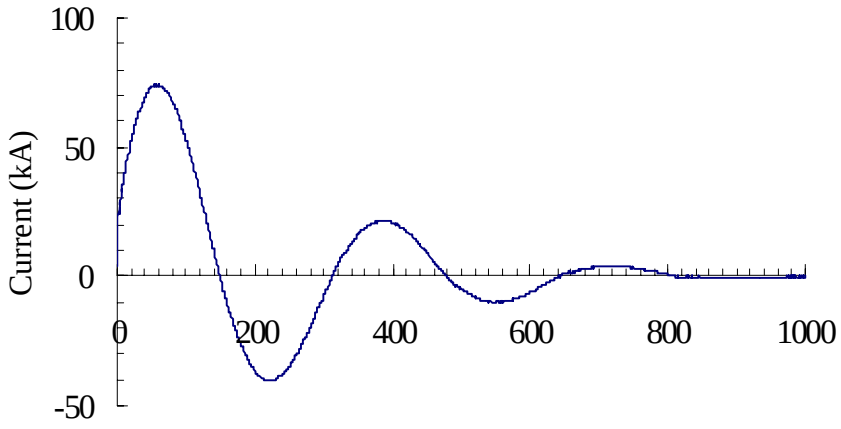

Figure 4.3 Measured current profile with the main gap and the series resistor short circuited. C=1035 μF, T=330 μs, L = 1/ (ω^2C)= 2.66 μH. V=4.0 kV

Similar to the inductance, the sources of the system resistance were very complicated and could only be indirectly estimated from the current profile of a discharge. The system resistance came from the main capacitor bank, cables, SF_6 switch, main arc and a 0.23 Ω external resistor. The external resistor (a thin steel sheet in a low-inductance configuration) was connected in series with the main capacitor bank (Figure 4.1) and served to form the discharge current to match a natural lightning stroke. During a natural lightning flash, the return stroke currents are always unidirectional and overdamped by the large resistance. If the main capacitor bank was directly discharged through a gap between electrodes, the spark current oscillated as in Figure 4.3. This additional resistor overdamped the main discharge and made the current match the waveform of natural lightning.

We estimated the system resistance by matching a typical experimental current profile with the computed current profile of a LRC discharge (Figure 4.4). When an LRC discharge is overdamped, it discharges with current

$$I=I_0(e^{-\alpha t} - e^{-\beta t}) \tag{4.2}$$

Where

$$I_0 = V/R \tag{4.3a}$$

$$\alpha = \frac{R}{2L}\left(1 - \sqrt{1 - \frac{4L}{R^2C}}\right) \approx \frac{1}{RC} \tag{4.3b}$$

$$\beta = \frac{R}{2L}\left(1 + \sqrt{1 - \frac{4L}{R^2C}}\right) \approx \frac{R}{L} \tag{4.3c}$$

The system capacitance was measured as1035 μF, and the system inductance was estimated with Eq. 4.1 as 2.66 μH. Fitting the computed current profile to a

measured profile (Figure 4.4),we found the overall resistance to be 0.37 Ω.

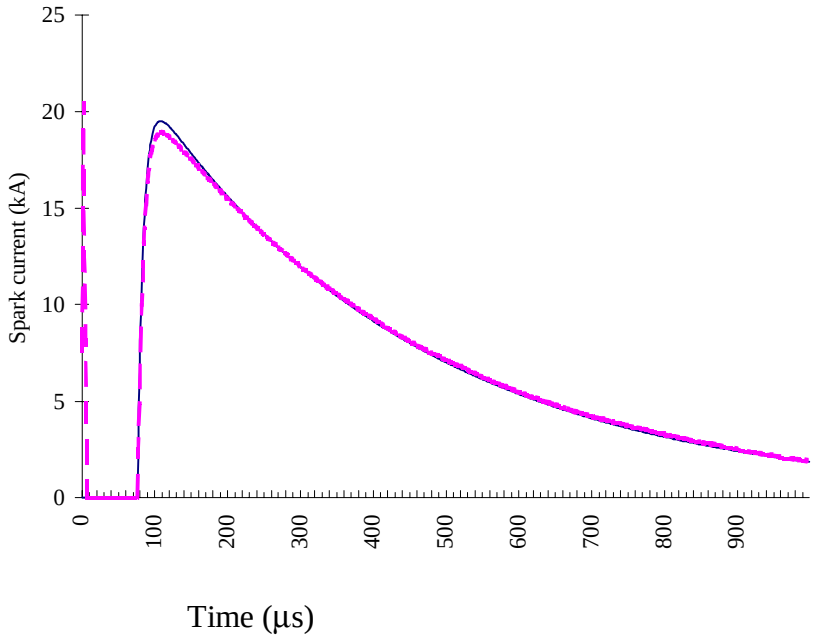

Figure 4.4. Current profile of main arc. Solid line -- Current of calculated LRC discharge; Broken Line -- Measured current of spark. The spike at the beginning indicates the Marx pulse. V=7.0 kV, d=3.2 cm, P=1 atm.

4.2. Spark Diagnostics

A. Current measurements

Discharge currents of experimental sparks were measured using a Rogowski coil that wrapped around the discharge cable on the grounded side of the main capacitor bank. When current flows through the discharge cable, variation of the associated magnetic field induces a voltage across the Rogowski coil. If the coil makes a closed turn around the cable, this induced voltage is proportional to the rate of current variation dI/dt and the current can be calculated by integrating the voltage

signal from t =0.

In our experiments, the voltage signal from the Rogowski coil was directed into a RC integrator. This integrator outputs a voltage signal that was proportional to the current flowing through the hole of the Rogowski coil. The RC integrator may cause an error in current measurement in recording a long pulse. This error was corrected numerically using

$$\int_0^t V_{in}(t)dt = V_{out}(t) + \frac{1}{RC}\int_0^t V_{out}(t)dt \qquad (4.4)$$

Where $V_{in}(t)$ is signal from Rogowski coil signal to RC integrator, V_{out} is signal after the RC integrator, and RC =5 ms is the time constant of the integrator.

B. Voltage measurements

Voltage across a spark was measured using a current transformer (Pearson model 410A) to monitor the current flowing through a series of carbon composition resistors. A current transformer was used because it is isolated from the main discharge system. In our experiments, it's advantage over a resistive or capacitive voltage divider is that it avoids the problem that the ground potential of the system may change when the main capacitor bank discharges. However, a current transformer cuts off the low frequency component. The adopted Pearson transformer cuts off at about 125 Hz with 3dB in low frequency regime. We compared the Pearson transformer to a resistive divider with signals from a function generator in various frequency regimes. The Pearson transformer agrees with the resistive divider very well in the frequency regime of the voltage of a typical experimental discharge.

Another problem in voltage measurement was the very large scale difference between Marx and main discharge voltages. Marx pulses differed by two or three orders from the main sparks in both voltage magnitude and signal length. The Marx generator outputs high voltage pulses over 250 kV that lasted only about one-half microsecond. The main capacitor bank may be charged up to 10 kV but its signal can last over one millisecond. Another scale difference existed between the resistive and inductive components of voltage across a spark. As shown in Figure 4.5, in the early phase($t \leq 50\ \mu s$) of a discharge, the voltage was very large and primarily inductive, while later the resistive component dominates. The profile labeled "d = 0" in Figure 4.5 shows the purely inductive voltage measured when the gap was closed to zero. The difference between the two curves represents the ohmic voltage across the arc. In our experiments, we clipped the Marx pulse in the output of the voltage signal using a Zener diode and numerically eliminated then inductive from the resistive component.

The measured voltage signal across a spark can be expressed as

$$V_m = V_r + L\frac{dI}{dt} \tag{4.5}$$

where V_m is measured voltage, V_r is resistive voltage across a spark, L is inductance of the discharge circuit, and L*dI/dt is inductive voltage across a spark.

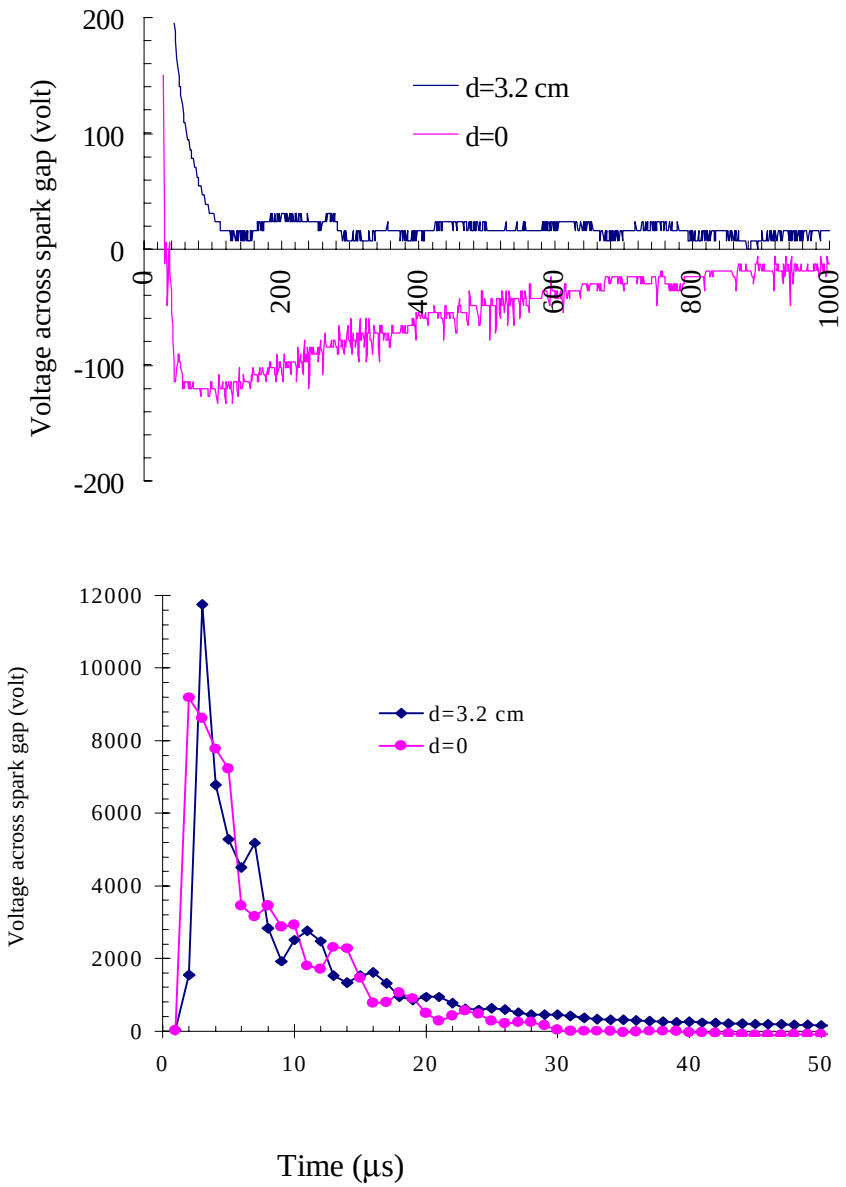

Figure 4.5. Voltage across an arc (Measured with a Pearson transformer).

P = 1 atm., I_{peak} =19.0 kA.

Upper -- voltage after 50 μs; Lower -- voltage of the first 50 μs.

C. Photographic diagnostics

We photographed the simulated lightning sparks with two systems. An

image-converter camera photographed the overall structure of a spark and a streak camera system recorded expansion of a spark center. The image-converter camera system consisted of an image converter tube, a camera control delay unit and the necessary focusing and imaging optics. The image converter tube was a vacuum

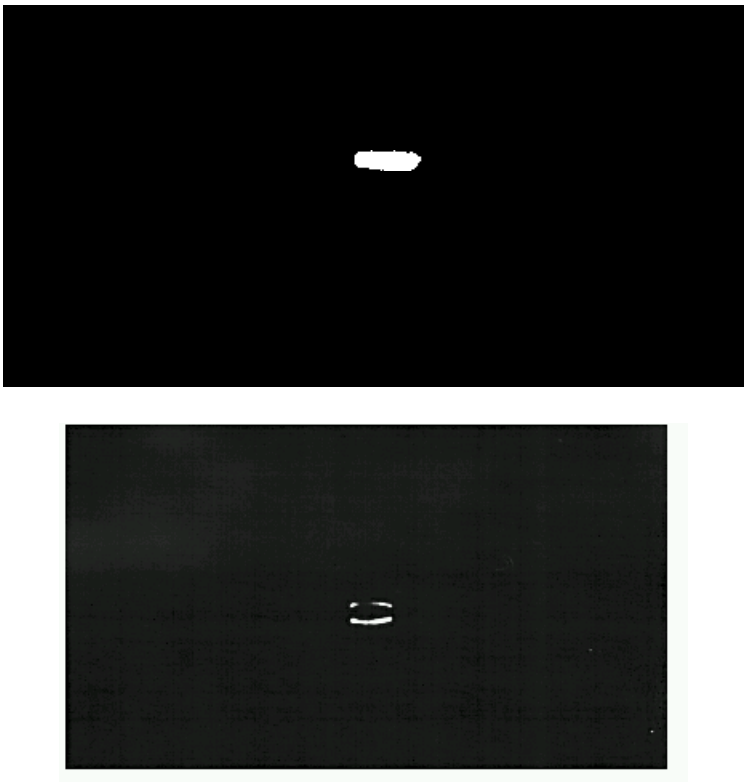

Figure 4.6 Images of simulated lightning sparks.

Gap = 3.2 cm, V = 7.0 kV, P = 1 atm, Exposure time = 100 ns

Upper -- Single Arc; Lower -- Double arc.

tube with a photocathode and an anode with phosphorescent coating at high potential. It works as a fast shutter and light amplifier. Electrons emitted by the cathode accelerate to the anode and produce an amplified image. The spark image on the anode was photographed by a Polaroid camera. This system was capable of taking a view of a spark at desired time interval with 5 nanoseconds exposure time.

Figure 4.6 shows images of a single arc and a double arc that obtained by the image converter system. Most sparks only had one channel, but double-channel sparks were occasionally observed (≅ one in ten). The double-channel sparks may be caused from branching or double initiating of leader channel by a Marx pulse. When a stepped leader initializes an ionized channel for the first return stroke, it always branches the leader channel. In our experiments, a branched leader channel was also observed when only Marx generator was discharged. Since only one camera was installed on the image-converter system, the leader channel and main spark could not be observed at the same discharge. The correlation was unclear between branching of the leader channel and the occurrence of double main spark.

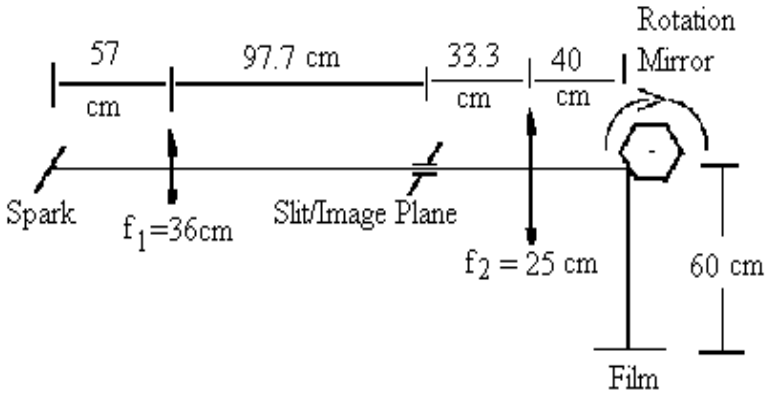

Figure 4.7 Optical alignment of streak camera.

The schematic of the streak camera system is shown in Figure 4.7. An objective lens f_1 imaged the horizontal spark on a narrow slit oriented vertically. The slit selected the center of the spark image, which was focused by the second lens f_2 the photographic film of a Polaroid camera. A mirror between f and the film swept the light image across the film to produce a time versus radius record (Figure 4.8). The vertical axis represents radius of a spark with its resolution determined by the magnification of the optical system. We measured spark radius from the visible image edge obtained by the streak camera system. The radius of the actual conductive channel could be large than the

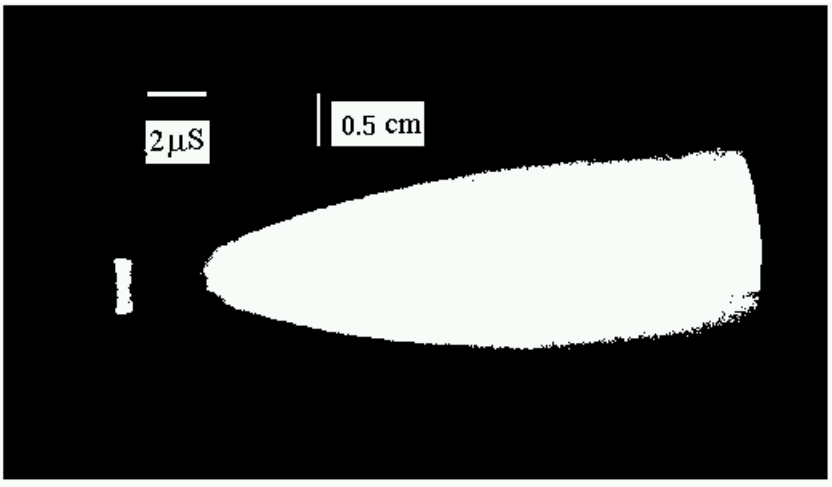

Figure 4.8. Photograph of spark expansion obtained with streak camera.

d = 3.2 cm, I_{peak} =19.0 kA, P = 1 atm., T =298 K. The image at the left is a time marker to indicate the beginning of the main current.

measured radius because the photographic film was only sensitive to visible light, but the outer layer of a discharge channel may not radiate visible light. The horizontal axis represented time with writing speed as

$$\frac{dx}{dt} = 4\pi\omega L \tag{4.6}$$

where L = 60 cm is the distance from rotating mirror to imaging film, and ω is rotation speed of the mirror in radians/second.

4.3 Diagnostic Results

A. Spark current

Figure 4.4 shows the current profile of a typical experimental spark, which was discharged at ambient pressure, charging the main capacitor at 7.0 kV and setting the gap length at 3.2 cm. The current reaches 63% of its peak value at about 5 μs and arrives at its peak in about 30 μs. It decays with a time constant about 350 μs after its peak. As the main capacitor charging voltage was changed from 3.0 kV to 10.0 kV at atmospheric pressure, the peak current of sparks of 3.2 cm length increase from 6 kA to 30 kA (Figure 4.9).

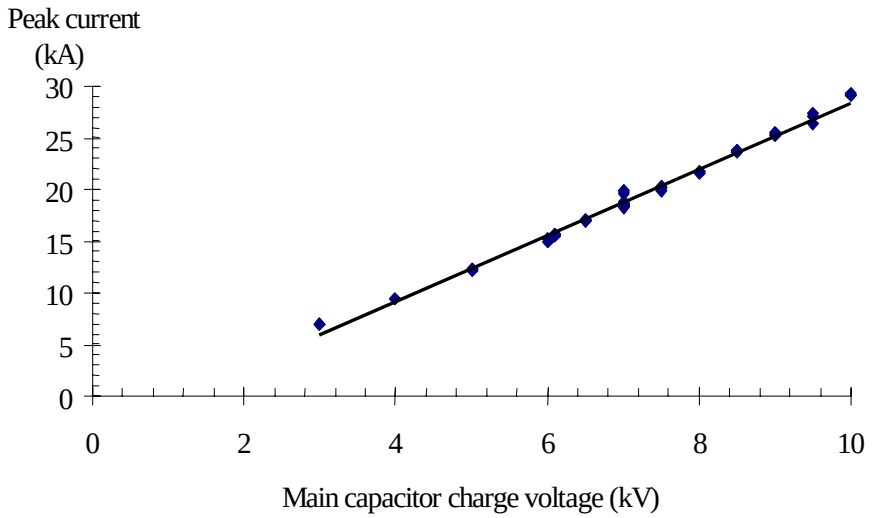

Figure 4.9 Spark peak current versus charging voltage of the main capacitor bank. d = 3.2 cm, P = 1 atm.

A LRC discharge is only a simple model to simulate lightning discharge. It matches a lightning discharge at very long times when the charges on the cloud dominate and the charge distribution on the leader channel is unimportant. The overall current waveforms of experimental sparks were close to overdamped LRC discharges but with a little difference in their current rising portion caused by the variation of system resistance during discharging process. They were dominated by the external circuit and were almost independent of spark length, air pressure, and the charge voltage of main capacitor bank. The currents matched the global average of natural lightning strokes in rise time, but have a longer decay time. They are more like the first negative return strokes that frequently occur and are important to NO_x production. Our experimental sparks have simulated about 50 % of cloud-ground lightning strokes in their current amplitude as they increased from about 5.0 kA to over 30 kA. The current amplitudes fell in the range of return stroke currents

of the order of 10^4 Amperes (Krider et al., 1968).

B. Energy dissipation

During a discharge of our system, only a small portion of the energy stored in the main capacitor bank was dissipated in the spark channel. The "net" energy could be calculated from the measured current profile and voltage across the spark.

$$E(t) = \int_0^t I(t') V_r(t') dt' \qquad (4.7)$$

where $V_r(t')$ is resistive voltage across the spark and I(t') is spark current. Figure 4.4 shows the spark voltage measured as described in Section 4.2.B. The curve denoted by d=0 means that two electrodes were replaced by a copper tube of 2" diameter (i.e. the circuit was shorted to ground). The recorded signal would be only the inductive voltage term of Eq. 4.5 since the resistive increase over the copper tube should be very small. The another curve is the voltage of a typical spark of d= 3.2 cm long and with I_{peak} = 19.0 kA.

Actually, we do not need to know the exact function $V_r(t')$ in Eq. 4.7 to estimate total energy dissipation. Substituting $V_r(t')$ expression from Eq. 4.5, energy dissipated by a spark is

$$\begin{aligned} E(t) &= \int_0^t I(t') V_r(t') dt' \\ &= \int_0^t I(t') V_m(t') dt' - \int_0^t I(t') L \frac{dI(t')}{dt'} dt' \\ &= \int_0^t I(t') V_m(t') dt' - \frac{L}{2} \int_0^t dI^2(t') \end{aligned} \qquad (4.8)$$

where V_m is the measured voltage. The second term of Eq. 4.8 indicates the effect of the circuit inductance on the energy transport. It does not contribute anything to the

"net" energy and becomes zero when the integration goes to infinity. In our work, we took the upper limit of the integration as one millisecond which makes the inductive term negligible comparing with errors from other sources.

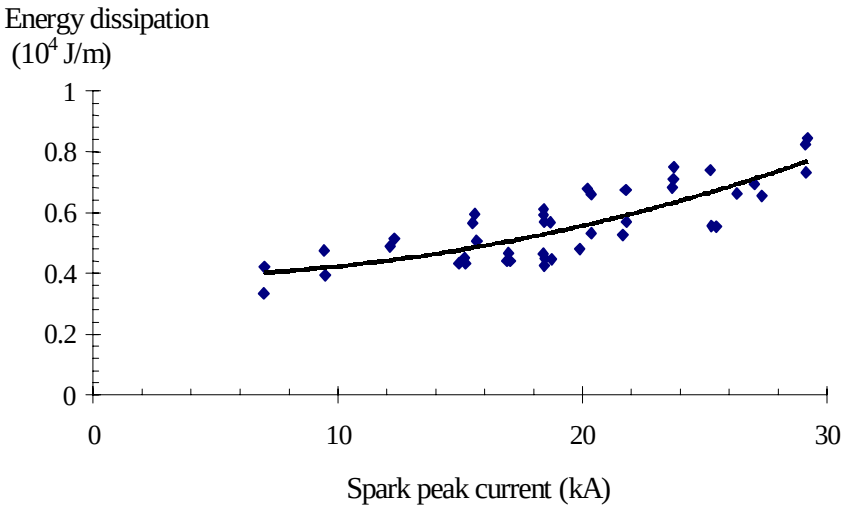

Figure 4.10 Spark energy dissipation versus spark peak current. A quadratic least squares fit is also shown.

d = 3.2 cm, p = 1 atm, T = 298 K.

Figure 4.10 shows spark energy dissipation calculated with Eq. 4.8 versus spark peak current. The data were obtained with a 3.2 cm gap at atmospheric pressure, and energy dissipation was represented as energy amount dissipated per unit spark length. A least squares quadratic regression of the data gives

$$E_0 = 0.393 - 1.95\times10^{-3}\, I + 5.09\times10^{-4}\, I^2 \qquad (4.9)$$

where the unit of E_0 is 10^4 J/m and the unit of I is kA. The square of the correlation coefficient is $r^2 = 0.673$ indicating the variance between the regressed values and the original data, which was calculated

$$r^2 = 1 - \frac{\sum_i (E_i - \hat{E}_i)^2}{\sum_i E_i^2 - n\overline{E}^2} \qquad (4.10)$$

where $\hat{E}_i$ denoted the predicated values and $\overline{E}$ was average of experimental data.

The energy dissipation by a lightning stroke can only be estimated from some primary lightning measurements such as, currents, electric field changes, light radiation intensities, or shock wave intensities. Large uncertainties always exist in all estimates (Table 2.2) because of their indirect approaches. On the basis of air heating and radiation transport of lightning channels, the energy dissipation of a stroke depends more strongly on stroke current than on other stroke parameters. Plooster suggested that the energy dissipated by a spark is $E_0 \propto I_p^{1.2} t_r^{-.08} t_d^{0.45} Q^{0.45}$. Where I_p is the peak current, t_r is the current rise time, t_d is the current decay time and Q is charge transported by stroke. Our results show the quadratic dependency of the E_0 on peak current for I > 10 kA. The difference may be caused from lack of high current data in our experiments.

Our measured E_0 agrees very well with the results of simulations and the field measurements of lightning dissipation, all ~10^4 J/m (Hill, 1979). It indicates that our experimental sparks also simulated lightning discharges energetically. If the function, Eq. 4.9, is used to extrapolate global lightning energy dissipation, we will be able to narrow the large uncertainty existing on that issue since lightning current is better known than any other parameters.

C. Spark expansion

The framing photographs of sparks were taken from different shots with

exposure time of 0.1μs with controlled time delay after starting of main current. After the start of the main current, a visible spark channel appeared at about 2 μs with a radius about 0.5 cm. This visible channel expanded to a radius about 1 cm in 15 μs. The observations with the streak camera system showed the visible spark channel appears at about 2 μs after main current with a radius only about 0.2 cm and it reaches about 0.5 cm in 8 μs.

Plooster (1971) expressed the diameter of a lightning stroke with spark peak current and time as

$$D \cong 18.7\, I^{1/3} t^{1/2} \qquad (4.11)$$

where r is in centimeter, I is in amperes, and t is in seconds. Our observed spark diameter is only half of that predicted with Eq. 4.11 (Figure 4.11), but the visible channel expanded with a behavior as Eq. 4.11.

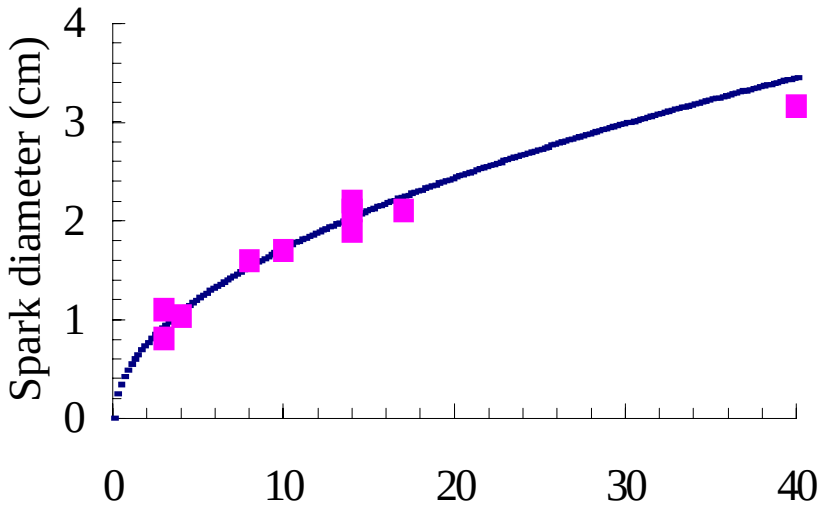

Figure 4.11 Spark expansion (obtained with image-converter camera). Fitting curve:

$D = 9.35\, I^{1/3} t^{1/2}$, I is in Amperes, t is in seconds and D is in cm.

I = 19.0 kA, d = 3.2 cm, T=298 K, P = 1atm.

Long arc discharges of Marx pulses in air have been studied experimentally in both the propagation of electric discharges and the dynamics of the resulting channels (Greig et al., 1978; Picone et al., 1981). Picone produced a spark 15 cm long in air with a high voltage pulse from a Marx generator with an erected voltage of ~ 250kV. The Marx pulse formed a hot, smooth, curved channel with a radius of ~1.4 cm within 8 μS of the initiation of the discharge at which time the accompanying shock wave had already decoupled from the hot channel. The channel remained roughly stable until 100 μs. At that moment, the interior temperature of the channel was ~ 5000 K, gas density was ~ 10^{18} cm^{-3} and electron density was ~ 10^{14} cm^{-3}. Instability did not become obvious until 250 μS after the initiation of the discharge. Similar results were obtained in studies of discharges guided along a path designated by laser/aerosol interaction (Greig et al., 1978). In our experiments, the main discharge flows through the ionized leader channel initiated by a Marx pulse after about 80 μS. The radius of the leader channel could be close to 1 cm when the main current starts. Photographic results shows that the main current of the spark starts with a radius ≤ 0.5 cm. Therefore, the dimension of the current channel of a simulated lightning spark may be different from the visible channel. Further work is necessary to relate current channel with visible spark current.

4.4 Summary

We have successfully simulated natural lightning flashes with arcs at

ambient conditions. Each simulated flash consisted of a low ionized leader channel initialized by a 250 kV pulse and a stroke driven by discharging a capacitor bank of 1035 μF through the pre-ionized leader channel. The simulated strokes matched natural lightning strokes in current amplitude, current waveform and energy dissipation per unit length. The peak current of simulated strokes has been varied from 5.0 kA to over 30 kA, which covers about 50 % of global strokes in amplitude. Similar to natural strokes for which the current waveform are primarily determined by the resistance within clouds, the waveform of our simulated stroke was dominated by an external additional resistor. In the early phase of a simulated stroke, it agreed very well with the global average of natural strokes. In the phase of current decay, it decays with a time constant that is a little longer than the global average of all strokes that was very close to the global average of the first negative strokes.

Energy dissipation of simulated sparks has been calculated using directly measured spark current profile and voltage across spark. The measured voltage across spark included both the resistive voltage and the inductive voltage associated with inductance of the discharge system. The inductive voltage early in the discharge was larger than the resistive voltage across a spark, but the contribution of inductive voltage to the energy was cancelled automatically in our calculation. The results shows that our simulated lightning sparks dissipated energy with the same order as natural lightning. A quadratic fit function was derived on the correlation between spark peak current and the energy dissipated per unit of the spark length.

We have developed photographic techniques to diagnose our simulated

sparks, which included an image converter camera and streak camera with rotating mirror. Like the first negative strokes of natural lightning, branching leader channel and double arc were occasionally observed in our experiments. The occurrence of a double arc was unpredictable and the correlation between branching leader and double arc is not clear. Dynamic expansion of the spark channel has been studied with the observed images of the visible channel that agrees very well with previously reported simulation of natural lightning channel and observed long laboratory sparks.

Chapter V. NO_x Production by Simulated Lightning

Throughout our work, NO_x produced by simulated lightning sparks has been measured with a chemiluminescent NO/NO_2 analyzer (Thermo Environmental, model 42). This chapter discusses the measuring technique and NO_x production by various sparks. NO_x production has been studied by changing parameters including the spark peak current, pressure of the initial air, and presence of water in the air. These measurements enable us to derive analytical expressions that are necessary to extrapolate NO_x production to a long lightning channel from a cloud to ground. We here estimate the annual global NO production using the lightning data obtained in the United States and measured global lightning frequency. In order to compare our results with the works reported by other researchers, we also have studied the correlation of NO_x production by a spark and the energy dissipation of the spark.

5.1 Experimental Methods

A. Principle of operation

In our experiments, the gas mixture after a discharge was sampled (Figure 4.1) by a chemiluminescent NO_x analyzer installed with a NO_x-NO molybdenum converter, measuring the concentrations of NO and NO_2 sequentially. The analyzer measures NO content via the gas phase reaction,

$$NO + O_3 \text{ --> } NO_2^* + O_2 \qquad (5.1)$$

The product NO_2^* is created in an electronically excited state. When the excited NO_2 molecules rapidly decay to lower energy states photons are emitted that are detected by a photomultiplier.

$$NO_2^* \text{-->} NO_2 + h\nu \quad (5.2)$$

Under stable conditions, if NO is completely oxidized by O_3, the intensity of the characteristic luminescence is linearly proportional to the NO concentration. Thus, a quantitative measurement requires that the reactant O_3 concentration exceeds the concentration of NO, and the gas mixture stays long enough in the reaction chamber of NO_x analyzer.

Only NO can be measured by the chemiluminescent reactions 5.1 and 5.2. If NO_2 is to be measured, it must be transformed into NO before entering the reaction chamber of NO_x analyzer. The transformation is performed by a molybdenum converter installed in the NO_x analyzer. When the converter is heated to approximately 325 ^oC, molybdenum reacts with NO_2 to form NO and MoO_3:

$$3\ NO_2 + Mo \text{----->}\ 3\ NO + MoO_3 \quad (5.3)$$

Molybdenum participates in the reaction 5.3 to be oxidized into the MoO_3, so that the conversion efficiency should be calibrated regularly to get reliable data.

When the sampled gas enters the analyzer through a single flow control capillary, it is routed by a solenoid valve either through the NO_2--NO converter or around it. If sampled gas flows through the converter, NO_2 is converted into NO and the analyzer measures total amount of NO_x ($NO+NO_2$), while bypassing the converter allows measurement of NO content only. The solenoid valve switches with a set period between measurements of NO and NO_x, so that concentrations of NO and NO_x may be measured sequentially.

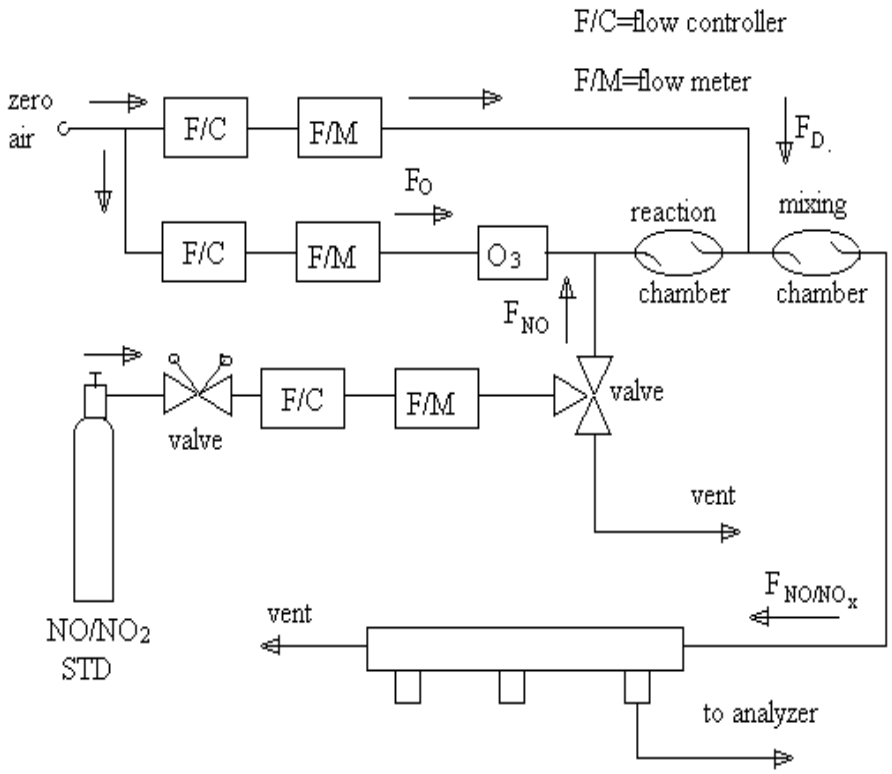

Figure 5.1 Gas phase titration system to calibrate NO/NO_2 analyzer. In this figure, F_0 is the flow rate of zero air (the air free of contaminants such as NO, NO_2, O3, and water) to O_3 generator; F_{NO} is the flow rate of NO mixture from standard cylinder; F_D is the flow rate of dilution zero-air; $F_{NO/NOx}$ is the flow rate of NO/NO_x mixture

B. Calibration of NO_x analyzer

The NO analyzer was calibrated with an NO standard which was a mixture of NO in N_2 containing 1.23±0.012 ppm of NO, prepared and calibrated by the National Institute of Standards and Technology (NIST). The NO_2 to NO conversion efficiency was measured with a GPT (gas phase titration) system. The GPT is

illustrated in Figure 5.1, where all connections between components were made with glass, Teflon, or stainless steel. An O_3 generator took zero-air (The air is essentially free of contaminants such as NO, NO_2, O_3, and water) and produced a gas mixture with stable O_3 content. The gases from the standard NO cylinder mixed with the gas mixture from the O_3 generator were directed into an external reaction chamber (Figure 5.1) with NO mixing ratio as

$$[NO]_{in} = \frac{[NO]_{std} F_{NO}}{F_{NO} + F_O} \tag{5.4}$$

where F_{NO} and F_O refer to the flow rates of the NO standard and the O_3 mixture. $[NO]_{std}$ is NO concentration in the gas mixture from the NO standard cylinder. In the reaction chamber, some NO was oxidized into NO_2^* by O_3 via the reaction 5.1. If the NO amount was excessive and the gas mixture stayed in the reaction chamber long enough, O_3 could be completely reacted. When the gas mixture left the reaction chamber, the NO and NO_2 concentrations in the mixture were related by

$$[NO]_{in}=[NO]_{out}+[NO_2]_{out} \tag{5.6}$$

where $[NO]_{out}$ and $[NO_2]_{out}$ are concentrations of NO and NO_2 in the gas mixture leaving the reaction chamber, and $[NO]_{in}$ is given by Eq.5.5.

If the O_3 generator was off, the NO_x analyzer measured the NO and NO_2 concentrations in a mixture of zero-air and NO from the standard NO cylinder. As O_3 generator was turned on, the NO reading decreased while the NO_2 reading increased (Figure 5.2). The decrease of NO concentration on the calibrated NO channel was equivalent to the increase of NO_2. The conversion efficiency of the converter was

$$CE = \frac{[NO_2]_m}{[NO_2]_{out}} \qquad (5.6)$$

Where CE is the conversion efficiency of the NO_2--NO converter, $[NO_2]_{out}$ is same as in Eq. 5.5, $[NO_2]_m$ is the measured concentration of NO_2. It should be pointed out that this calibration system is not sensitive to the exact concentration of O_3 from generator. Most commercial O_3 generators are suitable.

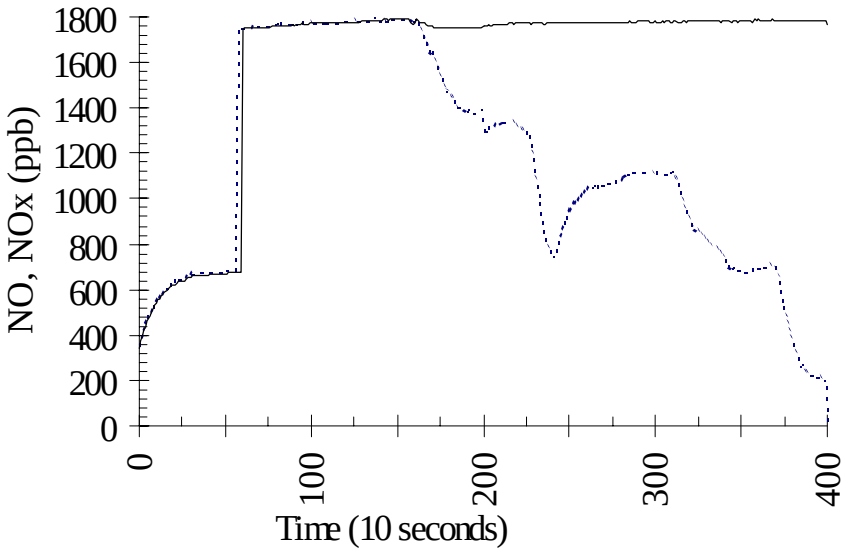

Figure 5.2. Calibration of NO/NO_2 chemiluminescent analyzer

The solid line is NO_x concentration, the broken line is the NO concentration. The sampling speed corresponds to10 seconds/point.

C. Determinations of NO_x production

Following a discharge, air in the reaction vessel was flushed out by means of a small pump while an MKS mass flow meter monitored the flow rate. The flushed air was sampled and analyzed by a chemiluminescence NO/NO_2 analyzer to determine the concentrations of NO and NO_2 in the flushed air simultaneously.

Figure 5.3 shows NO and NO_x concentrations in the flushed air stream from the vessel after a typical discharge. The NO/NO_x levels increase from significantly below 100 ppb before discharge to their peak values at about 2 minutes. After that they fall exponentially with a time constant of about 5 minutes and return to background readings in about 30 minutes. The detector sampled at the speed of 10 seconds/point in all experiments. It measured the concentration of NO and NO_x every other sampling point respectively.

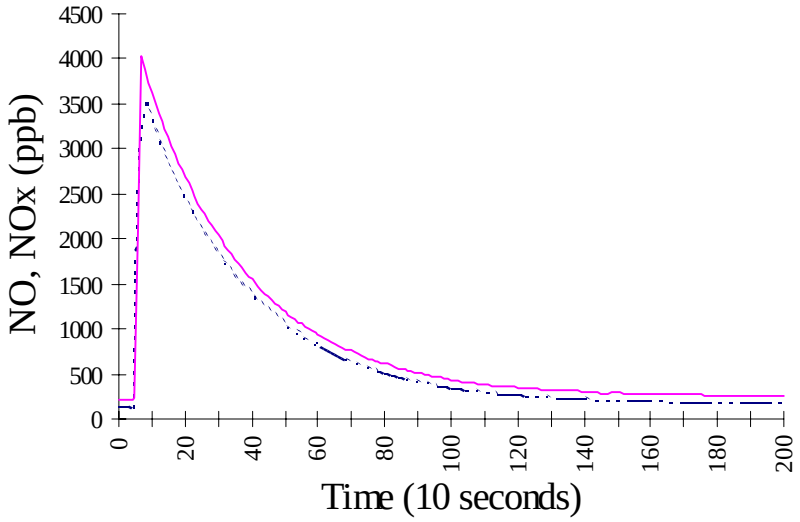

Figure 5.3. NO/NO_2 measurements with a chemiluminescent analyzer.

Air sampling flow rate = 200 liters /minute. Analyzer sampling speed = 10seconds/point, V = 7.0 kV, P= 1 atm., T=298 K, d = 3.2 cm, I_{peak} = 19.0 kA. The solid line is the NO_x concentration, and the broken line is the NO concentration.

The yield of NO or NO_2 was computed by integrating the NO or NO_x concentration in the flushed air stream over the sampling time interval

$$Q=\int F_{flush}c(t)dt \qquad (5.4)$$

where Q is the amount of NO or NO_2 produced by a discharge, F_{flush} is the mass flow rate of air and c(t) is the concentration of NO or NO_2 in that flow.

D. NO_x Production and simulated lightning

The current profiles of natural lightning strokes change from flash to flash and from stroke to stroke in a wide range. In our experiments, current waveforms of the simulated lightning were determined by the circuit components (Chapter IV) and the peak values could be varied by changing the charge voltage of the main capacitor bank. We first studied NO production by the simulated sparks as their peak currents were changed from 5.0 kA to 30 kA.

The atmospheric density varies along a lightning flash channel from a cloud to ground. We simulated this density variation by making sparks in room air at a single pressure created in a range from ambient 760 mmHg down to 160 mmHg. The lower pressure sparks were operated as follow, the steel discharge vessel (Figure 4.1) was pumped to the desired pressure, then the system was charged and discharged as normal. After discharging, the vessel was refilled with room air to ambient pressure. Finally, the vessel was flushed and the NO/NO_2 concentration was measured as usual.

Water is of concern in any study of NO_x production by lightning because it has a widely varying concentration in the air in which lightning occurs. In our experiments, we varied the mixing ratio of water vapor in the vessel air and studied the effect of humidity on the NO_x formation. The humidity of vessel air was

regulated though mixing dry air and humid air. The dry air came from a bottle of compressed air with humidity very close to zero. The wet air was the ambient air bubbled through a water tank. After a discharge, the vessel air was sampled and analyzed for its NO and NO_2 concentrations as usual.

5.2 Results and Discussion

A. Spark current and NO production

We have investigated the dependence of NO production on spark peak current (I_{peak}) with sparks 3.2 cm long under ambient pressure. Figure 5.4 shows the measured NO production as I_{peak} increased from 5.0 kA to 30 kA, by charging the main capacitor from 2.4 kV to 10 kV. The value of n_{NO} (NO production per unit length of the simulated lightning channel) increases with I_{peak}. The dependence of n_{NO} on I_{peak} was derived by a quadratic fit of the experimental data, which gives

$$n_{NO}(I)=0.148 + 0.0256\ I_{peak} + 0.0025\ I^2_{peak} \qquad (5.11)$$

where I_{peak} is in kA, and n_{NO} is in 10^{21} NO/meter. The square of the correlation coefficient

is r^2=0.785 (Defined in Chapter IV).

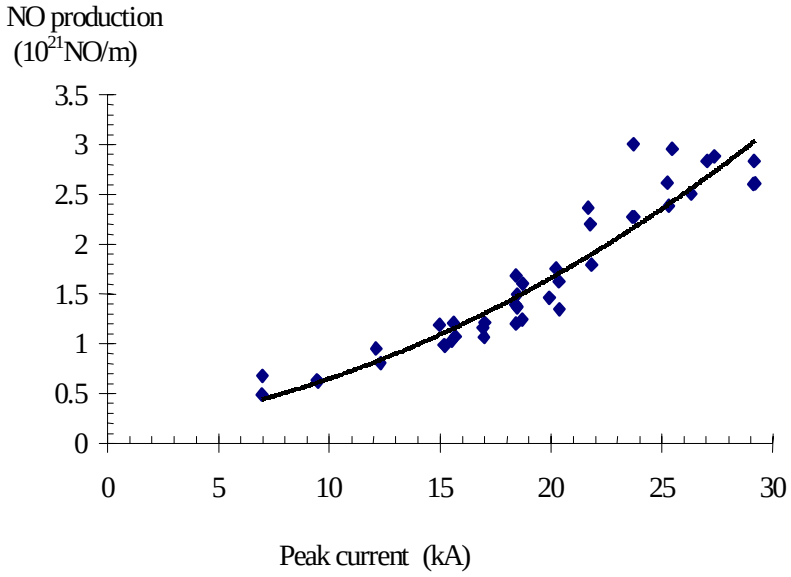

Figure 5.4. NO production per unit length of spark vs. spark peak current

p = 1 atm., T = 298 K, d = 3.2 cm.

In our experiments, 5.0 kA was the minimum peak current for which the system discharged reproducibly. Eq. 5.11 may inadequately represent NO production in the current range below 5.0 kA because we lacked experimental data with lower current. For example, n_{NO} should be zero at some value of peak current greater than zero since for small current inadequate heating may result in no NO production. The observed increase of NO production with spark peak current may be due to a combination of an increase of energy dissipation, spark temperature, and the volume of air involved, or due to the change in turbulent mixing. More detailed information of the spark dynamics is needed to clearly understand this mechanism.

However, the low current range is not important to estimate NO production by lightning because few lightning flashes occur with their peak current less than 5.0 kA. We believe Eq. 5.11 is useful to extrapolate NO production by a long lightning channel or even to estimate global NO production by lightning.

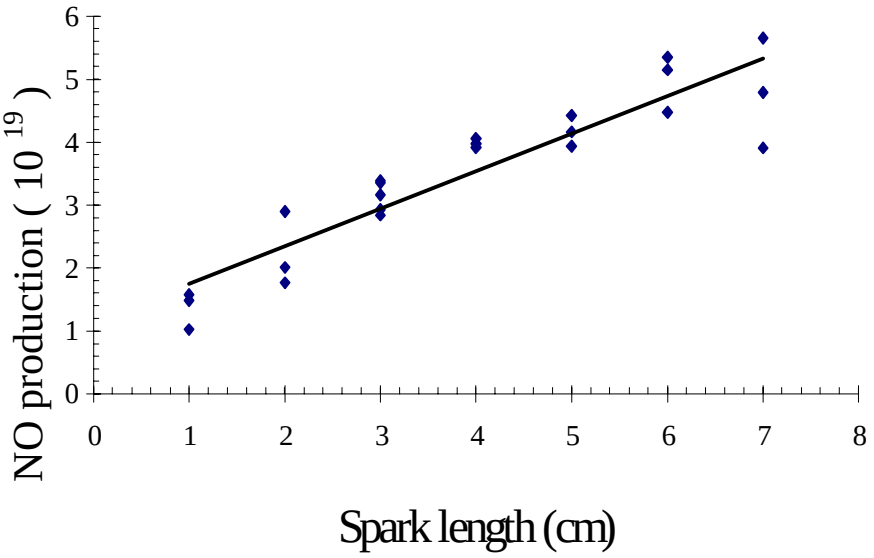

Figure 5.5. NO Production vs. spark length for p = 0.34 x 10^5 Pa., T=298 K, and I_{peak} = 19.0 kA.

B. Electrode end effects on NO production

The scale difference of discharge length has always been a potential problem for extrapolating NO production from experimental sparks to natural lightning strokes because of concerns with electrode end effects. We evaluated the end effects by measuring the NO production as a function of spark length under a fixed pressure

of 0.34×10^5 Pa with room air. The system was operated under a lower pressure than ambient pressure because it was possible to create longer sparks with the possible range of charging voltage on main capacitor bank. When the main capacitor banks were charged to a voltage of 7.0 kV, it could successfully discharge with a spark up to 7.0 cm in length.

Figure 5.5 shows the NO production by sparks with length from 1.0 cm to 7.0 cm. The main capacitor was charged at 7.0 kV so that the spark peak current was 19.0 kA for all of these measurements. A polynomial fit represents the experimental data as

$$N_{NO} = 1.15 + 0.60\ L \qquad (5.12)$$

where L is spark length in centimeters and N_{NO} is NO production in 10^{19} molecules. The square of correlation coefficient is r^2=0.85. The NO production linearly increased with spark length in our experimental range. The polynomial fitting line has an offset of 1.15 x 10^{19} NO molecules at zero of spark length, which implies that there was the electrodes tend to increase the NO production in their vicinities.

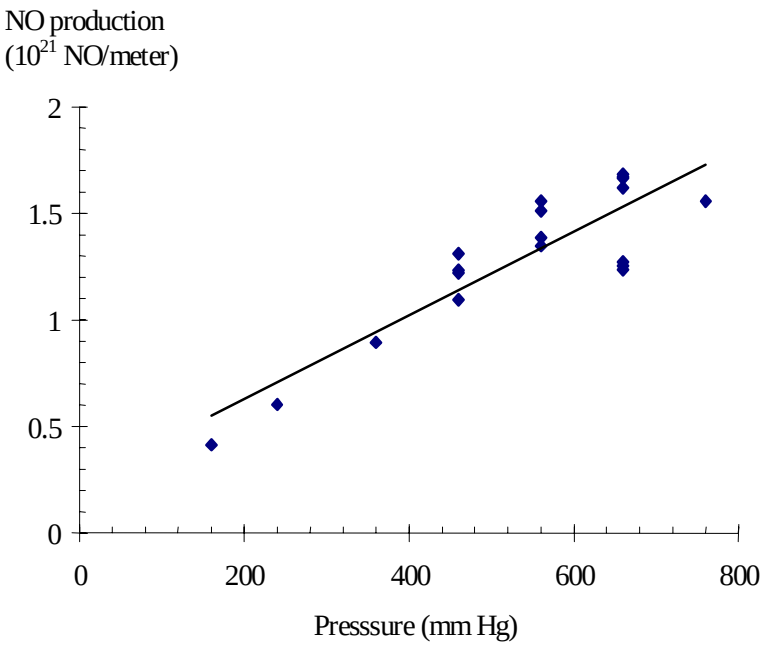

Figure 5.6. NO Production vs. air pressure for p=1 atm, T=298 K, d=3.2 cm, and I_{peak} = 19.0 kA.

C. Air pressure and NO production

Figure 5.6 shows the dependence of NO production on air pressure varying from ambient pressure to 160 mm Hg. It simulated the variation of air density along a lightning flash channel from ground to about 12km. In these measurements, the spark gap was set as 3.2 cm with I_{peak} at 19.0 in room air at a constant temperature (298 K).

The value of n_{NO} is proportional to the air pressure in the pressure range of our observations. A polynomial fit of the data gives

$$n_{NO} = 0.236 + 0.00196\ p \qquad (5.14)$$

where p is in unit of mm Hg, n_{NO} is in unit of 10^{21} NO/meter. The square of the correlation coefficient is $r^2 = 0.776$. The fit curve has an offset of 0.236 $x10^{21}$ NO/meter. It could be caused from the error of NO concentration measurements or because of the different chemical and physical process involved in the NO production as the air density tends to zero. If it was from measurement error, this offset corresponds to an average NO concentration of 28.8 ppb at flushing rate of 200 Liters/minute, which is much greater than the experimental error. Thus, the NO production mechanism as air density tends to zero may well be different from that at ambient pressure. Although it may be incorrect at very low density, the above equation should be applicable to NO production by natural cloud to ground and cloud to cloud lightning.

D. Spark energy dissipation and NO production

The correlation between spark energy and NO production (Figure 5.7 and Figure 5.8) was investigated with the group of discharges presented in Figure 5.4. The energy dissipated in a spark column (referred as spark energy) was directly calculated with Eq. 4.7 using the profile of spark current and the voltage across the spark (Chapter IV). As the spark peak current increased from 5 kA to 30 kA, the spark energy increased from 4 to 9 kJ/meter. NO production, n_{NO}, increases with the spark energy as usually assumed, but the data are very scattered (Figure 5.7) and it is very difficult to figure out the dependence of n_{NO} on spark energy. If the data are fit with a quadratic function, the square of correlation coefficient is only r^2=0.593.

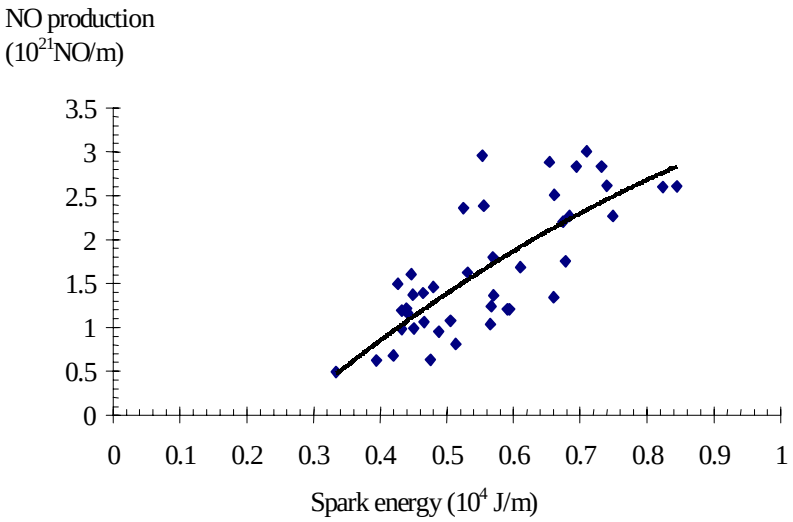

Figure 5.7. NO production vs. spark energy dissipation with p= 1 atm., d= 3.2 cm, T=298 K, and I_{peak} = 5 ~ 30 kA.

As discussed in chapter III, the NO yield of a lightning stroke is usually determined by two parameters: the NO mixing ratio when NO is "frozen out" from a spark channel and the amount of air mixture involved. The mixing ratio is determined by the thermochemical equilibrium of NO formation and destruction which depend on the energy transport process as well as the total amount of energy dissipated. The air amount is determined by the increase in radius of the discharge channel and its turbulent mixing with the surrounding air. Therefore, the turbulent mixing phase of a spark channel with its surrounding air may impact strongly on the "freezing" of the produced NO from the hot spark channel. Hill (1980) pointed out that if the hot channel expands adiabatically and only loses its energy by radiation, over 43% of the formed NO would be reconverted to N_2 and O_2 when the hot channel cools to ambient temperature. If the hot channel cools down rapidly to

ambient temperature by a quickly mixing with the surrounding cold air, only 2% of the formed NO are destroyed.

Figure 5.8 plots the p_{NO} (NO production per unit of energy) as a function of spark peak current I_{peak}. It has a similar dependence to n_{NO} shown in Figure 5.4 in that p_{NO} depends on I_{peak}. As I_{peak} increases from 5.0 kA to 30 kA, p_{NO} increases from 10 to 40×10^{16} NO/Joule. A quadratic fit of the data gives

$$p_{NO}(I) = 0.211 + 1.699\ I_{peak} - 0.0104\ I_{peak}^2 \qquad (5.13)$$

where the unit of $p_{NO}(I)$ is 10^{16} NO/J and the unit of I_{peak} is kA. The square of correlation coefficient is r^2=0.645.

The value of p_{NO} has been taken as the basis of estimating the NO_x production by lightning in theoretical calculations and experimental simulations with pulse sparks (Chameides et al., 1977; Levine, 1981; Peyrous and Lapeyre, 1982; Stark et al., 1996). It has been taken as a constant that is independent of the discharge process, and NO production by a lightning flash has been calculated by multiplying p_{NO} with lightning energy (Lawrence et al, 1995; Price et al., 1997). Results of our experimental demonstrate that the correlation between NO production and spark energy is very complicated rather than a linear dependence. Further study of energy transformation processes and the dynamic expansion of the spark channel are necessary to understand the dependence of NO production on spark energy dissipation.

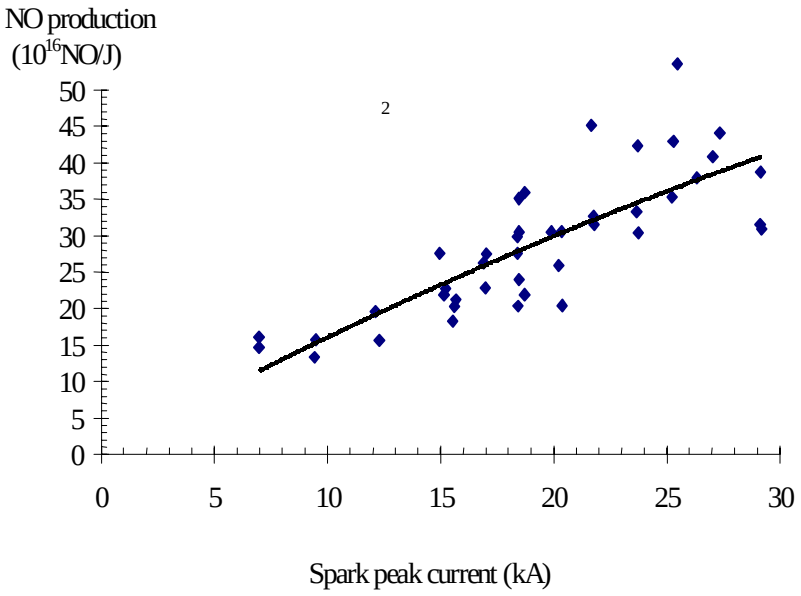

Figure 5.8. NO production per unit energy vs. spark peak current with p = 1 atm, d = 3.2 cm, and T=298 K.

The observed p_{NO} is greater than the previously reported results of simulations or observation in laboratory sparks. For example, the p_{NO} of a typical natural lightning spark has been reported from 1.6 to 17×10^{16} NO/Joule (Lawrence et al, 1995; Stark et al., 1996). The p_{NO} by a simulated spark with peak current of 30 kA (the mean of peak current for the first strokes of natural lightning is about 36 kA), is 40×10^{16} NO/Joule in our experiments. This discrepancy of the p_{NO} values may be caused by the different energy accounting used in our results. In most previously reported works, the stored energy was used as the energy to calculate NO (Chameides et al., 1977; Levine, 1981; Stark et al., 1996). In our experiments, only the energy dissipated in a spark was used as the energy to produce NO. The diagnostics of experimental sparks in the last chapter has showed that less than 1%

of the energy stored in the capacitor bank was dissipated in the discharge channel. If this stored energy was accounted as the energy to produce NO, p_{NO} would be 0.15 – 0.30 x 10^{16} NO/Joule for the sparks with peak current from 5.0 kA to 30 kA.

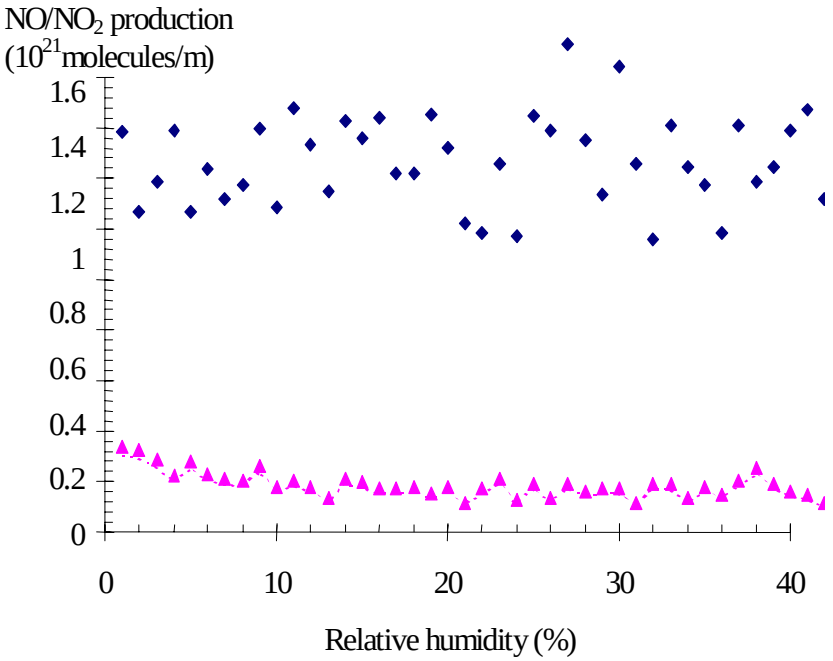

Figure 5.9. NO/NO_2 production vs. humidity of vessel air with P= 1atm, d = 3.2 cm, and I_{peak} = 19.0 kA. The water mixing ratio is normalized to the relative humidity at 298 K under ambient pressure. Upper series-- NO production, lower series -- NO_2 ($NO_2 = NO_x - NO$) production.

E. Air humidity and NO production

Figure 5.9 shows NO_x production versus the humidity of the initial vessel air under ambient pressure. The spark gap was set to 3.2 cm and discharges with a peak current of 19.0 kA were used. The temperature and humidity were monitored for each discharge, and the results are presented with humidity normalized to 298 K

under atmosphere pressure. As the normalized relative humidity increases from 0% to 40%, NO production is almost a constant at 1.5×10^{21} NO/meter, with a standard deviation of 7%. About 11% of NO produced oxidized into NO_2.

The effect of water vapor on NO_x formation by lightning sparks has previously been examined experimentally (Chameides et al., 1977; Levine et al., 1981; Peyrous and Lapeyre, 1982; Stark et al., 1996). Different results were reported on either total NO_x yield or NO/NO_2 ratio produced by lightning discharges but no convincing mechanism has been proposed. Our experiments show that water has little effect on NO_x production, and that the variation of the NO amount and the NO/NO_2 ratio was less than experimental uncertainty in a wide humidity range.

F. NO oxidation

The humidity of vessel air was regulated over a large range and the initial air temperature varied day by day, but Figure 5.9 shows that the NO/NO_2 ratio is almost constant for all of these sparks. The results confirm Hill's (1980) simulation and the observations of Stark et al. (1996). The NO oxidation is dominated by the long time oxidation by O_3 after discharge (Hill, 1980) rather than the simultaneous reaction between O_2 and NO in the hot spark channel.

Before we discuss NO oxidation quantitatively, let us estimate the NO concentration in the reaction vessel immediately following a discharge. The NO yield was 5.2×10^{19} molecules by a typical spark of 3.2 cm longth with peak current of 19.0 kA. The volume of the reaction vessel is about $1m^3$. Thus, the NO concentration was approximately 5.2×10^{13} cm^{-3} or 2.1 ppm after completely

mixing, which is about the same order as that in atmosphere after a lightning flash (Chapter III).

In Chapter III, we had estimated that the half lifetime of NO is about two days for an initial concentration of 1 ppm if it was only oxidized by atmospheric O_2. In our experiments, the flushing rate was set about 200 L/minute, so the resident time of an air mixture in the reaction vessel was about 5 minutes. In 5 minutes, less than 1% of the produced NO could be oxidized by atmospheric O_2. The atmospheric O_3 should less than 0.05 ppm. As an extreme case, suppose all the atmospheric O_3 reacted with the NO before the NO produced were directed into the NO_x analyzer, then about 0.05 ppm or 2.5% of the NO produced would have been oxidized. Figure 5.9 shows that about 11% of NO produced by a simulated lightning spark were oxidized into NO_2. Therefore, NO oxidation was enhanced by the O_3 produced during discharge.

O_3 production by lightning discharges has been studied in field observations (Orville, 1967) and in pulsed discharges at ambient pressure (Donole et al., 1977). Absorption by ozone of the radiation emitted by the return stroke channel has been observed, but without being able to determine the ozone's location (Orville, 1967). A convincing model of O_3 production by lightning discharges has also been developed (Hill, 1979). It suggests that a hot lightning channel generates strong UV radiation, especially during the ohmic heating phase of the spark. The UV radiation photolyzes the oxygen molecules and produces a large amount of O_3 in the corona discharge sheath of the spark channel (Stark et al., 1996). Hill (1979) estimated that at microsecond times there is a significant percentage (~ 1%) of oxygen molecules,

which is photolyzed into O_3, in a thin cool layer of ambient air surrounding the channel.

However, if it is accepted that NO_2 is formed by the reaction of O_3 with NO after a discharge, then the presence of water must have a significant effect on the NO/NO_2 ratio. Figure 5.9 shows that the NO/NO_2 ratio has been a constant over a large range of water mixing ratio. Thus, in order to understand the mechanism of NO oxidation, it is necessary to directly measure O_3 production and to monitor the variation of the concentrations of NO, NO_2 and O_3 in future work.

5.3 Summary

The measurements of NO production showed that NO production by a lightning flash strongly depends on the current, the energy deposition and the dynamic discharge process. We have estimated the NO production per unit of energy, p_{NO}, based on the observed energy dissipation. The p_{NO} increases with the energy dissipated in spark channel, rather than being a constant as assumed in most estimates of the global NO_x production by lighting. The observed value of p_{NO} was always greater than the previously reported data.

The NO production per unit of spark length, n_{NO}, strongly depends on the spark peak current and is proportional to the density of initial air in the range that correspond to the atmospheric density from a cloud to ground. The results imply that the NO production by a long lightning channel could be predicted with its peak current and the variation of air density along the spark channel. Once the peak current and discharge path of a lightning are known, the n_{NO} could be uniquely

determined along its discharge channel from ground to its origin in a cloud. Because the peak current is a better known parameter of global lightning flashes, we will be able to limit the uncertainty to estimate the global NO_x production by lightning using the peak current data of global lightning.

Neither the total amount of NO_x nor the ratio of NO/NO_2 was affected by the presence of water in the initial air. About 11% of NO produced by a spark oxidized into NO_2. The oxidation appears to be dominated by the long time oxidation by O_3 after a discharge. The oxidation was enhanced by the O_3 produced during discharging.

Chapter VI Estimates of Global NO_x Production by Lightning

In the following discussion, we estimate global NO_x production by lightning using the Flash-Extrapolation-Approach (FEA) (Lawrence et al., 1995). The approach calculates global NO production by lightning as

$$G_{NO} = g_{NO} f_{flash} \quad (6.1)$$

where g_{NO} is average number of NO molecules produced by a typical lightning flash, and f_{flash} is global lightning flash frequency. The g_{NO} is estimated from the experimental results reported in the previous chapter and lightning data obtained over the US (Orville, 1994; Price et al., 1997). The f_{flash} is determined from the recently reported data of global lightning flashes (Lawrence et al., 1995; Price et al, 1997). After calculating G_{NO} with Eq. 6.1, we discuss the global NO_x production by lightning with inclusion of the oxidation the NO after the discharge.

The typical lightning flashes used in Eq. 6.1 are defined as ideal CG flashes, which have an average number of strokes, discharge along an average channel of lightning flashes from cloud to ground, and yields an average NO amount. There are different kinds of lightning flashes, but this typical lightning flash only represents the "average" of cloud-ground flashes (CG), one of the two primary types of lightning flashes (Chapter II), because they have been better understood in their characteristics and frequency. Similarly, the f_{flash} only includes the global CG flashes. Intracloud flashes (IC) are not discussed in detail because of the great uncertainty surrounding them.

6.1 Determination of NO Production Per Flash

The value of g_{NO} has previously been estimated from field observations of NO_x enhancements under thunderstorms, theoretical simulations of NO_x production by lightning strokes and studies of NO_x production by laboratory discharges. The field observations calculated g_{NO} from the enhanced NO_x concentrations in the vicinity of lightning flashes and the estimated volumes of the storms (Noxon, 1976, 1978), as well as from the enhanced NO_x concentrations from distant lightning flashes and the modeling NO_x dispersion after lightning flashes (Drapcho et al., 1983; Franzblau and Popp, 1989). Theoretical and laboratory approaches generally estimated g_{NO}

$$g_{NO} = p_{NO} E_f \qquad (6.2)$$

where p_{NO} is NO production per unit of discharge energy, and E_f is the energy dissipated by a typical lightning flash.

A. Estimate of NO production from lightning peak current

The use of a constant parameter p_{NO} has always been a potential problem in previous estimates of NO production (Hill, 1979; Goldenbaum and Dickerson, 1993; Stark et al., 1996. For example, p_{NO} of IC flashes could be different from that of CG flashes because IC flashes occur in atmospheric regions with pressure much lower than ground pressure, and they usually dissipate much less energy than CG flashes. The experimental results reported in the last chapter demonstrated that p_{NO} strongly depends on lightning characteristic, such as discharge current, and energy dissipated. In order to avoid the large uncertainty caused by using p_{NO} to estimate

g_{NO}, we utilize a different parameter, n_{NO}, the NO production per unit of spark length based on experimental results.

In the last chapter, observations showed that n_{NO} depends on spark peak currents and the air pressure in which the discharges occur. The dependence of n_{NO} on spark peak current and the pressure of initial air were expressed in Eq. 5.14 and Eq. 5.15 respectively with polynomial fitting to the experimental data. In Chapter IV, we discussed that our laboratory sparks match natural lightning flashes very well in current profile, energy dissipation and the expansion of discharge channel. Therefore, if similar correlations exist between NO production by natural lightning discharges and their peak current, we could extrapolate these equations to a long lightning spark channel. Then, the NO yield of a vertical lightning stroke with peak current I is

$$q_{NO}(I) = \int_0^h n_{NO}(I, z)\, dz \qquad (6.3a)$$

where h is length of a lightning stroke from ground to the lightning origin in cloud, I is peak current of the stroke, and $n_{NO}(I,z)$ is NO production per unit length of the stroke at altitude z. Because peak currents are better known than all other parameters of natural lightning flashes, the accuracy of g_{NO} could be greatly improved by using observation data of lightning currents.

Most CG flashes have more than one return strokes through the discharge channel initialized by the first stroke. NO production by a multi-stroke flash should include that produced by all of its strokes,

$$
\begin{aligned}
Q_{NO}(I_1) &= \sum_j q^j_{NO}(I_j) \\
&= \int_0^h \sum_j n_{NO}(I_j, z)\, dz \\
&= \int_0^h m_{NO}(I_1, z)\, dz
\end{aligned}
\tag{6.3b}
$$

where j denotes the multiplicity of a multi-stroke flash, I_j is the peak current of the stroke j, and I_1 is the peak current of the first return strokes or I_j at j=1. NO production per unit length of discharge channel at altitude z is expressed as $m_{NO}(I_1,z)$, which sums NO production of all return strokes in that flash and is referred to I_1. In a multi-stroke flash, all strokes always flow through the same discharge channel, so the order of summation and integration are exchangeable in Eq. 6.3b.

Calculating the NO yield of each lightning flash using Eq.6.3b, then NO production by an "average" lightning flash can be determined as

$$
\begin{aligned}
g_{NO} &= \frac{\sum_k Q_k(I_{1k})}{f_{flash}} \\
&= \frac{\sum_k \int_0^{Hk} m_{NO}(I_{1k}, z) dz}{f_{flash}}
\end{aligned}
\tag{6.4}
$$

where H_k is the length of discharge channel of a multi-stroke flash, and I_{1k} is the peak current of the first stroke of that flash. The summation is over all CG flashes that occur annually over the globe.

B. Average NO production per unit length of flash channel

To calculate g_{NO} with Eq. 6.4, it is necessary to know the discharge path and current information of all global lightning flashes. Practically, this calculation has to be simplified because only statistical information is available for global lightning

flashes. Suppose all flashes discharge through an "average" channel, then the g_{NO} can be computed by

$$\begin{aligned} g_{NO} &= \int_0^{\infty} F(I_1)dI_1 \int_0^{H} m_{NO}(I_1, z)dz \\ &= \int_0^{H} dz \int_0^{\infty} m_{NO}(I_1, z)F(I_1)dI_1 \\ &= \int_0^{H} m_{NO}(z)dz \end{aligned} \tag{6.5}$$

where $F(I_1)$ is the normalized distribution function of flash frequency vs. I_1, the peak currents of the first strokes. The g_{NO} is obtained by integrating the $m_{NO}(z)$, NO production by per unit of discharge channel of the "average" discharge at altitude z, along an average discharge channel.

If all multi-stroke flashes have the same multiplicity, the same flash frequency distribution function $F(I_1)$ can be used to represent the frequency distribution of all the corresponding subsequent strokes. Then $m_{NO}(z)$ could be determined from Eq. 6.3b and $F(I_1)$ as

$$\begin{aligned} m_{NO}(z) &= \int_0^{\infty} m_{NO}(I_1, z)F(I_1)dI_1 \\ &= \int_0^{\infty} [\sum_j n_{NO}(I_j, z)]F(I_1)dI_1 \\ &= \sum_j [\int_0^{\infty} n_{NO}(I_j, z)F(I_1)\, dI_1] \\ &= \sum_j n_{NO}^{j}(z) \end{aligned} \tag{6.6}$$

where I_j is the peak current of the j^{th} stroke of a multi-stroke flash. The term of $n_{NO}^{j}(z)$ is the NO production per unit length of the spark of the j^{th} stroke at altitude z along the "average" flash channel, and $m_{NO}(z)$ is NO production by all strokes in the "average" flash.

The data leading to Eq. 5.13 were obtained with simulated lightning sparks under ambient pressure. If this equation is extrapolated to the NO production of

natural lightning strokes, it represent the NO production per unit of a natural lightning stroke at z=0. The global average NO production by a stroke at ground level could be determined using the $n_{NO}(I)$ expression of Eq. 5.13 and the flash frequency distribution function $F(I_1)$. Figure 2.3 shows the frequency distribution on peak current for negative (98.7% of these flashes) and positive flashes. It is extracted from the lightning data over the US that was obtained by the US National Lightning Detection Network (NLDN) (Orville, 1994; Price, 1997) for the period June-August 1988. The NLDN network observed only CG flashes, supplying information on polarity, multiplicity, and the peak current of the first return stroke.

Substituting the flash frequency distribution function $F(I_1)$ and $n_{NO}(I, z)$ at z=0 into Eq. 6.6, the average n_{NO} by the first return stroke of negative flashes at z=0 is

$$n_{NO}^{-1}(z=0) = 5.5 \times 10^{21} \text{ NO/meter} \qquad (6.7a)$$

Price et al. (1997) suggested that subsequent strokes have a peak current about 43% of that of the primary stroke. Using the corresponding peak current and the same flash frequency distribution function, the average n_{NO} by a subsequent stroke at z=0 level is

$$n_{NO}^{j}(z=0) = 1.4 \times 10^{21} \text{ NO/meter}, \quad j > 1 \qquad (6.7b)$$

Price et al. also represented the average multiplicity (strokes/flash) as a function of lightning frequency (flashes/minute) in Figure 2 of their paper, which indicates an average multiplicity of 2.8 strokes/flash. If the NO produced by each stroke is "frozen out" to its surrounding air before a subsequent stroke, the average n_{NO} over global negative flashes at z=0 is

$$n^{-}_{NO}(z=0) = n^{-1}_{NO}(z=0) + 1.8\, n^{-j}_{NO}(z=0)$$

$$= 6.8 \times 10^{21} \text{ NO/meter} \qquad (6.7c)$$

If positive and negative flashes are equivalent in NO production, the average NO production $m_{NO}(z)$ at z=0 over global positive flashes can be calculated using the flash frequency distribution function for positive flashes shown in Figure 2.3b. The majority of positive flashes have only one return stroke (Price et al., 1997; Berger et al., 1975), so the average n_{NO} for global positive flashes at z=0 is

$$n^{+}_{NO}(z=0) = 13.0 \times 10^{21} \text{ NO/meter} \qquad (6.7d)$$

Positive flashes occur much less frequently than negative flashes. Price et al. reported that there is less than 2% of flashes are positive in their data of the lightning in the US. Berger et al. found that about 20% of flashes were positive in observations at Mount San Salvatore. Assuming 5% of global flashes are positive flashes, the value of n_{NO} for global "average" typical lightning flash at z=0 is

$$m_{NO}(z=0) = 0.95\, n^{-}_{NO}(z=0) + 0.05\, n^{+}_{NO}(z=0)$$

$$= 7.1 \times 10^{21} \text{ NO/meter} \qquad (6.8)$$

C. Average NO production per flash

The undisturbed atmosphere could be modeled as an ideal gas with a linear lapse rate of temperature $B=6.5 \times 10^{-3}$ K/m (Seinfeld, 1986). Since the air pressure at each altitude is the weight of all the air above, the pressure differential is

$$dp = - g\rho(z)dz \qquad (6.9)$$

Eliminating ρ with the ideal gas equation

$$p = \frac{RT}{M}\rho \tag{6.10}$$

After integration over z, the pressure can be expressed as

$$p = p_0 \exp(-\int_0^z \frac{gM}{RT} dz) \tag{6.11}$$

Substituting the temperature lapse rate into (6.11), then it becomes

$$p = p_0 (\frac{T_0 - Bz}{T_0})^{\frac{gM}{BR}} \tag{6.12}$$

where R = 8.314 J/mol.K, g = 9.8 ms^{-2} , M = 28.96 g/mol. T_0 = 288 K is the model atmosphere temperature at ground level, $p_0 = 1 \times 10^5$ Pa is the model pressure at ground level. Using the idea gas equation, atmosphere density is

$$\rho = \rho_0 (\frac{T_0 - BZ}{T_0})^{\frac{gM}{BR} - 1} \tag{6.13}$$

where ρ_0 =1.209 kg/m^3, the model atmosphere density at ground level.

Eq. 5.14 represented NO production by simulated lightning sparks with a constant peak current of 19.0 kA under different air pressure. The value of $n_{NO}(I)$ is proportional to air pressure in a pressure range from ground to cloud. Actually, $n_{NO}(I)$ with a constant peak current should depend on air density if the variation of initial temperature is negligible. We can rewrite Eq. 5.14 as

$$n_{NO}(I, \rho) = a + b\rho \tag{6.14}$$

Using the ideal gas equation and the coefficients in Eq. 5.14, NO production by a spark with peak current I_{peak}=19.0 kA is

$$n_{NO}(z) = 0.236 + 1.470 \times 10^{-5} \times \frac{RT_{lab}\rho}{M} \tag{6.15}$$

where ρ is air density, T_{lab} = 294 K is the laboratory temperature at which the

measurements leading Eq. 5.14 were made. Modifying the coefficients of Eq. 6.15 by multiplying the ratio of $m_{NO}(z=0)/n_{NO}(I=19.0\ kA, z=0)$, NO production per unit length of discharge channel by an "average" typical flash at altitude z is

$$m_{NO}(z) = 1.093 + 6.805\times10^{-5} \times \frac{RT_{lab}\rho(z)}{M} \tag{6.16}$$

where $\rho(z)$ is atmosphere density varying along the flash channel.

Substituting Eq. 6.16 into Eq. 6.5 and integrating it along the "average" lightning path, the NO yield of the "average" lightning flash is

$$g_{NO} = 1.093\,H + 6.805\times10^{-5} \times \frac{RT_0\rho_0}{M} \times \frac{T_{lab}}{B\delta}(1-A^{\delta}) \tag{6.17}$$

where $\delta = gM/BR = 5.254$, $A=1-BH/T_0$. A typical cloud ground flash origin from about 6 km above earth surface, or H=6000 m, thus g_{NO} is given by

$$g_{NO} = 3.78\times10^{25}\ \text{NO/flash} \tag{6.18}$$

This is the NO yield of a lightning flash discharging vertically from cloud to ground, globally averaging over both positive and negative flashes with multi-strokes.

The discharge channel of a natural lightning flash is always tortuous. This tortuosity should be accounted to extrapolate g_{NO} from our experimental results of sparks which are considerably shorter than natural lightning. It was estimated as $H_{total}/H = 3.6$ for a typical lightning path of 6 km long (Wang et al., 1998), using a theoretical model based on a random walk of constant step between two endpoints. Including the tortuosity of discharge channel, the average NO production by a typical CG lightning flash is

$$g_{NO} = 1.36\times10^{26}\ \text{NO/flash.} \tag{6.19}$$

6.2 Global Flash Frequency

Price and Penner (1997) estimated the frequencies of CG and total flashes using the International Satellite Cloud Climatology Project (ISCCP) data set intervals from July 1983 to June 1991, which provided global convective cloud data at three hour interval (Rossow and Schiffer, 1991). They used the top height of the convective cloud as the predictive variable to estimate total lightning frequencies over a thunderstorm. The fraction of CG lightning in a storm was determined by the thickness of the cold cloud portion of the cloud (0 ^{o}C to cloud top) using an empirical method. They found that lightning primarily occurs over continental regions, mainly in the summer hemisphere, 64% of which (annual mean) occurs in the northern hemisphere because of large land areas. Consequently, lightning frequency exhibits a clear annual cycle with a maximum during the northern hemisphere summer. The annual mean of total global flash frequency is about 90 flashes/s with a monthly maximum of 101 flashes/s in July and a monthly minimum of 71 flashes/s during January. The annual mean of the global CG flash frequency is about 25 flashes/s, the monthly maximum is 30 flashes/s in July and the monthly minimum is 19 flashes/s in January.

Lawrence et al. (1995) reviewed the data of global frequencies adopted in the estimates of NO production by lightning. They found that global flash frequencies obtained from different observations were remarkably consistent. Much of the variation in the estimates of global flash frequencies could be attributed to confusion over the roles of CG and IC flashes. Some studies have assumed that the

value of 100 flashes/s includes both CG and IC. Others have assumed that the value of 100 flashes/s from ground-based observation only accounted for CG, requiring the addition of IC. They suggested that a total global flash frequency of 100 (70-150) flashes/s including both the CG and IC flashes, which agrees very well with the results of Price and Penner's calculation about the total lightning frequency.

In this calculation, we take 25 flashes/s and 100 flashes/s as the lower and upper limit of the global total CG flash frequency respectively.

6.3 Global NO_x Production

Combining the estimated NO production by a typical CG flash and the global flash frequency, we can determine the global NO productions by CG lightning with the FEA,

$$G_{NO} = g_{NO} f_{flash} \qquad (6.1)$$

Using $g_{NO} = 1.36 \times 10^{26}$ NO/flash, G_{NO} is 2.56 TgN/year for the global CG lightning frequency of 25 flashes/s and 10.3 TgN/year for 100 flashes/s. Experimental results discussed in the last chapter showed that about 11% of the NO produced oxidized into NO_2 after the discharges (Chapter V). Including the NO_2 produced, the NO_x yield of an "average" CG flash is 1.51×10^{26} NO_x/flash and the global NO_x production by lightning is from 2.84 to 11.4 TgN/year.

In the above calculation, we derived the global NO_x production from lightning data obtained in the US that may be different from global data. For example, Price et al estimated (1997) the mean peak current as 36 kA for the first return strokes of negative CG flashes using the lightning data obtained in the US.

Other observations reported the mean peak current of CG flashes from 20 to 30 kA. In addition, we adopted a similar average flash frequency for both the first return strokes and their subsequent return strokes of multi-stroke flashes. It assumes implies that on average all multi-stroke flashes have the same number of strokes and the same ratio of stroke peak currents. Actually, the numbers vary from storm to storm and from flash to flash.

Although there might be a considerable error in this estimate, we believe that 11.4 TgN/year is the upper limit and 2.84 TgN/year should be the lower limit. The upper limit was given by a lightning flash frequency of 100 flashes/s that includes both CG and IC flashes. It may overestimate the global NO_x production because CG and IC were accounted equivalently to produce NO_x. The lower limit was given by a lightning flash frequency of 25 flashes/s that ignored all IC flashes. It may underestimate the global NO_x production.

6.4 Conclusion

We have estimated NO_x yield of an "average" CG flash as 1.51×10^{26} NO_x/flash using the lightning data obtained in the US and the experimental measurements of NO_x production by the simulated lightning. The total NO_x production by the "average" flash includes the NO_x produced by all its strokes. The "average" CG flash was modeled as an annul average of CG flashes that annually occur over the globe, which averages the global CG flashes with the following values

Channel length = 6.0 km

Channel tortuosity = 3.6

Stroke multiplicity of negative flashes = 2.8 strokes/flash

Stroke multiplicity of positive flashes = 1 strokes/flash

Negative flashes = 95% of global flashes

Positive flashes = 5% of global flashes

The "average" flash occurs in an ideal atmosphere which was modeled with the following parameters:

Temperature lapse rate along flash channel = 6.5×10^{-3} K/m

Atmosphere temperature at ground level = 288 K

Atmosphere pressure at ground level = 1×10^{5} Pa.

The global NO_x production by lightning was estimated as 2.84 to 11.4 TgN/year using the Flash-Extrapolation-Approach. The lower limit was calculated by a global CG flash frequency of 25 flash/s ignoring the NO_x produced by IC flashes. The upper limit was calculated with a total global flash frequency of 100 flashes/s (including both the CG and IC flashes) assuming IC flashes and CG flashes are equivalent in producing NO_x. This estimate implies that lightning may have been overestimated as a source of atmospheric NO_x. In urban areas, the NO_x produced by lightning is swamped by the NO_x production from burning of fuel and biological processes at a combined rate of about 30 TgN/year (Chapter I). In remote areas, the NO_x produced by lightning may be responsible for the atmospheric NO_x because the NO_x levels there are 10^{-3} -- 10^{-4} times lower than that in urban areas (McFarland et al., 1979; Emmons et al., 1997).

More work remains to be undertaken to reach a more reliable estimate of the

global NO_x production by lightning. The lightning characteristics should be examined on a more specific aspects, such as multiplicity of flash, current profile of each stroke, and tortuosity of each flash channel, rather than simply on the peak current of its first return stroke. More field observations in regions other than the U.S., particularly in remote tropical regions, are necessary to evaluate the budget of lightning NO_x. To apply the experimental observations to a natural lightning stroke, more measurements are necessary to study NO_x by simulated lightning with varying other parameter, such as the current rise time, large peak current. More theoretical and experimental work is necessary to understand the dynamics of a lightning channel in order to evaluate the NO_x production by a lightning spark.

Appendix. Atmospheric Nitrogen Oxides

The atmospheric nitrogen oxides (NO and NO_2) are emitted by natural and anthropogenic sources. Globally, the total of natural sources has been estimated to be approximately the same as anthropogenic emissions. In urban regions, anthropogenic emissions are greater than that from natural sources, while remote tropic regions are dominated by the natural emissions. These compounds participate importantly in atmospheric chemistry. In the troposphere, they are responsible for the photochemical production of smog, production of other atmospheric oxidants, and acid deposition; in the stratosphere, they are involved in the depletion of the ozone layer. This appendix will describe the sources of the atmospheric NO_x and their influence on atmospheric chemistry.

A.1. Sources of Atmospheric NO_x

Estimated global emissions of NO_x have been given in Table 1.1. The global anthropogenic emissions are primarily attributed to fossil-fuel combustion and soil release from fertilizers. The natural processes include biomass burning, lightning fixation, the ionization of N_2 by cosmic radiation and other small contributions. In order to evaluate the impact of NO_x on atmospheric chemistry and global climate change, both the anthropogenic and natural sources must be considered and their relative importance needs to be evaluated.

A.1.1. Biological sources

Nitrogen in living matters is largely as amino compounds or ammonium ions, while amino acids present can be broken down into ammonia,

$$NH_2CH_2COOH + \frac{3}{2}O_2 \rightarrow 2CO_2 + H_2O + NH_3 \quad (A.1)$$

Ammonia and ammonium ion can be absorbed by plants directly. When environmental conditions are reasonable alkaline, ammonium ions in living matters and soils could be released directly into the atmosphere as gaseous ammonia.

Microbial activities, including nitrification and de-nitrification, take nitrogen-containing compounds such as NH_3, N_2O, and HNO_3 and release NO_x into the atmosphere (Burns and Hardy, 1975). Nitrification, performed by some specialized microorganisms, oxidizes ammonia into nitrite. These bacteria use ammonia as an energy source in the same way as other cells use the reduced carbon compounds such as carbohydrates

$$NH_3 + \frac{3}{2}O_2 \rightarrow NO_2^- + H_2O + H^+ \quad (A.2)$$

Nitrobacteria further oxidize nitrite into nitrate

$$NO_2^- + \frac{1}{2}O_2 \rightarrow NO_3^- \quad (A.3)$$

De-nitrification is the reverse process performed by numerous micro-organisms. Often these processes are performed by nitrate respiration of aerobic bacteria, which use nitrate to oxidize carbohydrates when oxygen becomes limited.

$$C_6H_{12}O_6 + 6NO_3^- \rightarrow 6CO_2 + 3H_2O + 6OH^- + 3N_2O \quad (A.4)$$

$$5C_6H_{12}O_6 + 24NO_3^- \rightarrow 30CO_2 + 18H_2O + 24OH^- + 12N_2 \quad (A.5)$$

These reactions emit N_2 or N_2O into atmosphere. The N_2O, predominantly emitted

by biological activities from soil and water, has a very long residence time (~100 years) in the atmosphere. It could also diffuse into the stratosphere. Where it may be further oxidized into NO as the principal natural source of NO_x in the stratosphere.

A.1.2. Atmospheric sources

Reactions in the atmosphere are the major direct sources of atmospheric NO_x. These reactions include fixation of nitrogen by lightning, reactions induced by incoming cosmic radiation, and a small portion from extraterrestrial materials. Lightning has long been recognized as the most important natural source of atmospheric NO_x. Especially in remote tropical region, where it is believed to be the dominant source.

Lightning heats air in its discharge column to high temperature and fixes nitrogen via the reaction

$$O_2 + N_2 \leftrightarrow 2NO \qquad (A.7)$$

and further

$$O_2 + 2NO \leftrightarrow 2NO_2 \qquad (A.8)$$

At high temperature, the oxidation of nitrogen (A.7) proceeds rapidly. As the hot air column cools quickly by its cold surrounding air, the thermochemical reaction A.7 does not remain in equilibrium during cooling and the NO formed at high temperature could be “frozen out”. The NO yield of a lightning depends on both the temperature and the rate of cooling. If the reacted gas mixture cools slowly the yield of nitrogen oxides is low because there is enough time for the reactants to be reformed. Large uncertainty exists in the estimates of the global NO_x production

because of the quantitative uncertainty of the NO_x production mechanism by a lightning discharge and the limited resources of global lightning data.

A.1.3. Combustion of fuels

Combustion is the major anthropogenic source of atmospheric nitrogen oxides, resulting from both the interaction of nitrogen in the fuel with oxygen in air and the chemical conversion of atmospheric nitrogen and oxygen at the high temperature of combustion. Estimated global emissions of NO_x from fossil-fuel combustion increased from 18.1 TgN/year in 1973 to 24.3 TgN/year in 1986 (Hameed and Dignon, 1992). The nitrogen contained in fuel can be converted to ammonia or hydrogen cyanide and then rapidly form NO. Combustion takes place in air which predominantly consists of nitrogen and oxygen, so the high temperatures in the combustion process may encourage NO_x formation with the same reactions that occur in the hot air column of lightning (A.7, A.8).

In an internal combustion engine, the reaction rates may be too slow to allow direct NO_x production. However, NO could be produced indirectly during the combustion of fuels. In the case of the combustion of hydrocarbons, the presence of the CH radical can lead to the rapid formation of hydrogen cyanide

$$N_2 + CH \rightarrow HCN + N \qquad (A.9)$$

The hydrogen cyanide can be converted to cyanide radical (CN) and then oxidized into NO by O_2.

Combustion of fossil fuels is the major anthropogenic source of the primary pollutants such as SO_2, NO_2, CO, Pb, and other organic or particulate matter. The

levels of NO_x observed in the low troposphere are greatly enhanced in urban and continental areas. In the free troposphere at altitudes of 8 to 12 km, aircraft emissions are potentially responsible for the NO_x levels because they are predominantly emitted at these altitudes.

The other sources of atmospheric NO_x may include volcanoes, rocks, and oceans. Volcanoes release NO_x and various gases into atmosphere and rocks can be the source of a small amount of the atmospheric NO_x. Oceans can also represent a significant source of various gases although many of these actually originate through biological activities within the oceans.

A.2. Photochemistry of NO_x in Troposphere

Although the thermal reactions, which may involve NO, O_2, O_3, and other gases, are very common in the atmosphere, many essential reactions are photochemical because the concentrations of all these trace gases are very low. These photochemical reactions are initiated by absorption of photons rather than by intermolecular collisions which drive thermal reactions. When the solar radiation enters the atmosphere, it is absorbed and scattered by atmospheric constituents. Only sunlight with wavelength exceeding about 290 nm reaches the troposphere, which lies in the spectral region absorbed by NO_2 (Seinfeld and Pandis, 1998). Therefore, NO/NO_2 play an important role in the chemistry of the troposphere because they are photolyzed by solar radiation and provide the atomic oxygen (O) to the oxidation reactions in the troposphere. O_2 is not a source of the atomic oxygen

as it is in the stratosphere because it only absorbs radiation of wavelength shorter than 290 nm.

A photon of wavelength less than 424 nm can dissociate a NO_2 molecule via the reaction,

$$NO_2 + h\nu \rightarrow NO + O(^3P) \qquad (A.10)$$

The oxygen atoms produced in A.10 can subsequently lead to the formation of O_3,

$$O(^3P) + O_2 + M \rightarrow O_3 + M \qquad (A.11)$$

where M is a third body, i.e., a molecule such as N_2 or O_2, which carries off excess energy that might disrupt the O_3 molecule. This O_3 formation is balanced by the reaction between O_3 and NO,

$$O_3 + NO \rightarrow NO_2 + O_2 \qquad (A.12)$$

and O_3 photolyzes

$$\begin{aligned} O_3 + h\nu &\rightarrow O(^3P) + O_2 \\ &\rightarrow O(^1D) + O_2 \end{aligned} \qquad (A.13)$$

In reactions A.10 and A.13, ^3P refers to the ground spectral states of the oxygen atom, and ^1D is the excited state. The reaction A.13 can only be initiated by a photon of wavelength less than 1,100 nm. When the wavelength is less than 315 nm, the reaction only produces an oxygen atom in the excited state.

Ground state oxygen atom will probably recombine with an oxygen molecule to form O_3 (A.12). The excited state oxygen atom may be de-excited to ground state by colliding with a molecule such O_2 or N_2,

$$O(^1D) + M \rightarrow O(^3P) + M \quad \text{(A.14)}$$

More importantly, the excited state atomic oxygen reacts with a water molecule and produce a hydroxyl radical (OH)

$$H_2O + O(^1D) \rightarrow 2OH \quad \text{(A.15)}$$

If water is present during the reaction A.10, the product NO will restore a NO_2 molecule immediately,

$$H_2O + NO \rightarrow NO_2 + OH \quad \text{(A.16)}$$

In the presence of an photon, NO_2 can initiate another cycle of the chain reaction from A.10 to A.16 producing OH, O_3, and O. Each NO_x molecule is responsible for the production of many molecules of these oxidant species before it is removed from the atmosphere.

OH is the most important radical in tropospheric chemistry and it determines the oxidizing and cleansing efficiency of the troposphere. It can produce atomic hydrogen or hydroperoxy (HO_2) when it meets CO in the atmosphere

$$OH + CO \rightarrow CO_2 + H \quad \text{(A.17)}$$

$$H + O_2 + M \rightarrow HO_2 + M \quad \text{(A.18)}$$

Similarly, OH could react with other organic or inorganic trace species in the troposphere producing various atmospheric oxidants and radicals. These highly reactive species, OH, H_2O, O_3, $O(^1D)$ and others, oxidize and remove the pollutants in atmosphere.

OH can also terminates the chain reactions when it meets NO_2 to form

nitrate acid

$$OH + NO_2 + M \rightarrow HNO_3 + M \qquad (A.19)$$

where M is the third body to remove excess energy. The product HNO_3 can be removed by dry or wet deposition.

If the photochemical reaction A.10 is considered as a common chemical reaction by taking a flux of photons with a distribution with respect to wavelength, then the reaction reduces to a pseudo first order reaction. The NO concentration varies

$$\frac{d[NO]}{dt} = -\frac{d[NO_2]}{dt} = J[NO_2] \qquad (A.20)$$

where J is the special first order reaction constant that embraces the absorption coefficient of NO_2, quantum efficiency of the reaction, and the solar spectrum and intensity at the altitude and latitude under consideration. A typical mid-latitude midday value of J is 5×10^{-3} s^{-1} (Brimblecombe, 1986) for reaction (A.10), which suggests a half-life time about 140 seconds for NO_2 photolysis. Actually, the lifetime of NO_x is longer in the troposphere. They could stay in atmosphere for a couple of days before they are removed by dry or wet deposition because the photolysis of NO_2 is balanced by the reverse processes.

A.3. Depletion of Stratospheric Ozone by NO_x

Most of the atmospheric ozone exists in the stratosphere with a peak density at an altitude between 20 to 30 km, which is termed as ozone layer. The O_3 ozone

layer in the stratosphere absorbs almost all of the solar radiation of wavelength from 240 to 290 nm, and it shields organisms on the Earth from damaging ultraviolet radiation. There is only a small amount of O_3 in the atmosphere. For instance, if all the O_3 in the Earth's atmosphere were brought to ground level it would constitute a layer of pure O_3 only 3 mm thick at standard temperature and density.

The stratosphere (altitude from 20 to 40 km) is dominated by photochemical reactions because where the air is so dry and cold that liquid water no longer plays the major role as in the troposphere (altitude less than 20 km). The stratospheric O_3 is formed by the photolysis of O_2, involving ultraviolet radiation with wavelength less than 242 nm.

$$O_2 + h\nu \rightarrow O(^3P) + O(^3P) \qquad (175<\lambda\leq 242 \text{ nm}) \qquad \text{(A.21)}$$

$$O_2 + h\nu \rightarrow O(^3P) + O(^1D) \qquad (\lambda\leq 175 \text{ nm}) \qquad \text{(A.22)}$$

The excited state of the atom oxygen $O(^1D)$ is de-excited by a molecule such as O_2 or N_2 (A.15), and ground state of oxygen $O(^3P)$ reacts with O_2 to forms O_3 (A.12). Reactions A.16 and A.17 do not occur because the water concentration is very low in the stratosphere. The global O_3 levels are stable because the O_2 photolysis production of O_3 is balanced by the O_3 photolysis absorbing a photon in the wavelength range from 242 nm to 320 nm

$$\begin{aligned} O_3 + h\nu &\rightarrow O(^3P) + O_2 \\ &\rightarrow O(^1D) + O_2 \end{aligned} \qquad \text{(A.14)}$$

or the reaction between O_3 and the atomic oxygen $O(^3P)$

$$O_3 + O(^3P) \rightarrow 2O_2 \qquad \text{(A.23)}$$

This is the Chapman mechanism that governs the formation and destruction of O_3 in the stratosphere. However, since 1970 the stratospheric ozone levels have decreased significantly. This has been conclusively linked to anthropogenic emissions of various air pollutants such as the species containing halogen or nitrogen.

The stratospheric NO_x, produced in stratosphere or transported from the troposphere, are involved in the O_3 destruction process with the catalytic cycle

$$NO + O_3 \rightarrow O_2 + NO_2 \quad \text{(A.24)}$$

$$NO_2 + O \rightarrow NO + O_2 \quad \text{(A.25)}$$

and the indirect reactions through the production of hydrogen-containing radicals such as H, OH, and HO_2. These radicals destroy O_3 through the catalytic cycles

$$H + O_3 \rightarrow O_2 + OH \quad \text{(A.26)}$$

$$HO + O \rightarrow H + O_2 \quad \text{(A.27)}$$

and

$$OH + O_3 \rightarrow O_2 + HO_2 \quad \text{(A.28)}$$

$$HO_2 + O \rightarrow O_2 + OH \quad \text{(A.29)}$$

In each of these pair reactions, O_3 and atomic oxygen are destroyed while restoring NO, H or OH. These processes are catalytic until being terminated by the reaction between NO_2 and a water molecule (A.20). The water vapor is very low in stratosphere so the reaction A.20 can only occur on the surface of aerosol particle. The lifetime of NO_x is very long since the density of aerosol particles is so low in the stratosphere that each NO_x molecule may destroy many ozone molecules.

The anthropogenic emissions of NO_x are very effective in damaging the stratospheric O_3 layer. The NO_x produced in troposphere with high chemical stability could diffuse up to the stratosphere and damage the O_3. Especially, the NO_x from combustion in supersonic jets flying in the stratosphere could directly involve in the depletion process of the stratospheric O_3.

A.4 Summary

Most of the atmospheric NO_x molecules are emitted into the troposphere by both anthropogenic and natural resources. In the troposphere NO_x are the essential compounds to determine the cleansing efficiency of the atmosphere. They dominate the photochemistry of the troposphere because NO_2 absorb the solar radiation with wavelength longer than 290 nm which is beyond the absorption region of O_2. The UV photons dissociate NO_2 into NO and atomic oxygen. The product NO could be further oxidized into NO_2 by O_3, O_2, H_2O restoring the photolysis reaction of NO_2, while atomic oxygen initiate a series of gas-phase reactions producing O_3, H, OH, HO_2 and other active species. In urban or continental areas, the anthropogenic emissions are primary sources of atmospheric NO_2. These NO_x emissions always produce locally high levels of atmospheric oxidants because of the short resident time of NO_x in the troposphere. The lifetime of the tropospheric NO_x could be as long as a couple of days before entering the stratosphere or being removed by wet and dry deposition.

The stratospheric NO_x, either drifting from the troposphere or produced by

atmospheric reactions in the stratosphere, are potentially responsible for the depletion of the ozone level (Lacis et al., 1990). Each NO_x molecule could damage many O_3 molecules by a series of recyclable and catalytic reactions. These NO_x molecules reside in the stratosphere with a much longer lifetime than in the troposphere because the water vapor density is very low and hence NO_x are not easily removed. Once the NO_x molecules are emitted into the stratosphere, they impact the depletion of stratospheric ozone layer globally.

References

Alfven, H. and C. G. Falthammar, *Cosmical electrodynamics*, p180, Oxford at the Clarendon Press, London, 1963

Ammann, P. R. and R. S. Timmins, Chemical reactions during rapid quenching of oxygen-nitrogen mixture from very high temperatures, AICHE J., 12, p956-963 (1966)

Barlow, J. S., G. W. Frey and J. B. Newman, Very low frequency noise power from the lightning discharge, *J. Franklin Inst.,* 258, p187-203 (1954)

Barasch, G. E., Spectral intensities emitted by lightning discharges, *J. Geophys. Res.,* 100, p1,049-1,057 (1970)

Baskin, D., Lightning without clouds, *Bull. Am. Meteor. Soc.*, 33, p348-452 (1952)

Beck, J. P., C. E. Reeves, F. A. A. M. de Leeuw, and S. A. Penkett, The effect of aircraft emissions on tropospheric ozone in the northern hemisphere, *Atmos. Environ., Part A26*, p17-29(1992)

Benkovitz, C. M., M. T. Benkovitz, J. Pacyna, L. Tarrason, J. Dignon, E. C. Voldner, P. A. Spiro, J. A. Logan, and T. E. Graedel, Global gridded inventories of anthropogenic emissions of sulfur and nitrogen, *J. Geophys. Res.*, 101, p29,239-29,253 (1996)

Berger, K. and E. Vogelsanger, Photographichische blitzuntersuchungen der Jahre 1955-1965 auf dem Monte San Salvatore, Bull.SEV., 57, p1-22 (1966)

Berger, K., R. K. Anderson, H. Kröninger, Parameter of lightning flashes, *Electra*, 40, p101-119 (1975)

Berger, K., The earth flash, in *Lightning*, ed. by R. H. Golde, p119-190, Academic,

San Diego, CA, 1977

Borovsky, J. E., An electrodynamic description of lightning return strokes and dart leaders: Guided wave propagation along conducting cylindrical channels, *J. Geophys. Res.*, 100, p2697-2726 (1995)

Borucki, W. J. and W. L. Chameides, Lightning: Estimates of the rates of energy dissipation and nitrogen fixation, *Rev. Geophys. And Space Phys*., Vol. 22, p363 (1984)

Braginskii, S. I., *Transport processed in a plasma, in Review of plasma physics, vol.1*, ed. by M. A. Leontovich, p221, Consultant Bureau, New York, 1965

Brimblecombe, P., *Air, composition & chemistry*, Cambridge University Press, 1986

Brook, M. and T. Ogawa, *The cloud discharge, in Lightning, Vol. 1: Physics of lightning*, ed. by R. H. Golde, Academic Press, New York, 1977

Bruce, C. E. R. and R. H. Golde, The Lightning discharge, J. Instn. *Elect. Engrs.*, 88, Part II, p487-520 (1941)

Burns, R. C. and R. W. Hardy, *Nitrogen fixation by bacteria and higher plants*, Spring-Verlag, 1975

Chameides, W., Tropospheric odd nitrogen and the atmospheric water vapor cycle, *J. Geophys. Res.*, 80, p4989-4996 (1975)

Chameides, W. L. J. C. G. Walker and A. F. Nagy, Possible chemical input of planetary lightning in the atmospheres of Venus and Mars, *Nature*, 280, p820-822 (1979)

Chameides, W. L., Effect of variable energy input on nitrogen fixation in instantaneous linear discharges, *Nature*, 277, p123-125 (1979b)

Chameides, W. L., D. H. Stedman, R. R. Dickerson, D. W. Rusch and R. J. Cicerone, NO_x production in lightning, *J. Atmos. Sce.*, 34, p143-149 (1977)

Connor, T. R., Efficiency of conversion of electrical energy into visible radiation in lightning return strokes, *Eos. Trans. AGU*, 49, p686(1968)

Cooray, Vernon, Energy dissipation in lightning flashes, *J. Geophys. Res.*, 102, p21401-21410(1997)

Crutzen, P. J., he role of NO and NO_2 in the chemistry of the troposphere and stratosphere, *Ann. Rev. Earth Planet. Sci.*, 7, p443-472 (1979)

Dawson G. A. , Nitrogen fixation by lightning, *J. of Atmos. Sci.*, 37, p174 (1980)

Dhar, N. R. and A. Ram, Variation in the amounts of ammoniac and nitric nitrogen in rainwater of different countries and the origin of nitric nitrogen in the atmosphere, *J. Indian Chem. Soc.*, 10, p125-133 (1993)

Donohoe, K. G., F. H. Shair and O. R. Wulf, Production of O_3, NO, and N_2O in a pulsed discharge at 1 atm., *Ind. Eng. Chem. Fund.*, 16, p208-215 (1977)

Drapcho, D. L., L. D. Sisterson and R. Kumar, Nitrogen fixation by lightning activity in a thunderstorm, *Atmos. Environ.*, 17, p729-734 (1983)

Ehalt, D. H. and J. W. Drummond, The tropospheric cycle of NO_x, in *Chemistry of the unpolluted and polluted troposphere,* ed. by H.W. Georgii and W. Haeschke, D. Reidel, Hingham, Masss., p219-251 (1982)

Eremin, E. N., Fundamentals of chemical thermodynamics--translated from the Russian by Artavaz Beknazarov, Moscow : Mir, p156-173(1981)

Eriksson, E., Composition of atmospheric precipitation I. Nitrogen compounds, *Tellus*, 4, p215-232 (1952)

Fehsenfeld, F. C., D. d. Parrish, D. W. Fahey, The measurement of NO_x in the non-urban troposphere, in *Troposphere ozone*, Isaksen, S. A., Ed.; D. Reidel Publishing Co., p185-215 (1988)

Fofana, I., A. Be'roual, Modeling of the leader Current with an equivalent electrical network, *Geophys. Res. Letts.*, 21, P305-318(1994)

Franzblau, E. and C. J. Popp, Nitrogen oxides produced from lightning, *J. Geophys. Res.*, 94, p11,089-11,104 (1989)

Garbagnati, E., E. Giudice, F. B. Piparo and U. Magagnoli, Survey of the characteristics of lightning stroke currents in Italy--Results obtained in the years from 1970 to 1973. *E.N.M.L. Report* R5/63-27

Gaydon, A. G. and I. R. Hurle, The shock tube in high temperature chemical physics, *Rheinhold*, 1963

Gifford, T., Aircraft struck by lightning, *Meteorol. Mag.*, 79, p121-122 (1950)

Glasstone, S., K. J. Laidler and H. Eyring, The theory of rate processes, in *The kinetics of chemical reactions, viscosity, diffusion and electrochemical phenomena*, McGraw-Hill, New York, 1941

Goldenbaum, G. C. and R. R. Dickerson, Nitric oxide production by lightning discharges, *J. Geophys. Res.*, 98, p18,333-18,338 (1993)

Greig, J. R., W. Koopman, R. F. Fernsler, R. E. Pechacek, I. M.Vitkovitsky and A. W. Ali, Electrical discharges guided by pulsed CO_2 -- laser radiation, *Phys. Rev. Lett.*, vol. 41, p174-177 (1978)

Griffing, G. W., Ozone and oxides of nitrogen production during thunderstorms, *J. Geophys. Res.*, 82, p943-950 (1977)

Guo, C. and E. P. Krider, The optical and radiation field signatures produced by lightning return strokes, *J. Geophys. Res.*, 87, p8,913-8,922 (1982)

Haagen-Smith, A. J., Air conservation: With discovery of the sources and chemical reactions of pollutant: the stage is set for conservation, *Science*, 128, p869-879 (1958)

Hameed, S., O. G. Paidoussia and R. G. Stewart, Implications of natural sources for the latitudinal gradients of NO_y in the unpolluted troposphere, *Geophys. Res. Lett.*, 8, p591-594 (1981)

Hameed, S., and J. Dignon, Changes in the geographical evaluations of global emissions of NO_x and SO_x from fossil fuel combustion between 1966 and 1980, *Atmos. Environ.*, 22, p441-436 (1988)

Hameed, S., and J. Dignon, Global emissions of nitrogen and sulfur oxides in fossil fuel combustion 1970-1986, *J. Air Waste Manage. Assoc*., 42, p159-163 (1992)

Hao, W. M., M. H. Liu, and P. J. Crutzen, Estimates of annual and regional releases of CO_2 and other trace gases to the atmosphere from fires in the tropics, based on FAO statistics from the period 1975-1980, paper presented at Third International Symposium on Fir Ecology, Friburg Univ., Frieburg, Germany, 1989

Hill, R. D., On the production of nitric oxide by lightning, *Geophys. Res. Letts.*, 6, p945-947 (1979)

Hill, R. D., R. G. Rinker and H. Dale Wilson, Atmospheric nitrogen fixation by lightning, *J. Atmos. Sci.*, 37, p179-192 (1980)

Hutchinson, G. E., The biogeochemistry of the terrestrial atmosphere, in *The earth*

as a planet, ed. by G. P. Kuiper, The University of Chicago Press, p337-433 (1954)

Kasibhatla, P. S., J. Levy II, W. J. Moxim, and W. L. Chameides, The relative impact of stratospheric photochemical production of tropospheric NO_y levels: A model study, *J. Geophys. Res.*, 96, p18,631-18,646(1991)

Kotaki, M., I. Kuriki, C. Katoh, and H. Sugiuchi, Global distribution of thunderstorm activity observed with ISS-b, *J. Radio Res. Lab.*, 28, p49-71 (1981)

Kowalczyk, M. and W. Bauer, Lightning as a source of NO_x in the troposphere, Rep. FAA-EE-82-4, U.S. Dept. of Transp., Washington, DC, (1982)

Krehbiel, P. R., M. Brook and R. A. McCrory, An analysis of the charge structure of lightning discharges to ground, *J. Geophys. Res.*, 84, p2432-2456 (1979)

Krehbiel, P. R., The electrical structure of thunderstorms, in *The Earth's electrical environment*, p90-113, Natl. Acad. Press, Washington DC, (1986)

Krider, E. P., Some photoelectric observations of lightning, *J. Geophys. Res.*, 71, p3,095-3,098 (1966)

Krider, E. P., G. A. Dawson and M. A. Uman, Peak power and energy dissipation in a single-stroke lightning flash, *J. Geophys. Res.*, 73, p3,335-3,339 (1968)

Kumar, P. P., Global distribution of nitric oxide produced by lightning and its seasonal variation, *J. Geophys. Res.*, 100, p11,203-11208 (1995)

Lacis, A. A., D. J. Wuebbles and J. A. Logan, Radiative forcing of climate by changes in the vertical distribution of ozone, *J. Geophys. Res.*, 95, p9,971-9,981 (1990)

Lawrence, M. G., W. L. Chameides, P. S. Kasibhatla, H. Levy, II, and W. Moxim, Lightning and atmospheric chemistry: The rate of atmospheric NO production, in *Handbook of Atmospheric Electrodynamics*, vol.1, ed. by H. Volland, p189-203, CRC Press, New York, 1995

Levy, H., II, Normal atmosphere: Large radical and formaldehyde concentrations predicted, *Science*, 163, p141-143 (1971)

Levy, H., II, W. J. Moxim, P. S. Kasibhatla, and J. A. Logan, The global impact of biomass burning on tropospheric reactive nitrogen, in *global Biomass Burning: Atmospheric, Climatic and Biospheric Implications*, edited by J. S. Levine, p363-369, MII Press, Cambridge, Mass., 1991

Levy, H., II, and W. J. Moxim, Simulated global distribution and deposition of reactive nitrogen emitted by fossil fuel combustion, Tellus, 41, p256-271(1989)

Levy, H., II,, W. J. Moxim, and P. S. Kasibhatla, A global three-dimensional time-dependent lightning source of tropospheric NO_x, *J. Geophys. Res.*, 101, p22,911-22,922 (1996)

Levine, J. S. , R. S. Rogowski, G. L. Gregory, W. E. Howell, and J. Fishman, Simultaneous measurements of NO_x, NO , and O3 production in a laboratory discharge: Atmospheric implications, G*eophys. Res. Lett*., 8, No.4, p.357 (1981)

Liaw, Y, P., D. L. Sisterson and N. L. Miler, Comparison of field, laboratory, and theoretical estimates of global nitrogen fixation by lightning, *J. Geophys. Res.*, 95, p22,489-22,494 (1990)

Lin, S. C. Cylindrical shock waves produced by instantaneous energy release, *J. Appl. Phys.*, 25, p54-57 (1954)

Little, P. F., Transmission line representation of a lightning return stroke, *J. Phys. D: Appl. Phys.*, Vol. 11, p1,893-1,910 (1978)

Liu, S. C., M. McFarland, D. Kley, O. Zafiriou and B. Huebert, Tropospheric NO_x and O_3 budgets in the equatorial Pacific, *J. Geophys. Res*., 88, p1,360-1,368 (1983).

Logan, J. A., Nitrogen oxides in the troposphere: Global and regional budgets, *J. Geophys. Res.*, 88, p10,783-10,807 (1983)

Logan, J. A., M. J. Prather, S. C. Wofsy and M. B. McElroy, Tropospheric chemistry: A global perspective, *J. Geophys. Res.*, 86, p7,210-7,254 (1981)

Mackerras, D., Photoelectric observations of the light emitted by lightning flashes, *J. Atmos. Terr. Phys.*, 35, p521-535(1973)

Malan, D. J., *Physics of lightning*, English University Press, London (1963).

Müller, J. F., Geographical distribution and seasonal variation of surface emissions and deposition velocities of atmospheric trace gases, *J. Geophys. Res.*, 97, p3,787-3,804 (1992)

Noxon, J. F., Atmospheric nitrogen fixation by lightning, *J. Geophys. Res. Lett.*, 3, p463-465 (1976)

Noxon, J. F., Tropospheric NO_2, *J. Geophys. Res.*, 83, p3,051-3,057(1978)

Ogawa, T. and M. Brook, The mechanism of the intracloud lightning discharges, *J. Geophys. Res.*, 69, p514-519 (1964)

Ortega, P. et al, Long air gap discharges under non standard positive impulse voltages, Proc. 7th ISH, Dresden, p105-108 (1991)

Orville, R. E., Calibration of a magnetic direction finding network using measured

triggered lightning return stroke peak currents, *J. Geophys. Res.*, 96, p17,135-17,142 (1991)

Orville, R. E., Ozone production during thunderstorms, Measured by the absorption of UV radiation from lightning, *J. Geophys. Res.*, 72, p3,557-3,561 (1967)

Orville, R. E., Cloud-to-ground lightning flash characteristics in the contiguous United States: 1989-1991, *J. Geophys. Res.*, 99, p10,833-10,841(1994)

Penner, J. E., C. S. Atherton, J. Dignon, S. J. Ghan, J. J. Walton, and S. Hamed, Tropospheric nitrogen: a three-dimensional study of sources, distributions, and deposition, *J. Geophys. Res.*, 96, p959-999 (1991)

Peyrous, J. M. and R. M. Lapeyre, Gaseous products crested by electrical discharges in the atmosphere and condensation nuclei resulting from gaseous phase reactions, *Atmos. Environ.*, 16, p959 (1982)

Picone, J. M., J. P. Boris, J. R. Greig, M. Raleigh and R. F. Fernsler, Notes and correspondence: Convective cooling of lightning channels, *J. of the Atmospheric Science*, 38, p2,057-2,062 (1981)

Pierce, E. T., Atmospherics and radio noise, *in Lightning, vol. 1, Physics of lightning*, ed. By R. H. Golde, Academic Press, 1977

Plooster, M. N., Numerical simulation of spark discharge in air, *Phys. Fluids*, 14, p2,111-2,123 (1971)

Price, C. and M. Prather, personal communication (1998)

Price, C., J. Penner and M. Prather, NO_x from lightning: 1. Global distribution based on lightning physics, *J. Geophys. Res.*, 102, p5,929-5,941 (1997)

Price, C. and J. Penner, NO_x from lightning: 2. Constraints from the global

atmospheric electric circuit, *J. Geophys. Res.*, 102, p5,943-5,951 (1997a)

Raizer, Y. P., The formation of nitrogen oxides in the shock wave generated by a strong explosion in air, *Zh. Fiz, Khim.* 33, p700-709 (1959)

Rakov, R. A. and M. A. Uman, Origin of lightning electric field signatures showing two return-stroke waveforms separated in time by a millisecond or less, *J. Geophys. Res.*, 99 p8,157-8,165 (1994)

Ramstetter, D. -Ing, Messungen der meschwindigkeit $2NO_2 \Leftrightarrow 2NO + O_2$, in Bodenstein, M., Bildung und Zersetzung der Hoheren Stickoxyde, *Z. Physik. Chem. (Leipzig)*,100, p62-123 (1922)

Rhodes, C. T., X. M. Shao, P. R. Krehbiel, R. J. Thomas, and C. O. Hayenga, Observations of lightning phenomena using radio interferometry, *J. Geophys. Res.*, 100, p13,069-13,082 (1995)

Rhouma, A. B. and P. Auriol, Modeling of the whole electric field changes during a close lightning discharge, *J. Phys. D: Appl. Phys.*, 30, p598-602(1997)

Rossow, W. B., and R. A. Schiffer, ISCCP cloud data products, *Bull. Am. Meteorol. So.*, 72 p2-20 (1991)

Seinfeld, John, N., *Atmospheric chemistry and physics of air pollution*, John Wiley & Sons, Inc., p453(1986)

Seinfeld, John N. and Spyros N. Pandis, *Atmospheric chemistry and physics: from air pollution to climate change*, John Wiley & Sons, Inc., p234 (1998)

Stark, M. S., J. T. Harrison and C. Anastasi, Formation of nitrogen oxides by electrical discharges and implications for atmospheric lightning, *J. Geophys. Res.*, 101, p6,963-6,969 (1996)

Stekolnikov, I. S., The parameters of the lightning discharge and the calculation of the current waveform, *Elektrichestvo.*, 3, p63-68 (1941)

Tuck, A. F., Production of nitrogen oxides by lightning discharges, Q, J. R. *Meteorol. Soc*., 102, p749-755 (1976)

Turman, B. N., Analysis of lightning data from the DMSP satellite, *J. Geophys. Res.*, 83, p5,019-5,024(1978)

Uman, M. A., *Lightning*, McGraw-Hill, New York, 1969

Uman, M. A., *Lightning*, McGraw-Hill, New York, 1978

Uman, M. A., *The lightning discharge*, Academic, San Diego, CA, 1987

Viemerster, P. E., Lightning and origin of nitrates found in precipitation, *J. Meteor.*, 17, p681-683 (1960)

Visser, S., Chemical compositions of rain water in Kampala, Uganda, and its relation to meteorological and topographical conditions, *J. Geophys. Res.*, 77, p3,759-3,765 (1961)

von Liebig, J., Une note sur la Nitrification, *ann. Chem. Phys*., 35, p329-333 (1857)

Wang, Y., A. W. DeSilva, G. C. Goldenbaum and R. R. Dickerson, Nitric oxide production by simulated lightning: Dependence on current, energy and pressure, *J. Geophys. Res.*, 103, p19,149-19,159(1998)

Williams D. P., and M. Brook, Magnetic measurement of thunderstorm currents, (1) Continuing currents in lightning, *J. Geophys. Res.*, 68, p3243-3247 (1963)

Wilson, C. T. T., Investigations on lightning discharges and on the electric field of thunderstorms, *Philos. Trans. R. Soc*., London, A 221, p73-115 (1920)

Winn, W. P., G. W. Schwde and C. B. Moore, Measurement of electric fields in

thunderstorms, *J. Geophys. Res.*, 79, p1761-1767 (1974)

Wuebbles, D. J., D. Maiden, R. K. Seals Jr., S. L. Baughcum, M. Metwally, and A. Mortlock, Emissions scenarios development: Report of the Emissions Scenarios Committee, in *The Atmospheric Effects of Stratospheric Aircraft: A Third Program Report, edited by R. S. Stolarski and H. L. Wesoky, NASA Ref. Publ.*, p1,313(1993)

Yienger, J., and H. Levy II, Empirical model of global soil-biogenic NO_x emissions, *J. Geophys. Res.*, 100, p11,477-11,464 (1995)

Zel'dovich, Y. B. and Y. P. Raizer, *Physics of shock waves and high-temperature hydrodynamic phenomena*, vol.1, Academic Press, New York and London, (1966)

Zel'dovich, Y. B., P. Y. Sadovnikov and D. A. Frank-Kamenetskii, The oxidation of nitrogen by combustion, *Izdat. Akad. Nauk SSSR*, Moscow, 1947

Appendix. Atmospheric Nitrogen Oxides

The atmospheric nitrogen oxides (NO and NO_2) are emitted by natural and anthropogenic sources. Globally, total of natural sources has been estimated approximately same as anthropogenic emissions. In urban or continental regions, anthropogenic emissions are greater than that from natural sources, while remote tropic region is dominated by the natural emissions. These compounds participate importantly in atmospheric chemistry. In the troposphere, they are responsible to the photochemical production of smog, production and other atmospheric oxidants, and acid deposition; in the stratosphere, they are involved in the depletion of ozone layer. This appendix will describe the resources of the atmospheric NO_x and their influence on the atmospheric chemistries.

A.1. Resources of Atmospheric NO_x

Estimated global emissions of NO_x have been given in Table 1.1. The global anthropogenic emissions are primarily attributed to fossil-fuel combustion and soil release from fertilizers that tend to be located in or near urban areas. The natural processes include biomass burning, lightning fixation, the ionization of N_2 by cosmic radiation and other small contributions. In order to evaluate the impact of NO_x on atmospheric chemistry and the global climate change, both the anthropogenic and natural sources must be considered and their relative importance needs to be evaluated.

A.1.1. Biological resources

Nitrogen in living matters is largely as amino compounds or ammonium ion, while amino acids present can be broken down into ammonia

$$NH_2CH_2COOH + \frac{3}{2}O_2 \rightarrow 2CO_2 + H_2O + NH_3 \quad (A.1)$$

Ammonia and ammonium ion can be absorbed by plants directly. When environmental conditions are reasonable alkaline, ammonium ions in living matters and soils could be released directly into atmosphere as gaseous ammonia.

Microbial activities, including nitrification and de-nitrification, take the nitrogen-containing compounds and release NO_x into the atmosphere, as well as the other nitrogen-containing species such as NH_3, N_2O, and HNO_3. Nitrification, performed by some specialized microorganisms, oxidizes ammonia into nitrite. These bacteria use ammonia as an energy source in the same way as other cells use the reduced carbon compounds such as carbohydrates

$$NH_3 + \frac{3}{2}O_2 \rightarrow NO_2^- + H_2O + H^+ \quad (A.2)$$

Nitrobacteria further oxidize nitrite into nitrate

$$NO_2^- + \frac{1}{2}O_2 \rightarrow NO_3^- \quad (A.3)$$

De-nitrification is the reverse process performed by numerous micro-organisms. Often these processes are performed by nitrate respiration of aerobic bacteria, which use nitrate to oxidize carbohydrates when oxygen becomes limited.

$$C_6H_{12}O_6 + 6NO_3^- \rightarrow 6CO_2 + 3H_2O + 6OH^- + 3N_2O \quad (A.4)$$

$$5C_6H_{12}O_6 + 24NO_3^- \rightarrow 30CO_2 + 18H_2O + 24OH^- + 12N_2 \quad (A.5)$$

These reactions emit N_2 or N_2O into atmosphere. The N_2O, predominantly emitted by biological activities from soil and water, has a very long residence time (~100 years) in atmosphere. It could diffuse into stratosphere. Where it may be further oxidized into NO as the principal natural source of NO_x in the stratosphere.

A.1.2. Atmospheric resources

Reactions in the atmosphere are the major direct sources of atmospheric NO_x. These reactions include the lightning fixation of nitrogen in air, reactions induced by incoming cosmic radiation, and a small portion from extraterrestrial materials. Lightning has long been recognized as the most important natural source of atmospheric NO_x. Especially in remote tropical region, it is believed the dominant source.

Lightning heats air in its discharge column to high temperature and fixes nitrogen via the reaction

$$O_2 + N_2 \leftrightarrow 2NO \qquad \text{(A.7)}$$

and further

$$O_2 + 2NO \leftrightarrow 2NO_2 \qquad \text{(A.8)}$$

At high temperature, the oxidation of nitrogen (A.7) proceeds rapidly. As the hot air column cools quickly by its cold surrounding air, the thermochemical reaction (A.7) does not remain in equilibrium during cooling and the NO formed at high temperature could be “frozen out”. The NO yield of a lightning depends on both the temperature and the rate of cooling. If the reacted gas mixture cools slowly the yield of nitrogen oxides is low because there is enough time for the reactants to be

reformed. Large uncertainty exists in the estimates of the global NO_x production because of the uncertainty of NO_x production mechanism by a lightning discharge and the limited resources of global lightning data.

A.1.3. Combustion of fuels

Combustion is the major anthropogenic source of atmospheric nitrogen oxides, resulting from both the interaction of nitrogen in the fuel with oxygen in air and the chemical conversion of atmospheric nitrogen and oxygen at the high temperature of combustion. Estimated global emissions of NO_x from fossil-fuel combustion increased from 18.1 TgN/year in 1973 to 24.3 TgN/year in 1986 (Hameed and Dignon, 1992). The organic nitrogen contained in fuel can be converted to ammonia or hydrogen cyanide and then rapidly to form NO. Combustion takes place in air which predominantly consists of nitrogen, so the high temperatures in the combustion process may encourage NO_x formation with the same reactions that occur in the hot air column of a lightning (A.7, A.8).

In an internal combustion engine, the reaction rates may be too slow to allow NO_x production. However, NO could be produced by more rapid ways during the combustion of fuels. In the case of the combustion of hydrocarbons, the presence of the CH radical can lead to the rapid formation of hydrogen cyanide

$$N_2 + CH \rightarrow HCN + N \qquad (A.9)$$

The hydrogen cyanide can be converted to cyanide radical (CN) and then oxidized into NO by O_2.

Combustion of fossil fuels is the major anthropogenic source of the primary

pollutants such as SO_2, NO_2, CO, Pb, and other organic or particulate matter. The levels of NO_x observed in the low troposphere are greatly enhanced in urban and continental areas. In the free troposphere at altitudes of 8 to 12 km, aircraft emissions are potentially responsible for the NO_x levels because they are predominantly emitted at these altitudes rather than at the surface.

The other resources of atmospheric NO_x may include volcanoes, rocks, and oceans. Volcanoes release NO_x and various gases into atmosphere and rocks can be the source of a small amount of the atmospheric NO_x. Oceans can also represent a significant source of various gases although many of these actually originate through the biological activities within the oceans.

A.2. Photochemistry of NO_x in Troposphere

Although the thermal reactions, which may involve NO, O_2, O_3, and other gases, are very common in the atmosphere, many essential reactions are photochemical because the concentrations of all these trace gases are very low. These photochemical reactions are initiated by absorption of photons rather than by intermolecular collisions which drive thermal reactions. When the solar radiation enters the atmosphere, it is absorbed and scattered by atmospheric constituents. Only the sunlight of wavelength exceeding about 290 nm reaches the troposphere, which lies in the region absorbed by NO_2 (Seinfeld and Pandis, 1998). Therefore, NO/NO_2 play an important role in the chemistry of the troposphere that they are photolysised by solar radiation and provide the atomic oxygen (O) to the oxidation

reactions in the troposphere. O_2 is not a source of the atomic oxygen as it does in the stratosphere because it only absorbs radiation of wavelength shorter than 290 nm.

A photon of wavelength less than 424 nm can photolysis a NO_2 molecule via the reaction

$$NO_2 + h\nu \rightarrow NO + O(^3P) \qquad (A.10)$$

The oxygen atoms produced in A.10 can subsequently lead to the formation of O_3

$$O(^3P) + O_2 + M \rightarrow O_3 + M \qquad (A.11)$$

where M is a third body, i.e., a molecule such as N_2 or O_2, which carries off excess energy that might disrupt the O_3 molecule. This O_3 formation is balanced by the reaction between O_3 and NO

$$O_3 + NO \rightarrow NO_2 + O_2 \qquad (A.12)$$

and O_3 photolysis

$$\begin{aligned} O_3 + h\nu &\rightarrow O(^3P) + O_2 \\ &\rightarrow O(^1D) + O_2 \end{aligned} \qquad (A.13)$$

In reactions A.10 and A.13, ^3P and ^1D describe ground and excited spectral states of the oxygen atom. The reaction A.13 can only be initiated by a photon of wavelength less than 1,100 nm. When the wavelength is less than 315 nm, the reaction only produces oxygen atom in excited state.

Ground state oxygen atom will probably recombine with an oxygen molecule to form O_3 (A.12). The excited state oxygen atom may be de-excited to ground state by colliding with a molecule such O_2 or N_2.

$$O(^1D) + M \rightarrow O(^3P) + M \quad \text{(A.14)}$$

More importantly, the excited state atomic oxygen reacts with a water molecule and produce a hydroxyl radical (OH)

$$H_2O + O(^1D) \rightarrow 2OH \quad \text{(A.15)}$$

If water presents in the reaction A.10, the product NO will restore a NO_2 immediately

$$H_2O + NO \rightarrow NO_2 + OH \quad \text{(A.16)}$$

In the presence of photon, then NO_2 will initiate another cycle of the chain reaction from A.10 to A.16 producing OH, O_3, and O. Each NO_x molecule is responsible for the productions of many molecules of these oxidant species before it is removed from the atmosphere.

OH is the most important radical in tropospheric chemistry and it determines the oxidizing and cleansing efficiency of the troposphere. It can produce atomic hydrogen or hydroperoxy (HO_2) when it meets CO in the atmosphere

$$OH + CO \rightarrow CO_2 + H \quad \text{(A.17)}$$

$$H + O_2 + M \rightarrow HO_2 + M \quad \text{(A.18)}$$

Similarly, OH could react with other organic or inorganic trace species in the troposphere producing various atmospheric oxidants and radicals. These highly reactive species, OH, H_2O, O_3, $O(^1D)$ and others, oxidize and remove the pollutants in atmosphere.

OH can also terminates the chain reactions when it meets NO_2 to form

nitrate acid

$$OH + NO_2 + M \rightarrow HNO_3 + M \qquad (A.19)$$

where M is the third body to remove excess energy. The product HNO_3 can be removed by dry or wet deposition.

If the photochemical reaction A.10 is considered as a common chemical reaction by taking a flux of photons with a distribution with respect to wavelength, then the reaction reduces to a pseudo first order reaction. The NO concentration varies

$$\frac{d[NO]}{dt} = -\frac{d[NO_2]}{dt} = J[NO_2] \qquad (A.20)$$

where J is the special first order reaction constant that embraces the absorption coefficient of NO_2, quantum efficiency of the reaction, and the solar spectrum and intensity at the altitude and latitude under consideration. A typical mid-latitude midday value of J is 5×10^{-3} s^{-1} (Brimblecombe, 1986) for reaction (A.10), which suggests a half-life time about 140 seconds for NO_2 photolysis. Actually, the lifetime of NO_x is longer in the troposphere. They could stay in atmosphere for a couple of days before they are removed by dry or wet deposition because the photolysis of NO_2 is balanced by the reverse processes.

A.3. Depletion of Stratospheric Ozone by NO_x

Most of the atmospheric ozone exists in the stratosphere with a peak density at altitude between 20 to 30 km, which is termed as ozone layer. The O_3 ozone layer

in the stratosphere absorbs almost all of the solar radiation of wavelength from 240 to 290 nm, and it shields organisms on the Earth from damaging ultraviolet radiation. There is only a small amount of O_3 in atmosphere. For instance, if all the O_3 in the Earth's atmosphere were brought to ground level it would constitute a layer of pure O_3 only 3 mm thick.

The stratosphere (altitude from 20 to 40 km) is dominated by photochemical reactions because where the air is so dry and cold that liquid water no longer plays the major role as in the troposphere (altitude less than 20 km). The stratospheric O_3 is formed by the photolysis of O_2, involving ultraviolet radiation with wavelength less than 242 nm.

$$O_2 + h\nu \rightarrow O(^3P) + O(^3P) \qquad (175<\lambda\leq 242 \text{ nm}) \qquad (A.21)$$

$$O_2 + h\nu \rightarrow O(^3P) + O(^1D) \qquad (\lambda\leq 175 \text{ nm}) \qquad (A.22)$$

The excited state of atom oxygen $O(^1D)$ is de-excited by a molecule such as O_2 or N_2(A.15), and ground state of atom oxygen $O(^3P)$ reacts with O_2 to forms O_3 (A.12). Reactions A.16 and A.17 do not occur because the water concentration is very low in the stratosphere. The global O_3 levels are stable because the O_2 photolysis of O_3 formation is balanced by the O_3 photolysis absorbing a photon in the wavelength range from 242 nm to 320 nm

$$\begin{aligned} O_3 + h\nu &\rightarrow O(^3P) + O_2 \\ &\rightarrow O(^1D) + O_2 \end{aligned} \qquad (A.14)$$

or the reaction between O_3 and the atomic oxygen $O(^3P)$

$$O_3 + O(^3P) \rightarrow 2O_2 \qquad (A.23)$$

This is the Chapman mechanism that governs the formation and destruction of O_3 in the stratosphere. However, since 1970 the stratospheric ozone levels have decreased significantly that has been conclusively linked to anthropogenic emissions of various air pollutants such as the species containing halogen or nitrogen.

The stratospheric NO_x, produced in stratosphere or transported from troposphere, are involved in the O_3 destruction process with the catalytic cycle

$$NO + O_3 \rightarrow O_2 + NO_2 \quad \text{(A.24)}$$

$$NO_2 + O \rightarrow NO + O_2 \quad \text{(A.25)}$$

and the indirect reactions through the production of hydrogen-containing radicals such as H, OH, and HO_2. These radicals destroy O_3 through the catalytic cycles

$$H + O_3 \rightarrow O_2 + OH \quad \text{(A.26)}$$

$$HO + O \rightarrow H + O_2 \quad \text{(A.27)}$$

and

$$OH + O_3 \rightarrow O_2 + HO_2 \quad \text{(A.28)}$$

$$HO_2 + O \rightarrow O_2 + OH \quad \text{(A.29)}$$

In each of these pair reactions, O_3 and atomic oxygen are destroyed while restoring NO, H or OH. These processes are catalytic until being terminated by the reaction between NO_2 and a water molecule (A.20). The water vapor is very low in stratosphere so the reaction A.20 can only occur on the surface of aerosol particle. The lifetime of NO_x is very long since the density of aerosol particles is low in the stratosphere that each NO_x molecule may destroy many ozone molecules.

The anthropogenic emissions of NO_x are very effective in damaging the stratospheric O_3 layer. The NO_x produced in troposphere with high chemical stability could diffuse up to the stratosphere and damage the O_3. Especially, the NO_x from combustion in supersonic jets flying in the stratosphere could directly involve in the depletion process of the stratospheric O_3.

A.4 Summary

Most of the atmospheric NO_x are emitted into the troposphere by both anthropogenic and natural resources. In the troposphere NO_x are the essential compounds to determine the cleansing efficiency of the atmosphere. They dominate the photochemistry of the troposphere because NO_2 absorb the solar radiation with wavelength longer than 290 nm that is beyond the absorption region of O_2. The UV photons photolysis NO_2 into NO and atomic oxygen. The product NO could be further oxidized into NO_2 by O_3, O_2, H_2O restoring the photolysis reaction of NO_2, while atomic oxygen initiate a series of gas-phase reactions producing O_3, H, OH, HO_2 and other active species. In urban or continental areas, the anthropogenic emissions are primary resources of atmospheric NO_2, greatly enhanced NO_x levels have been observed. These NO_x emissions always produce high levels of atmospheric oxidants only locally because of the short resident time of NO_x in the troposphere. The lifetime of the tropospheric NO_x could be as long as a couple of days before entering the stratosphere or being removed by wet and dry deposition.

The stratospheric NO_x, drifted from the troposphere or produced by

atmospheric reactions in the stratosphere, are potentially responsible to the depletion of ozone level. Each NO_x could damage many O_3 molecules by a series of the recyclable and catalytic reactions. These NO_x reside in the stratosphere with a much longer lifetime than in the troposphere because water vapor is very low and NO_x are uneasy to be removed. Once the NO_x are emitted into the stratosphere, they impact the depletion of stratospheric ozone layer globally.